AN ABSTRACT OF THE THESIS OF

Colin R. Robins for the degree of Master of Science in Soil Science presented on 17 August 2004.

Title: Spatial Analysis of Soil Depth Variability and Pedogenesis Along Toposequences in the Troodos Mountains, Cyprus.

Abstract Approved: Redacted for privacy

Jay S. Noller

In unstable landscapes, modern pedological research explores the role of soils as products and indicators of geomorphologic change. Understanding the dynamics of hill slope pedogenesis is especially important in regions with limited, poor, or threatened soil resources. The island of Cyprus, situated in the eastern Mediterranean, is claimed by many authors to exhibit signs of severe soil degradation and is a prime site for comparative soil geomorphologic research. This study strove to 1) identify the controls of soil genesis and landscape stability within the Troodos Mountains of Cyprus using image and GIS analysis; 2) compare toposequence data to expected soil thickness trends from traditional models of xeric soil toposequences prevalent in current scientific literature; and 3) develop a predictive model for hillslope pedogenesis based on measured soil properties within the field area.

Study soils within the Troodos are thin, weakly developed Lithic and Typic Xerorthents formed in colluvium derived from fractured, igneous bedrock. Soil thickness was measured at 368 sites in seven transects across three watersheds in the Troodos, using interpretations of field profiles and image analysis of digital soil-bedrock profiles in photographed road-cuts along forestry paths. Soil thickness was compared through GIS and statistical analysis to landscape attributes derived from a 25-m DEM and other map data. Results indicate that lithology is the only factor of several studied to have a significant relationship with the variability of soil-profile thickness in the Troodos, and that soil thickness does not vary in a predictable manner across toposequences. These results, combined with differences between measured soil data and values predicted by the landscape stability model SHALSTAB, suggest that soil genesis in the Troodos is best described only within the context of a weathering-limited geomorphological system.

Short-term disruptive processes such as forest fires, land sliding, tree throw, and raindrop impact, combined with long-term processes such as tectonic uplift and stream incision, are the most likely driving forces behind the rapid erosion of hill slope sediments and the weak development of Troodos hill slope soils. These findings have important implications for DEM-based, predictive soil mapping in weathering-limited geomorphologic systems.

Spatial Analysis of Soil Depth Variability and Pedogenesis Along Toposequences in the Troodos Mountains, Cyprus.

by

Colin R. Robins

A THESIS

submitted to

Oregon State University

In partial fulfillment of
the requirements for
the degree of

Master of Science

Presented August 17, 2004
Commencement June 2005

Master of Science thesis of Colin R. Robins, presented on August 17, 2004.

APPROVED:

Redacted for privacy

Major Professor, representing Soil Science

Redacted for privacy

Head of the Department of Crop and Soil Science

Redacted for privacy

Dean of the Graduate School

I understand that my thesis will become part of the permanent collection of Oregon State University Libraries. My signature below authorizes release of my thesis to any reader on request.

Redacted for privacy

Colin R. Robins, Author

ACKNOWLEDGEMENTS

This research would not have been possible without generous financial and logistical support from Oregon State University and the Department of Crop and Soil Science. I would like to extend my sincerest thanks to the faculty, staff, and fellow students who encouraged and assisted me kindly every single step of the way.

I am especially grateful to my committee members, Herb Huddleston, Jim Thomson, and Dawn Wright, for their guidance, time, and interest; to Tracy Mitzel and Jayne Smith, for their humor and patient assistance with all of my departmental dilemmas; to John Baham, James Cassidy, and Herb Huddleston for their love of knowledge and inspirational teaching styles; to friends and office mates Cameron Bergen, Abdelhamid Elnaggaar, and Alicia Lyman-Holz for all their assistance, stories, and understanding; to Candace Banners, Eric Gale, Heath Keirstead, Jenn Moore, and Naoyuki Ochiai for their friendship and thesis advice; and to Justin Brant, Nick Chambers, Terry Luecker, and Laila Parker, for always being there with support, friendship, sanity, love, and laughter.

I am also forever indebted to the Troodos Archaeological and Environmental Survey Project for generous financial, logistical, and intellectual support during my two unforgettable summer field seasons as a geomorphological intern in Cyprus.

I would especially like to thank Michael Given for taking an interest in my research, and for providing appropriate doses of humor, kindness, wisdom, and logistical support whenever they were needed; fellow G.I.s Brian Blankespoor, Abel Lufafa, and Sheila Slevin of OSU for their friendship, advice, and sanity; Georgia Apostolou, Alexis Boutin, Hugh Corley, Annie Evans, Erin Gibson, Marios Hadjianastassi, Kristina Jacobson, Sarah Janes, Chris Parks, Sophi Pullar, Charlie Schriwer, Luke Sollars, Caroline Sauvage, Caroline Torres, and Thomas Tselios, for fantastic travels, great conversations, fine cuisines, brilliant stories, ridiculous moments, and for keeping me on my toes always.

Above all, I extend my most heartfelt thanks to Jay Noller, my advisor and mentor, whose wisdom, patience, humor, kindness, and love of knowledge have been and will always be an inspiration to me; and to Lisa Wells for her support, patience, hospitality, and kindness in Oregon and Cyprus.

TABLE OF CONTENTS

TABLE OF CONTENTS (Continued)

LIST OF FIGURES

LIST OF FIGURES (Continued)

LIST OF TABLES

This thesis is dedicated to my parents, Dr. Catherine H. Robins and Dr. C. Richard Robins, whose love, compassion, intelligence, and never-failing support have guided me always towards the best possible walks of life; and to Lane and Rob, for bein' the best darn sister and brother of all time.

Spatial Analysis of Soil Depth Variability and Pedogenesis Along Toposequences in the Troodos Mountains, Cyprus.

INTRODUCTION

Literature Review

Hans Jenny's landmark publication *The Soil Forming Factors* identified and detailed five broad factors of pedogenesis: climate, organisms, topography, parent material, and time (Jenny, 1941). These factors have since been widely accepted and cited by soil scientists around the world. The scope of each factor is so broad and complex, however, that entire subdisciplines of study have arisen to better detail the processes and variables comprising each one. Moreover, the factors are so intricately related that it often proves meaningless to analyze them as separate factors. For example, the analysis of topography in studies of pedogenesis includes landscape pattern variables such as hill slope gradient, curvature, and aspect. The effect of each variable may be compared to one or more soil properties to test for correlation, but the necessary exclusion of time-dependent processes by such methods greatly oversimplifies depictions of pedogenetic processes, especially in geomorphologically active landscapes.

In unstable landscapes, modern pedological research explores the role of soils as products and indicators of geomorphologic change. The fundamental factors of soil formation on unstable hill slope landforms are identical to those acting upon flatter terrain. Research in landscape pedology assumes that much of a soil's characteristics are an indirect product of geomorphologic processes, specifically the way water moves through and over the landscape (Moore *et al.*, 1993). The hydrology of a landscape both affects and is affected by climate, organisms, parent material, and topography. The specific effects of hydrogeomorphology on soil genesis become clear when all pedogenetic factors apart from topography are held constant. A toposequence, therefore, is a series or pattern of distinct soils imparted on a landscape by changes in hydrogeomorphologic processes with topography. The distinction between soil or landscape pattern and geomorphologic process becomes crucial when modelling soil genesis along a toposequence. Many attempts by soil scientists and geomorphologists to characterize soil spatial variability across hill slopes have not sufficiently linked pattern to process (Moore *et al.*, 1993).

Published toposequence studies range from simple regression analyses of soil properties along hill slope profiles (two dimensions) to more complex multivariate analyses that extend across landforms (three-dimensions). Soil properties investigated may include total profile thickness, specific horizon thickness, pH and the content of clay-sized particles, coarse fragments, organic matter, or specific nutrients.

Successful prediction of soil properties in a toposequence is considered an important goal of the field of pedometrics, given the new, detailed models of the Earth's surface: digital elevation models (DEMs) (McBratney *et al.*, 2003). Some researchers suggest that certain soil properties, particularly those of the subsoil, do not correlate with satellite topographic data (*e.g.* Park and Burt, 2002), whereas other studies present an opposing view. In the latter case, researchers (Tsai *et al.*,

2001) predict soil-depth characteristics across forest terrain based on multi-linear regression analysis.

In terms of general soil morphology, unstable landscapes are most frequently characterized by Entisols and Inceptisols because geomorphologic processes occur at rates or frequencies that preclude extensive soil-profile development. For this reason, soil thickness may serve as a proxy for soil development in the absence of diverse horizons or textural differentiation. In addition to representing long-term erosion, deposition, and soil building processes, soil thickness may also generally indicate water storage capacity, nutrient storage pool, and overall productivity, providing a basis for modelling the spatial distribution of landscape process zones.

The most informative toposequence studies relate pedogenesis to geomorphologic process by considering soil properties as a net by-product of the co-acting processes of soil or regolith development, soil and bedrock erosion, and tectonic uplift or subsidence (Heimsath *et al.*, 1999; D'Odorico, 2000; Gessler *et al.*, 2000; Braun *et al.*, 2001). This net effect of slope process and pedogenesis determines the spatial distribution of select soil properties (Park & Burt, 2002).

Once the relationship between geomorphology and hill slope pedogenesis is understood for a given site, soil properties may be extrapolated across landforms of similar morphology, and over geomorphologically significant time scales (Dietrich *et al.*, 2003). The question, then, is which pedogenetic factors and what level of geomorphologic detail are needed to accurately model soil development, or soil thickness, across a given hill slope system (Jenny, 1941). Because toposequences have been described for many distinct environmental and ecological regimes, the geomorphologic aspects of the traditional soil forming factors are well-constrained. The following review addresses the dynamics of organisms, parent material, and climate, on toposequence pedogenesis.

Factors in toposequence pedogenesis

Organisms affect soil in many ways, however, their geomorphologic significance consists mainly of the downslope transport of soil material through bioturbation, for example: burrowing, root growth, or tree throw. In many instances, the mechanical disruption of parent material through bioturbation is the dominant soil production mechanism (Heimsath *et al.*, 2001). Although bioturbation by an individual organism may affect only a small volume of soil or regolith, studies suggest that bioturbation, especially in forested hill slopes, thoroughly mixes soil layers over geomorphologic time-scales and limits the maximum soil depth (Roering *et al.*, 2002; Gabet *et al.*, 2003). Researchers have also detailed the effects of soil mixing on organic and inorganic nutrient levels along toposequences (Weitkamp *et al.*, 1996; Norton *et al.*, 2003).

Parent-material characteristics also affect pedogenesis. Specifically, the porosity, permeability, physical integrity, and mineralogy of a substratum influences hydrology and stability. Moreover, fractured bedrock has long been considered more susceptible than intact material to physical weathering and erosion via root growth, freeze-thaw, and other processes. Research indicates that chemical weathering of parent material increases laterally towards the increased surface area of rock fractures (Frazier & Graham, 2000; Ehlen, 2002). Therefore higher degrees of regolith production may be found in parent material exhibiting high bedrock fracture density. The relationship of soil thickness to bedrock fractures, however, depends also on the temporal stability of the landscape. Under a weathering-limited geomorphologic system, soil erosion is limited by the rate at which sediment is made available by weathering of parent material (Birkeland, 1999).

Under transport-limited conditions, soil develops in accumulating colluvium through time until erosional events disrupt pedogenesis and translocate sediments. Expected soil thickness trends for weathering- and transport-limited hill slopes are illustrated in Figure 1.1. The degree and depth of rock weathering profiles may help determine geomorphologic processes of erosional landscapes and

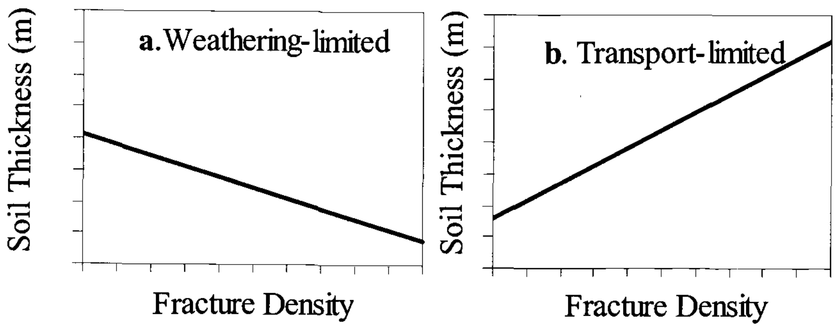

Figure 1.1. Expected relationship between fracture density and pedogenesis for distinct geomorphologic systems.

sediment features (Migoń & Lidmar-Bergström, 2001). That is, the properties that influence hill slope resistance to lowering through mass removal often depend less upon the original parent material than they do upon the physical and hydrological properties of soil and regolith (Taylor & Eggleton, 2001).

Climate exerts even greater pedogenetic controls on a landscape. The total amount of moisture received, the form of precipitation in which moisture arrives, the intensity of precipitation events, and the seasonal distribution of precipitation events all exert great influence on soil development and landscape stability (Birkeland, 1999). In turn, the flow of water is inherently dependent upon topography. Research by Moore *et al.* (1993) models pedogenesis as a function of the hydrologic characteristics, supported by slope and wetness index correlations, of a landscape. Other well-explored models include USLE (Wischmeier, 1976) and WEPP (Flanagan & Nearing, 1995), which employ similar topographic and hydrologic variables to characterize soil erosion rather than soil genesis. Where relief is high, orographic effects can greatly influence not only soil erosion, but also soil properties and regolith development at larger temporal and spatial scales. For the most part, however, toposequence study areas are developed at the kilometer scale, landform scale, or smaller and exhibit limited (tens to hundreds of meters) relief so climatic variability across modelled sites is often negligible.

Given the high number of studies describing different sub-processes of the soil forming factors, the geomorphologic aspects of traditional soil forming factors are well-constrained and may be applied to toposequence analysis. Because topography and hydrology are never uniform, geomorphologic processes vary even along individual hill slopes. Consequently, toposequences are usually subdivided into distinct hill slope position classes, based on natural breaks in hill slope gradient or curvature. Common classes include summit, shoulder, backslope, footslope, and toeslope positions (Ruhe and Walker, 1968). Recently, computer programs have been developed to automate the classification of hill slope position for comparison to soil and other landscape attributes (*e.g.* Coops *et al.*, 1998).

In two companion papers, Ruhe and Walker describe pedogenetic variability along toposequences as a function of hill slope gradient and landscape stability (Ruhe & Walker, 1968; Walker & Ruhe, 1968). Other researchers suggest that while pedogenesis may indeed depend partly on landscape position, slope length, and slope gradient, the spatial variation of pedogenesis is more significantly controlled by landform curvature (King *et al.*, 1983). The relationship between topography and pedogenesis has been explored in diverse toposequences across the globe. For example, the research of Ruhe and Walker (1968) maintains that, for a given hillside, shoulder and backslope positions should exhibit weak soil development due to steep gradients and high rates and incidences of erosion, while summit soils should be well developed due to greater stability through time (Figure 1.2). In contrast, other authors remark that summits of many toposequences in the western U.S. are poorly developed because they retain the least soil moisture of all positions in their respective hill slopes (Birkeland *et al.*, 2003). Results from another study, of rocky hill slopes in Mexico, suggest that summit, shoulder, and backslope segments are all predominantly unstable areas characterized by weak soil-profile development (Gama-Castro *et al.*, 2004).

These apparently conflicting results are explained in terms of the previously mentioned interaction of pedogenetic, geomorphologic, and geologic processes. The Iowa field site described by Ruhe and Walker (1968) falls within a tectonically

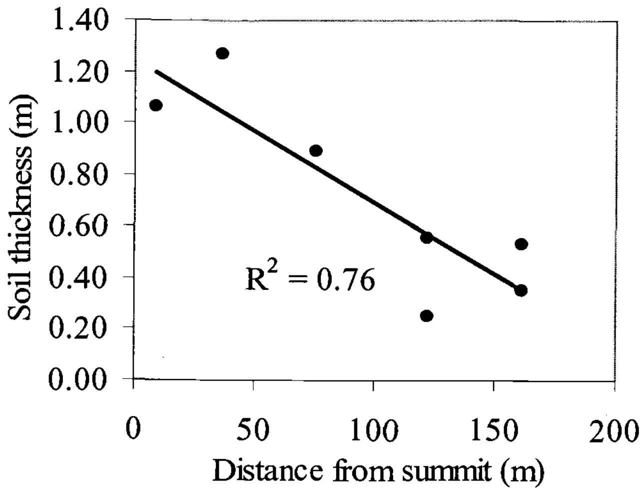

Figure 1.2 Measured soil depths and expected soil thickness trend between summit and backslope positions in Harrison County, Iowa (adapted from Ruhe & Walker, 1968).

stable region. In contrast, the authors of the study in Mexico suggest that landscape changes in their field site are rapid, and that episodes of change may be separated by long periods of stability (Gama-Castro *et al.*, 2004). Not all differences between toposequences may be explained in this manner. Researchers at other sites note, as a caveat, that erosion rate estimates are often only poorly constrained, not only due to the spatial variability of soil properties but also due to the short time period in which data may be collected (Reneau & Dietrich, 1991). Researchers comparing diverse toposequence and erosion studies must also consider that the apparent order, complexity, or variability of earth surface systems depends upon the spatial and temporal scales of study (Phillips, 1999).

Toposequences span distinct geomorphologic and geologic systems. Sediment-limited and transport-limited regimes comprise two extremes between which pedogenesis and hill slope processes fluctuate due to random forcing

(D'Odorico, 2000). Thus, soils within traditionally defined toposequence position classes are shown to vary depending on site geology, climate, topography, vegetation, and even human land use. The expectation, however, is that soil characteristics within a given toposequence may be predicted when the pedogenetic and geomorphologic context of the site can be clearly identified. Similarly, soil toposequences may be compared between sites that have closely similar pedogenetic and geomorphologic environments.

Understanding the dynamics of hill slope pedogenesis is especially important in geomorphologically unstable regions with limited, poor, or threatened soil resources. The regions bordering the Mediterranean Sea face the increasing threat of large-scale, progressive soil desertification and subsequent soil erosion (Secretariat of the UN CCD, 2002). The island of Cyprus, situated in the eastern Mediterranean, is claimed by many authors to exhibit signs of severe soil degradation. Centuries of use, it is argued, have degraded soil quality on the island, leaving many soils as thin, alkaline, humus- and nutrient-poor mantles of regolith atop highly permeable, rocky substrata (Keefe *et al.*, 1971). Analysis of historical land use records illustrates how millenia of extensive timber harvest and forest grazing by goats could have contributed to the diminution of the forests of Cyprus and the erosion of forest soils (Christodoulou, 1959).

Although hill slope processes have been detailed worldwide, much of the recent research (*e.g.*: Reneau & Dietrich, 1991; Heimsath *et al.*, 1997; Frazier & Graham, 2000; Anderson *et al.*, 2002) on hill slope processes and soil geomorphology has been conducted in the western mountains of North America.

Similar seasonal moisture patterns, geology, geomorphology, and land use make studies of landscape pedology in these regions ideal for comparison to the Troodos Mountains of Cyprus.

Although both provinces have Mediterranean climates, the mean annual precipitation (MAP) of the North American sites is much greater than that of Cyprus. Oregon data represent the wettest hill slopes, while studies conducted in California model landforms with intermediate MAP. Thus, research on hill slope soil processes in Cyprus may elucidate dynamics of drier (low MAP) regions under-represented in contemporary scientific literature. Models developed in wetter climate regimes can be applied to DEM and hydrologic data from the Mediterranean, and tested for applicability to drier climates. The island of Cyprus presents a virgin field for soil genesis and soil erosion research (Thirgood, 1987). Investigations of pedogenesis in forested toposequences of the Troodos Mountains extends the broader scientific knowledge of pedogeomorphologic processes to a region in great need of further geomorphologic and soil science research.

Objectives

The central hypothesis of this research holds that soil thickness within the Troodos Mountains varies in a predictable manner across geomorphic features due to topographic variations. Specifically, qualitative field observations made during the summer of 2003 suggest that soils are extremely thin (less than ten centimeters) or absent on summits and ridges, and thickest (greater than forty centimeters) along valley bottoms. This proposed toposequence departs from more traditional models (*e.g.* Ruhe and Walker, 1968), which hold that summit soils are more stable and, thus, better developed than backslope soils. A further tenet of this research is that soil-profile thickness is a reasonable proxy for degree of soil development.

The objectives of this study are: 1) to identify the controls of soil genesis and landscape stability within the Troodos Mountains of Cyprus; 2) to compare field measurements to expected soil thickness trends from traditional models of soil toposequences prevalent in current scientific literature; and 3) to develop a predictive model for hill slope pedogenesis based on measured soil properties within the field area.

Site Description

Field Area

The boundaries of three adjacent watersheds - the Atsas, Elia, and Kargotis - along the northern flank of the Troodos Mountains delineate the study area of this thesis (Figure 1.3). The Atsas, Elia, and Kargotis watersheds drain north into Morphou Bay and, above the plains of the Mesaoria, are representative of general watershed characteristics throughout the Troodos. Their drainages also traverse Cyprus Department of Forestry lands that are an integral component of ongoing government forest restoration and fire-suppression efforts. The following descriptions of the geology, geomorphology, and land use characteristics of these watersheds are essential to the contextual analysis of pedogenetic processes in the Troodos Massif.

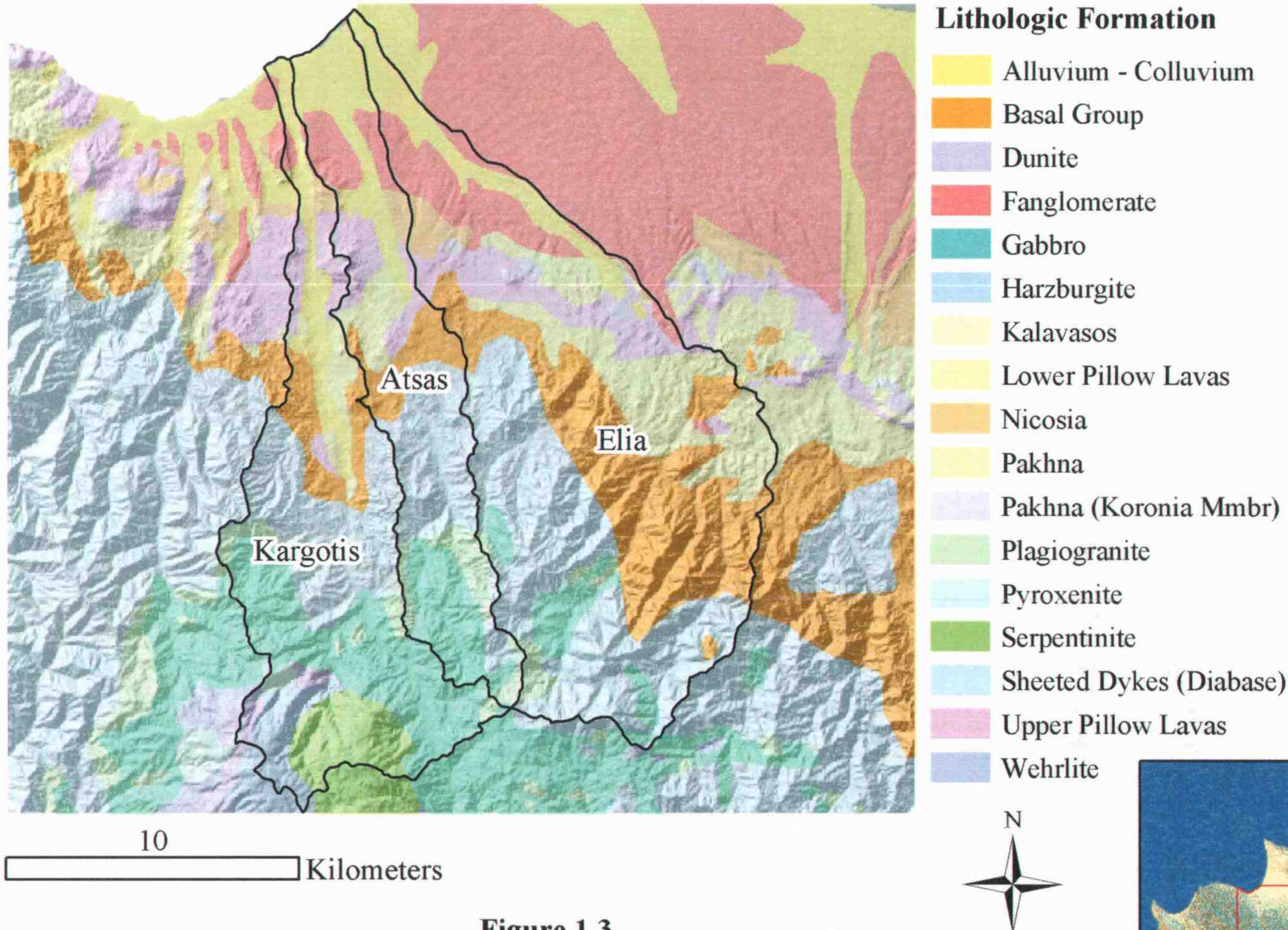

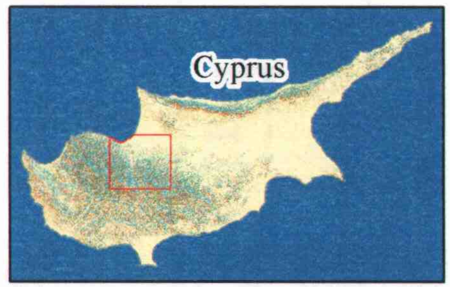

Figure 1.3.
Hillshade geological map of the Kargotis, Atsas, and Elia watersheds of the Troodos Mountains, Cyprus.

Geology and Geomorphology

The v-shaped valleys of the Troodos incise highly fractured intrusive and extrusive volcanic rocks of the Troodos Ophiolite. Intracontinental rifting initiated uplift of the ophiolite during the Late Triassic (Gass, 1975; Robertson & Woodcock, 1979). With time, channel incision and erosion produced a concentric outcrop pattern in which the oldest lithologic units of the ophiolite sequence are the most central (Gass, 1975). Within the study area, bedrock consists chiefly of the Upper Cretaceous Basal Group and Sheeted Dike (Diabase) units (Geological Survey Department, 1995). These units incorporate successions of basalt pillow lavas subsequently intruded by diabase dikes, but the prevalence and homogeneity of dikes increases down-section until the bedrock consists wholly of parallel dike bodies (Gass, 1975). In this way, laterally alternating dike swarms and pillow lavas characterize substrata in most of the field area.

Owing to the uplift and concurrent fluvial incision of the Troodos Ophiolite, the most characteristic landforms atop the igneous substrata consist of either long, linear bedrock spurs with narrow ridges and steep, contiguous side slopes, or conical bedrock landforms with triangular facets. Sheet, rill, and gully incision marks all landforms to varying degrees, and hill slopes may contain vegetated or bare, shallow colluvial hollows, or deep, rocky ephemeral gullies. Elevation across the complete Atsas, Elia, and Kargotis watersheds area ranges from mean sea level in the north to approximately 1900 meters above mean sea level in the south. The elevations of soil-profile sites analyzed in this research cover a significantly narrower range of 450 meters to 680 meters above mean sea level. Hill slope gradients generally range from zero to ten degrees atop ridgelines and along valley bottoms, and from 20 to 45 degrees along backslopes.

Thin layers of gravelly colluvium mantle the landscape between ridge shoulders and narrow deposits of alluvium along gully bottoms. Soils developed within the colluvium either exhibit only weakly developed horizons or lack distinct horizons entirely. Mineralogical and textural differences between individual igneous bodies cause lateral variations in rock color, texture, and hydrology that are apparent within even small outcrops and roadcuts. These lithologic and regolith variations impart similar, though more muted, color and textural variations to hill slope soils. Five- to ten-centimeter thick surface organic layers are common, typically comprised of mosses, lichens, mycorrhizal fungi, and decomposing plant matter. The humus content of these soils is low, ranging from 4.6% in pine forests in the upper Troodos Mountains to 1.5 percent or less in cultivated lowlands (McDonald, 1949, *as cited by* Christodoulou, 1959).

The gravelly nature of these silt loam and silty clay loam soils also indicates that mass creep entrains coarse fragments from the upper layers of the fractured bedrock. Many trees exhibit markedly curved trunks, further suggesting gradual but persistent soil creep. Ridge summits are typically rocky, their fine sediments likely removed by raindrop impact, runoff, wind, and mass creep. However, the isolated boulders and exposed bedrock blocks common on ridge summits often bear weathering rinds and lichen assemblages (*Rinocarpon sp.*) indicative of long periods of in-situ weathering and, thus, inferred stability. Hilltops may constitute stable surfaces for coarse boulders and bedrock blocks, while finer materials achieve stability only on footslope or toeslope terrain.

Besides igneous bedrock, some landforms developed on younger sedimentary substrata. Long, graded Pleistocene alluvial terraces composed of red channel gravels and silts demarcate ancient streams throughout the Troodos Massif and are readily discernable from surrounding igneous landforms. The alluvial landforms typically have a sub-uniform slope of five to fifteen degrees while the faceted bedrock spurs and rounded hill slopes have variable slopes that are generally steeper than 20 degrees. Where roadcuts have bisected multiple landforms, the red and grey silts and rounded cobbles of channel-form Quaternary sediments contrast strongly with the dominantly reddish yellow-brown, fractured bodies of the older, weathered volcanic bedrock. These alluvial landforms exhibit deeper soil profiles and are far more stable than surrounding colluvial slopes.

Historical Perspectives on Land Use and Soil Genesis in Cyprus

Because the soils of Cyprus have been tilled for the last 5,000 years, the long-term imprint of human land use on soils of the Troodos, especially the effects on soil erosion and soil cover, must be considered (Christodoulou, 1959). A commonly held theory suggests that Cyprus was once widely covered by forests, maquis, or scrub woodland but declined into progressively sparser assemblages of grasses and dwarf woody colonizers under persistent, heavy grazing and other poor land use practices (Thirgood, 1987). Compounding this history, it is thought, is the precipitation pattern. Precipitation occurs as intense, high energy events that typically take place only during winter months, so the parched soil profiles of Cyprus are able to maintain vegetative cover only with difficulty (Christodoulou, 1959). Roughly fifteen percent of the total area of Cyprus exhibits steep slopes (Secretariat of the UN CCD, 2002), and the effects of sheet erosion have been described as widespread and severe, yielding very thin soils on even gently sloping land (Christodoulou, 1959). Much of the landscape is subject to high erosion potential, and large areas are thought to have been completely denuded of once-thicker topsoil (Keefe *et al.*, 1971). This belief has led to the further, permanent modification of the Troodos landscape by humans, with the emplacement of extensive terraces and gully check dams.

As part of general restoration efforts, Department of Forestry practices over the last two centuries have focused on thorough terracing and reforestation of the Troodos, and the abolition of herds of goats and sheep from forest lands. Terraces emplaced within the study area vary in extent and morphology, perhaps dependent on contemporary land management policy. Terrace morphologies include large bulldozed earth and gravel; long, narrow, hand-dug, linear terrace cuts with path-like morphologies that contour hillsides; small scalloped excavations into bedrock; and pre-nineteenth century stacked stone terraces near abandoned or ruined settlements. Of these diverse morphologies, only the ancient check dams and terrace walls do not involve significant excavation and thus succeed in promoting rather than weakening local slope stability. Stone check dams of varying age are found in small, second- or third-order gullies near settlements, churches, or other sites. These structures consist of cobble- to boulder-sized stones stacked perpendicular to flow direction, and typically have reservoirs of less than one or two cubic meters. Of these structures, the younger generation were built near forestry trails to control soil erosion, while the purpose of older structures may have been to support individual family olive trees, or small herb gardens.

The geomorphology of the northern flank of the Troodos Mountains exemplifies the close ties between human activity, natural resources, landscape, and slope stability. Thorough understanding of soil genesis in the context of geomorphic process and historic land use is needed to address modern issues in soil and forest resource management.

MATERIALS

Image Data

A network of seasonally-maintained, bulldozer-constructed gravel roads traverses the forested northern Troodos Mountains. Because these roads comprise part of ongoing government fire-suppression efforts, their track foregoes more conventional, contoured routes to allow access by firefighters to even the most remote areas of the Troodos. Consequently, these Forestry Department roads cut through landforms of all slope and elevation ranges, and roadcuts afford excellent cross-sections of diverse geomorphic and pedologic features. In this way, these roadcuts represent a quasi-random sampling of soil-bedrock profiles in transects across multiple watersheds. Soil-bedrock relationships are easily discernable in these outcrops, and regular maintenance of the roadways insures fresh, stable exposures indicative of natural soil profile characteristics. Accurate descriptions of soil and bedrock properties are readily obtainable from the outcrops themselves or, alternatively, from high-resolution digital photographs of the outcrop faces.

During the summer of 2002 and the spring of 2004, several hundred digital photographs were taken of soil-bedrock profiles in stable roadcuts within the Elia, Kargotis, and Atsas watersheds (Figure 2.1, below). The images were taken at a constant distance of approximately 4.5-meters from profile faces and share a 50-millimeter focal length. The resolution of the images affords accurate, quantitative measurement of soil thickness (apparent depth to bedrock) and bedrock fracture characteristics across each outcrop. Sample images are displayed in Figure 2.2.

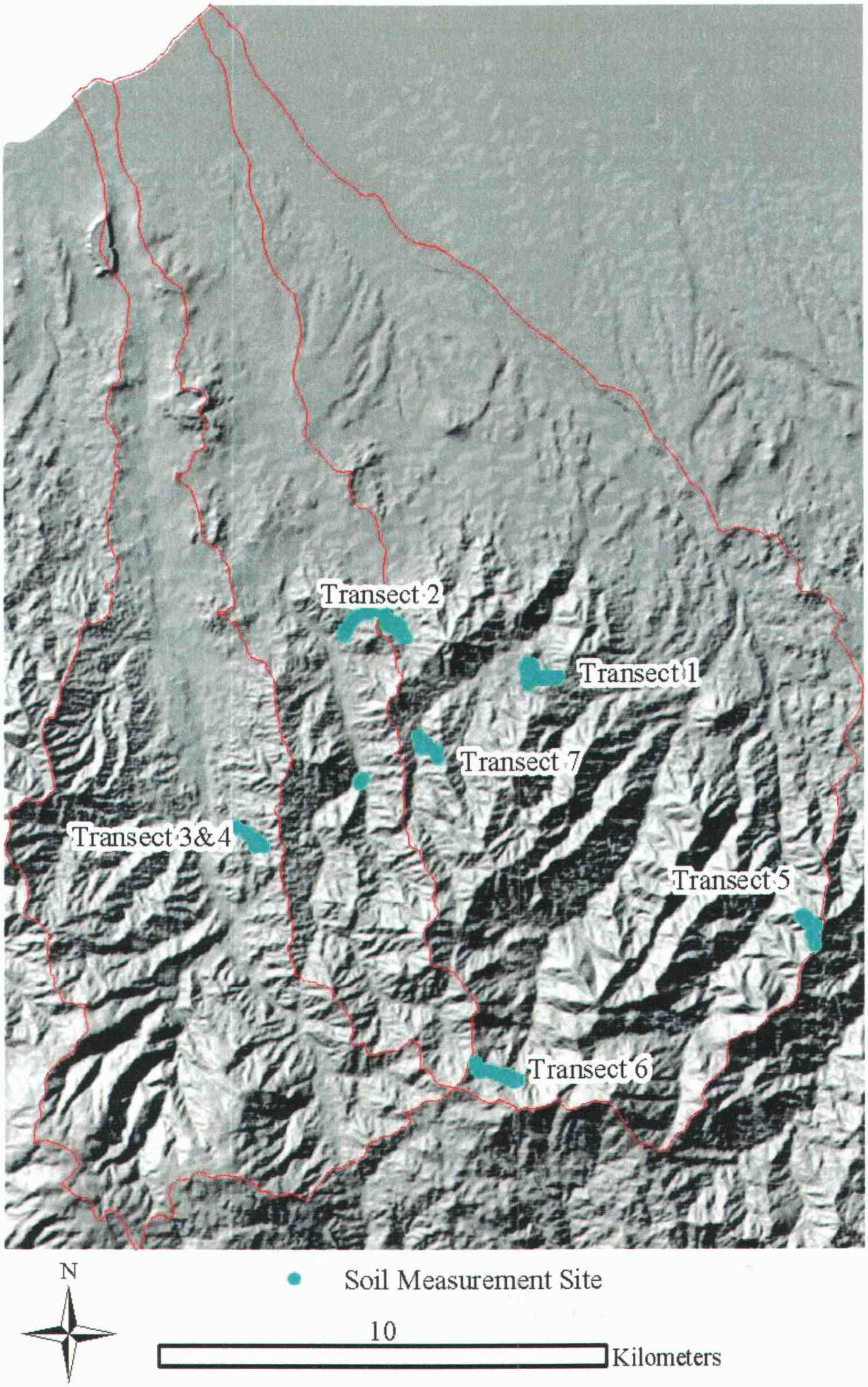

Figure 2.1. Locations of soil photograph and soil pit transects. Numbered transects are described in greater detail below.

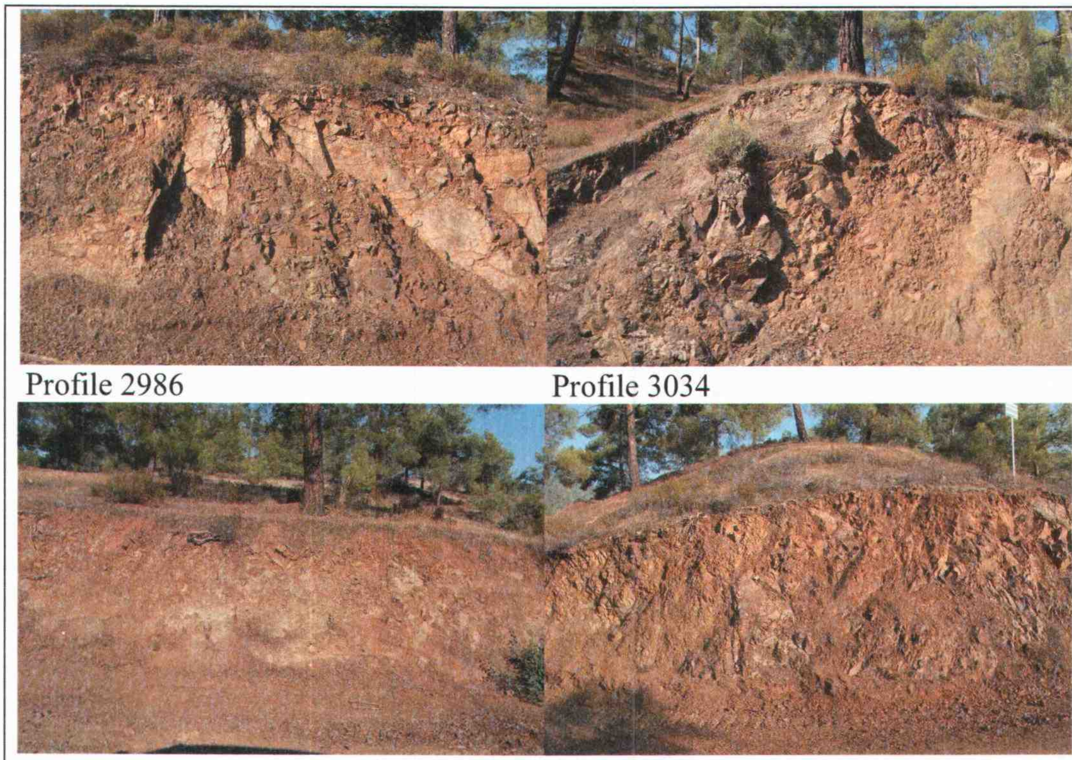

Profile 2986 Profile 3034

Profile 3046 Profile 3120

Figure 2.2. Examples of images used to measure area-normalized soil thickness and bedrock fracture density.

Concurrent global positioning system (GPS) data were collected at each outcrop using hand-held Garmin Gecko and Etrex GPS units.

Field Data

Field work conducted during the summer of 2003 and 2004 supplemented this research. Specifically, survey mapping performed in conjunction with the Troodos Archaeological and Environmental Survey Project (TAESP) provided a thorough, qualitative analysis of regional geology, geomorphology, land use, and vegetation. Survey work also facilitated the detailed description and classification of additional soil profiles from roadcut outcrops and hand-dug pits. Combined with ground-truthing of select roadcut profiles, this information verified the temporal integrity of the soil-bedrock profiles and the accuracy of photo-derived measurements. Thus, the combined dataset employed by this research comprises 367 mapped records.

GIS Data

This project also relied on GIS data obtained through the assistance and kind permission of both the government of Cyprus and TAESP. These data include a 25-meter digital elevation model (DEM); 1:50,000 scale stream data, and 1:250,000 scale lithologic, soil, hydrologic, and mean annual precipitation maps. The DEM was produced by the Cyprus Geological Survey between 2000-2003. Arc polyline shapefiles of elevation were hand-digitized from 1:50,000 topographic maps, and a triangular integrated network (TIN) was then developed from the contour polylines via ArcMap 3D Analyst. The TIN, in turn, was then gridded to a cell size of 25 meters, using TauDEM extension in ArcMap 8.2. TauDEM processing included the filling of voids in the DEM. Information provided by the DEM and the described digital maps was vital to the spatial and pedogenetic context and analysis of the soil data.

METHODS

The general organization schematic and progression of methods used is displayed in Table 2.1, below. Specific procedures for image analysis, fracture characterization, soil-landscape correlations, toposequence analysis, and predictive soil-stability mapping are outlined here.

Data Processing and Database Construction

Soil thickness (depth to bedrock) was measured by importing the digital photographs of soil-bedrock outcrops as .tif files into the software program ESRI ArcGIS Desktop 8.2. Based on the known focal length and lens-to-outcrop distance for all images, associated world files (.tfw) were created in the software program Geotiff. These companion files assigned a non-earth coordinate system with metric units to each image so that individual measurements of soil profile thickness, in meters, might be determined using geographic information system (GIS) software. The resolution of the digital photographs employed to measure soil thickness and bedrock fracture density in roadcuts and outcrops is sufficient to interpret pedogenetic and lithologic contacts. Possible variations in image scale cannot be discounted entirely, because the distance between camera lens and outcrop face may have varied on the order of centimeters or decimeters. Similarly, the slope of roadcut faces may have strayed slightly from the vertical. However, such variability translates to very low magnitude differences in soil thickness. Global positioning system (GPS) coordinates of image sites are accurate within two to ten meters, well

Table 2.1. General organization of data, showing target attributes and analyses.

Data Source	Attributes Provided	Data Values and Categories (units)
Digital Photographs	Soil, Fracture, and Spatial (GPS Coordinate) Information	Minimum, maximum, and mean soil thickness; soil and bedrock cross-sectional area; area-normalized fracture length; (meters)
Field Profiles	Soil Profile Descriptions; Landform Characteristics	Soil color, texture, structure, horizonation; root and bedrock fracture characteristics
Field Transects	Geomorphological and Archaeological Data; Land Resource Characterization	Hill slope stability, slope, aspect, substratum, morphology; Age of human land use; Historic land use industry, Toposequence Trends
Satellite Data	25-m DEM	Elevation (m), Slope (deg), Aspect, Hillshade Map, Relative Hill Slope Position, Ridgelines
Map Shapefiles	Geology, River, Watershed, Precipitation, and Hydrology	Parent lithology, stream order, stream proximity (m), watershed, MAP (mm)

below the scale of landforms within the study area, and permit detailed mapping and GIS analysis of the roadside soil-bedrock images. Universal transverse mercator (UTM) coordinates were used in this study.

Because soil thickness in the natural landscape can vary significantly across even small distances, and because the photographed profiles span up to five horizontal meters, the minimum and maximum soil profile thicknesses (depth to bedrock), the straight-line width of the weathering front from one side of the soil profile to the other, and the cross-sectional area of the soil profile were measured in each image. The mean soil depth at each site was defined as the ratio of the cross-sectional area of the soil profile divided by the straight-line distance between the lower left and lower right corners of the soil profile. This value mean soil depth per outcrop is more representative of field conditions than the average of the minimum and maximum soil depths per outcrop. Thus, the mean soil depth value was used in all analyses.

In most instances the soil-bedrock contact was abrupt, exhibiting strong textural contrast between fine-grained colluvial sediment and angular bedrock faces. In many images, coarse roots of *Pinus brutia* further demarcated and facilitated accurate delineation of the soil-bedrock contact. Roadcuts obscured by shadow, comprised of alluvial rather than bedrock substrata, graded at non-subvertical angles, unconstrained by spatial data, or otherwise deemed of poor quality were not analyzed.

General observations of soil texture, structure, depth, and color trends were noted on transects throughout the field area to characterize the general variation of soil properties. Field descriptions of representative soil profiles and their geomorphic setting facilitated generalized morphologic interpretations of the photographed soil sites. Data from the detailed field description of additional profiles from GPS-located sites permitted classification of regional soils to the family level following the USDA soil classification system (Soil Survey Staff, 2003).

In total, this analysis includes measurements from 302 photographs and sixty-five excavated field pits. The mean soil depth for each profile was then entered into a tabular database containing also the site identification and GPS coordinates for each profile. The 367 records were then converted to a point shapefile for processing in subsequent GIS analyses.

Testing for Correlation between Soil Depth and Pedogenetic Factors

Correlation between soil depth and bedrock fracture characteristics

The sheeted diabase dike, pillow basalt, and plagiogranite units of the Troodos Massif are extensively fractured. One postulate of pedogenesis maintains that, other factors held constant, soils atop fractured bedrock may experience greater development because the fracture networks afford increased surface area for chemical and physical weathering. If the fracture characteristics of substrata in the Troodos do affect pedogenesis, there should exist an identifiable correlation between soil thickness and the spatial density of bedrock fractures. Assuming geomorphologic systems in the Troodos operate near a state of natural equilibrium, identified relationships between pedogenesis and bedrock fracture density should match expected trends for either supply-limited or transport-limited conditions. A two-part analysis explored distinct means of quantifying fracture density and connectivity through image analysis and tested for possible correlations between soil depth and bedrock fracture density. One method was automated while the other was performed manually.

The first procedure employed Erdas Imagine 8.5 to cluster pixel signatures into two classes, essentially thresholding the images, and then exported pixel data to a spreadsheet program for additional analysis. Due to the nature of the soil mineralogy and bedrock lithology within the study area, the images afforded strong contrast between fracture pixels and pixels of soil and rock. Images exhibiting poor contrast or areas of shadow, roots, or vegetation were excluded because the similarity in spectral signature of such pixels to fracture pixels would otherwise inflate the measured fracture density. First, 13 vertical profiles extending from the soil surface down to bedrock were sub-sampled from the six images. Each profile was filtered using Erdas Imagine's 3x3 matrix cross edge detect spatial convolution. Next, an unsupervised classification was applied to both raw and filtered profile images. To ensure uniformity, the clustering options were held constant – each classification produced 10 classes through a maximum of 25 iterations, a convergence threshold of 0.99 and an automatic standard deviation function. Class interpretation was constant between profiles. Specific profile information for each classification is presented in Appendix A. Each signature group was interpreted as either "fracture" or "non-fracture" and assigned a class value of 1 or 0, respectively. Once the original ten class values had been recoded, and the new, processed image saved, the pixel table was exported into a Microsoft Excel spreadsheet. The depth to bedrock was previously measured in each image as described above. Because each fracture pixel had a value of 1, the total number of fracture pixels divided by the total number of pixels below the bedrock-soil contact, per profile, yielded a percent area of fracture to rock. This value was then compared to the soil thickness to test for correlation.

The second, simpler but more time-intensive test involved manual digitization of bedrock fractures in 44 images using ArcGIS 8.2. All fractures visible at a scale of 1:15 or coarser and longer than approximately three centimeters were digitized as polyline segments. Polygon traces of outcrop faces were also constructed. All produced shapefiles were then converted to coverages, and the total fracture length, in meters, per outcrop was calculated. The area of each outcrop polygon, in square meters, was also measured and used to calculate the total area-normalized fracture length per profile. The quantitative relationships of fracture density to soil depth in all images were then compared for possible trends.

Correlation between soil depth and the traditional soil-forming factors

To better understand the active controls of soil genesis in the Troodos, GIS and statistical methods were developed to determine the relative importance of each of the traditional soil-forming factors of time, organisms, parent material, climate, and topography. This simple analysis focused on each pedogenetic factor individually and did not address all contributors. Distinct methods were developed to address the more complex dynamics between multiple topographic and geomorphic factors, and will be presented in a separate section below.

In the simple GIS and statistical assessment of traditional pedogenetic factors described here, the role of time is not directly addressed because no age data currently exist for the studied soil profiles. Secondly, qualitative field observations indicate that vegetation is relatively uniform across the region and comprised most characteristically of *Cistus sp.* shrubs and the Calabrian Pine, *Pinus brutia*. Macrofauna assemblages are also relatively uniform across the region and include several reptile and small mammal species. Goats are no longer permitted within the Troodos forest (Thirgood, 1987). Because of the relative homogeneity of floral and faunal characteristics across the study area, the effect of biologic factors on soil-thickness variation is assumed negligible.

With the exception of plagiogranite substrata in upper elevations, the lithology of the igneous parent material does not vary greatly across the study area from sheeted diabase dike complexes and the basal group basalts they intrude. Moreover, soil development presumably varies only imperceptibly across geologic contacts because the boundaries between lithologic units are gradual (Morris, 1996). Nevertheless, the substratum lithology was identified for each data point using a 1:250,000 geologic map of Cyprus (Geological Survey Department, 1995) in polygon shapefile format. As in other portions of this research, soils derived from wholly alluvial sediments and landforms were excluded because such soils differ geomorphologically and genetically from the colluvial hill slope soils mantling the igneous substrata. Soil thickness between lithologic classes was compared via a fixed-effect one-way analysis of variance.

Climate variability across the study area also appears relatively slight, however, topography does impart local changes in total mean annual precipitation (MAP) and precipitation intensity. Soils were analyzed for climatic influences through simple linear regression of soil depth and MAP. Precipitation values were estimated for each site using interpolated values from a precipitation map of Cyprus in grid format. The precipitation map itself was derived from 308 measurement stations scattered across the island.

The effect of topography on pedogenesis was also investigated. The different variables addressed included elevation, slope gradient, aspect and, on a broader scale, watershed. All topographic data were derived from the 25-meter DEM utilizing ArcMap's 3D Analyst and the complementary software package TauDEM (Tarboton, 2002). Simple linear regressions were used to test for soil thickness correlation with slope, aspect, and elevation. Differences in mean soil depth between watershed classes were analyzed using one-way ANOVA.

Attribute values for lithology, MAP, elevation, slope gradient, aspect, and watershed for each soil site were added to the database of point records. Attribute values were assigned in ArcGIS by overlaying the soil-bedrock point shapefile with the appropriate map layer, converting the point features to 3-D in 3D Analyst, and then running the Easy Calculate command 'get point z-value' in Raster Calculator. Through this process, attributes (*e.g.* substratum lithology, elevation value, *etc.*), for the coordinates of each site were recorded in the GIS directly from corresponding locations on each map layer (*e.g.* geologic map shapefile, DEM raster, *etc.*). Complete point attribute (.dbf) tables were then exported to S-plus 6.0 and Microsoft Exel for statistical analysis. Statistical analyses included simple linear regression, ANOVA, and two-sample t-tests. In each case, the soil forming factors were the grouping variable and soil thickness the dependent, or response, variable.

Topography Revisited: Hill Slope Position

Simple statistical analyses of individual topographic elements may illustrate general trends, but more involved, multivariate approaches are required to explain in detail the topographic and geomorphologic controls of soil genesis. Soils vary depending upon slope gradient and morphology, erosion type, hydrology, and other factors (Birkeland, 1999). Thus, topography-dependent soil properties may be predicted across other hill slope soil traverses, or toposequences, under similar environmental conditions (Birkeland, 1999). Classical models (*e.g.*, Ruhe & Walker, 1968; Walker & Ruhe, 1968) delineate hill slope position at changes in slope gradient or curvature along a two-dimensional profile. Methods of automated three-dimensional toposequence analysis are also possible (*e.g.*, Coops *et al.*, 1998). Hill slope positions of all data points were identified to develop a working model for characteristic toposequences in the northern Troodos Mountains. Because implementation of a three-dimensional model is quite time and labor intensive, a more rapid, though less accurate, two-dimensional means of analyzing the variability of soil-profile thickness with topography was employed. The first, automated, method computed the position of all soil profiles based simply on their distance from topographic extremes, *i.e.* streams and ridgelines. The second method identified 32 apparent toposequences within seven larger-scale transects, and classified each component profile based on visual interpretations of its slope and curvature characteristics. Specific procedures for these two methods are outlined here.

Stream and ridgeline-derived classification of hill slope position

In this procedure, a three-class system was established by buffering all areas within defined distances of ridgelines and streams in ArcGIS to establish crude interpretations of summit and footslope classes, respectively. This method was thought to suit well the long, narrow, linear nature of ridges and hill slopes in the Troodos Mountains. In this study, all soil sites situated within 15 meters of a stream or gully were classified as footslope soils, while sites falling within a 15-meter buffer of the ridgelines were classified as summit soils. Soil sites between the buffers were simply classified as backslope soils. Several wider and narrower buffer widths were explored, however, the 15-meter buffer appeared to best-fit landform morphology within the study area.

Ridgelines were mapped by first inverting the DEM in ArcMap, employing TauDEM to create flow paths, and then re-inverting the flow path grid to reflect ridge order. The Geoprocessing Wizard tool in ArcMap was used to identify, select, and export records for the profiles (points) from each class. The data were then imported into S-plus for statistical analysis. Statistical methods employed include simple linear regression and fixed ANOVA, using hill slope position as the grouping variable and soil depth as the dependent variable.

One disadvantage of this method is that its simplified class definitions limit interpretation of toposequence trends to the two extremes of hill slope position: summit and footslope. To understand the processes and variability in effect within backslope and shoulder positions, and to explore uniformity of toposequence characteristics between hill slopes, a more detailed toposequence analysis is required. Automated GIS hill slope analyses classify DEM pixels into more detailed classes using a scale-dependent topographic position index algorithm. The algorithm developed by Weiss (2001) is a neighborhood, statistical method which classifies the elevation value and slope position of individual raster pixels. To better compare computer-automated and traditional methods, however, the five-position classification scheme of Ruhe and Walker (1968) was explored in this study.

Slope-derived classification of hill slope position

The second toposequence analysis was employed to better explore the role of slope processes on pedogenesis and soil thickness variability within the Troodos Mountains. This method was threefold, and involved: 1) a general identification of hill slope position for each site, similar to that discussed above; 2) identification of apparent catenas and their component profile characteristics; and 3) comparison of soil depth variability between individual catenas of similar geomorphology.

Because the majority of data points in this study lie along forestry roads or walked sampling lines, it proved feasible to construct seven distinct transects of profile data points. The transects ranged in length from 300 meters to 2 kilometers. Generalized topographic profiles were constructed in the GIS by digitizing each transect as a polyline with nodes established at each data point. The analytical tool ET Geowizards 8.7 calculated the distance along transect and the elevation of each node. In this way the generalized surface topographic profile for each transect could be drafted in a spreadsheet program. Classical hill slope positions were then assigned to all points along each cross-section through visual interpretation of the transect's surface topography. Hill slope class divisions were based on natural slope breaks and follow the definitions of Ruhe and Walker (1968) for summit, shoulder, backslope, footslope, and toeslope. As in the method described above, simple group-wise comparisons were used to explore statistical distinctions between hill slope classes.

In addition, the morphology of individual hillsides, as delineated in the generalized topographic profiles, was classified as rectilinear, curvilinear-convex, or curvilinear-concave, after Walker and Ruhe (1968). Soil thickness trends from summit to toeslope were compared for toposequences of similar morphology, to test the hypothesis that correlation between hill slope morphology and soil depth is more significant than that between slope gradient and soil depth (King *et al.*, 1983). Soil thickness values from summit to toeslope position were plotted for 25 individual hillsides, each containing at least three profiles, and the overall results were compared.

Predictive Soil Models

Predictive mapping through external slope stability models

One of the key objectives of this research was to compare data from the Troodos to external models of soil properties and slope stability. The benefit of such a comparison lies in the assessment of how well accepted landscape models characterize diverse geomorphic environments. There currently exist many models which strive to accurately describe and quantify soil development, soil erosion, landscape stability, and related pedogenetic and geomorphic processes across landforms. These process-based models have been developed from and applied to studies in varied geologic and climatic regimes. The Troodos present an ideal opportunity to test the applicability of such models to a landscape where slope processes and pedogenesis have not yet been fully addressed in current scientific literature.

SHALSTAB, a software program developed by William Dietrich at the University of California at Berkeley, maps potential shallow slope instability through GIS analysis of a digital elevation grid (Dietrich & Montgomery, 1998). Such stability maps may facilitate soil thickness prediction and modelling. For this reason, SHALSTAB was used to produce a landscape stability map of the northern Troodos, in keeping with the assumption that higher instability implies greater erosion and, consequently, thinner soils.

The "q/T" file output during SHALSTAB analysis represents a hydrologic-slope stability model, in which more negative values indicate decreased stability (Dietrich and Montgomery, 1998). If the SHALSTAB prediction adequately models active hill slope processes in the Troodos Mountains, there should exist a positive statistical correlation between mean soil thickness, slope, and the modelled stability values. To apply the model, the 25-meter resolution DEM was masked, or subsampled, to the three watersheds containing all described and photographed soil outcrops from this research. The smaller DEM was then processed in ArcView 3.3 following the methods put forth by Dietrich and Montgomery (1998).

The model provides two means of calculating the hydrologic ratio. A constant cohesion parameter is introduced in the first, while the alternative omits cohesion entirely (Dietrich and Montgomery, 1998). The model used in this analysis omitted cohesion, and specified parameters included an internal friction angle of 45 degrees and a bulk density of 1700 kg m^{-3}. SHALSTAB assumes uniform soil depth - for this analysis, soil depth was defined as 0.5 m. Once the q/T grid had been calculated, stability values were obtained for the soil sites using EZ Calculate "get_point_Z" command in ArcGIS 8.2. The mean soil depth values were then compared graphically and through simple linear regression to predicted stability to test for correlation.

Predictive mapping through analysis of northern Troodos data

Once the processes influencing pedogenesis and soil variability across the Troodos Mountains have been characterized, the logical progression is the development of a predictive model for hill slope soil development based on measured soil properties. Field observations suggest a general model wherein soils are thinnest on ridges and thickest along footslopes, however, a more specific model is needed. Towards that aim, results from the preceding analyses were compiled to attempt a working model of soil-depth variability across the greater field area. Multiple linear regression analysis of soil depth, elevation, aspect and slope gradient have been shown to facilitate predictive mapping of soil properties across landscapes (Tsai *et al.*, 2001). Similar methods are attempted here.

RESULTS AND ANALYSIS

General Soil-Profile Data

Soil-profile analyses performed in the field and laboratory yield a substantial matrix of results. General soil data are presented below, including soil thickness, regolith fracturing, and general profile descriptions. Statistical analyses of these data provide quantitative descriptions of correlation between soil thickness and pedogenetic factors.

Soil-thickness data

The core data of this research are the soil-thickness measurements obtained from digital photograph analysis and field soil-profile measurements. A data table containing all image analysis-derived and GIS analysis-derived values is presented in Appendix B. Summary statistics of the 367 site measurements are displayed in Table 3.1, and reveal an overall mean soil thickness of 17 centimeters. A histogram

Table 3.1 Summary of soil-thickness data.

Minimum Thickness (m)	0.00	Std Deviation (s)	0.155
Maximum Thickness (m)	0.96	Std Error of the mean	0.008
Mean Soil Thickness (m)	0.17	95% LCL mean	0.153
Sample Size (n)	367	95% UCL mean	0.185
Variance (s^2)	0.024		

illustrating the general distribution of soil-thickness values is displayed in Figure 3.1. The data exhibit a high skewness value of 2.04 due to the weak soil development that characterizes the region: 269 of the 367 samples, or 73 percent, have thicknesses of 20 centimeters or less.

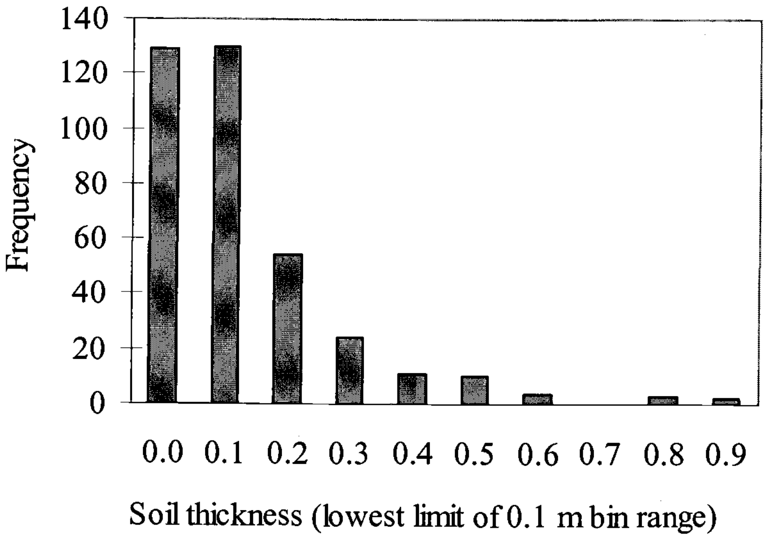

Figure 3.1. Histogram of all soil thickness measurements.

Morphology and classification of studied soils

Loamy, mixed, superactive, nonacid, mesic Lithic Xerorthents (less than 50 cm mean soil depth) comprise 348 of the measured soil sites, while the remaining 19 profiles classify as Loamy, mixed, superactive, nonacid, mesic Typic Xerorthents because their depth to a lithic contact is greater than 50 centimeters (Soil Survey Staff, 2003). Lateral variations in soil depth are common, with bedrock outcrops or extensive surfaces stripped of fine sediment. In general, the study soils are characterized by thin or absent O horizons and extremely weakly developed A horizons in thin (<< 1m) colluvium atop weathered bedrock. The A horizon may exhibit weak fine granular structure, but becomes structureless with depth (below 3-10 cm). No B horizons have been noted. Soil textures typically range from silt loam to silty clay loam, and may contain up to 30 percent fine or medium angular coarse fragments. Soil color hue ranges from 2.5YR to 10YR, with moist values of four or higher. Soil color varies according to the predominant lithologic characteristics of the igneous substratum. C horizons lack pedogenetic structure and typically contain higher percentages of rock fragments than the A horizons. The contact between the C horizon and weathered bedrock may be gradual or abrupt. The R layer consists of fractured and oxidized bedrock, and tree roots often delineate fracture paths as deep as 2 meters below the surface of the bedrock. Sample profile descriptions from this study are provided in Appendix C.

Testing for Correlation between Soil Depth and Pedogenetic Factors

Correlation between soil depth and bedrock fracture characteristics

The importance of bedrock-weathering characteristics to pedogenesis was addressed in the analysis of bedrock-fracture density, as discussed in the methods section above. The results of the thresholding method for testing correlation of soil thickness to bedrock-fracture density are displayed in Figure 3.2(a) and 3.2(b), below. Wide data scatter precludes statistically significant linear regression analysis, however, it remains clear that no precise correlation exists between fracture density and soil depth. The two accuracy assessments yielded overall classification accuracy of 86.71% and 85.71%, while the overall kappa statistics were 0.8340 and 0.7496, respectively. The user's accuracy for the three fracture classes was 100% in both assessments.

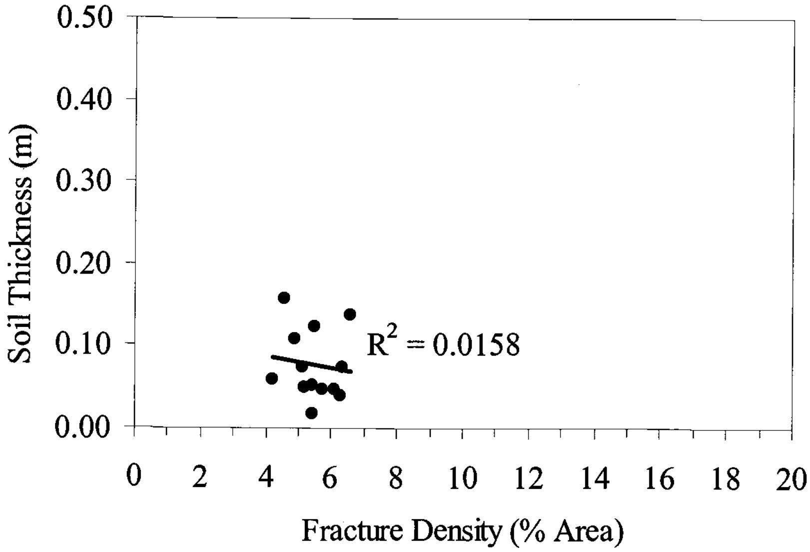

Figure 3.2(a). Correlation results from filtered classification.

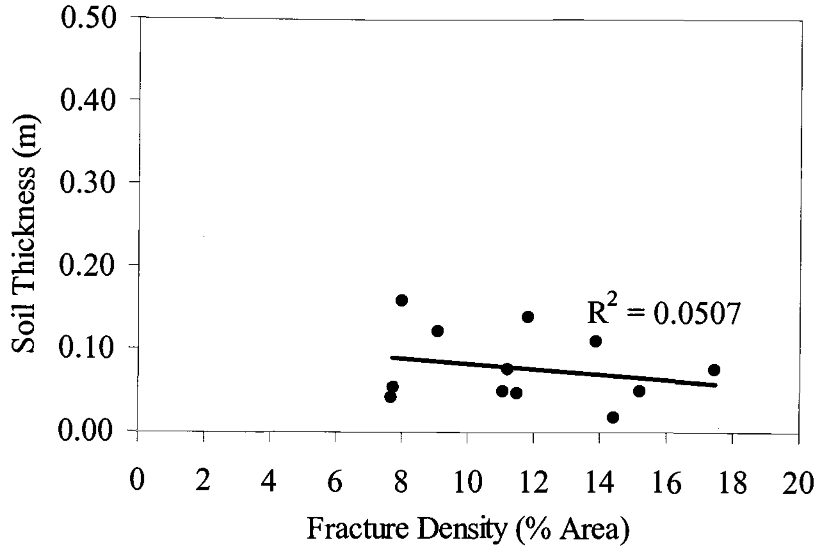

Figure 3.2(b). Correlation results from unfiltered classification.

Manual digitization of fractures yields trends that support the findings of the automated technique. A low correlation coefficient (R^2<<1.00) confirms the absence of statistically significant linear trends in the data (Figure 3.3). These findings reveal that the pedogenetic and geomorphologic processes operating in the

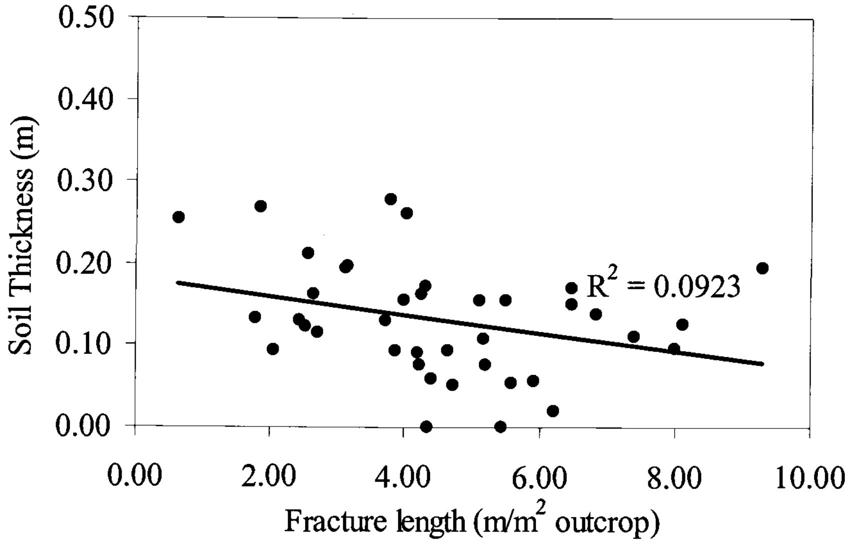

Figure 3.3. Results from manual fracture digitization.

Troodos Mountains are certainly not transport-limited. If the generally negative trends of the regression lines are considered, the data instead suggest that present-day conditions in the Troodos Mountains approach a supply-limited state. In such a scenario it would be impossible to expect historically thicker soils. Given the low magnitude of the correlation coefficients, however, any trends in the data that are consistent with supply-limited conditions are statistically inconclusive.

Correlation between soil depth and the traditional soil-forming factors

Soil-depth measurements also were compared to landscape-attribute values. Table 3.2 displays results from simple linear regression analyses of the elevation, slope, aspect, lithology, and precipitation effects on soil development. Low p-values (p-value < 0.05) suggest a high significance of correlation coefficients for all regressions except slope aspect, however, the individual linear regression models

Table 3.2. Summary of individual linear regression analyses for pedogenetic variables and soil thickness.

Variable	R^2	*p*-value
Lithology	0.083	<<0.001
Precipitation (MAP)	0.107	<<0.001
Elevation	0.081	<<0.001
Slope gradient	0.011	0.043
Aspect	0.004	0.219

for specific pedogenetic variables failed to account for enough of the variability to indicate any trend. That is, for all pedogenetic variables, R^2<<1.00. These findings are further illustrated by the wide scatter of data points in the plots of soil thickness versus precipitation, elevation, slope gradient, and aspect displayed in Figures 3.4(a), 3.4(b), 3.4(c), and 3.4(d).

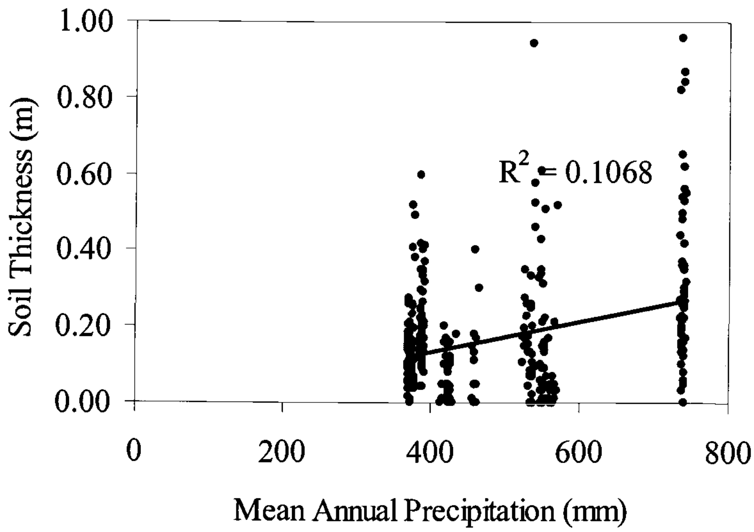

Figure 3.4(a). Regression test of correlation between M.A.P. and soil thickness.

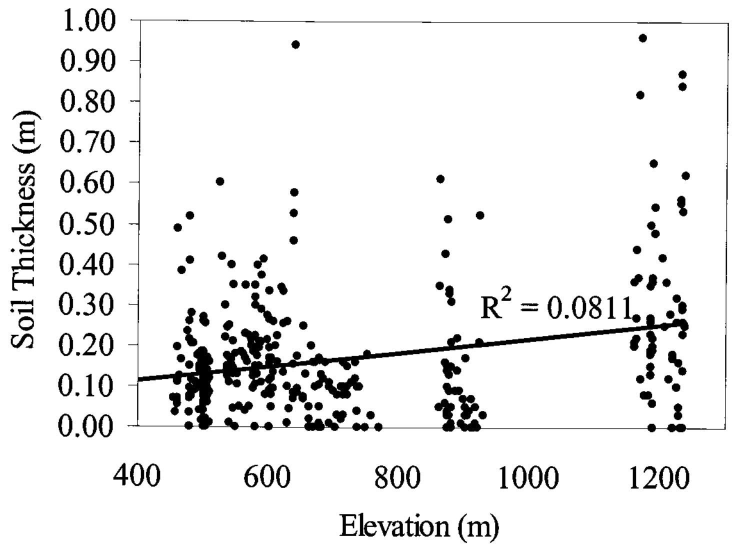

Figure 3.4(b) Regression test of correlation between elevation and soil thickness.

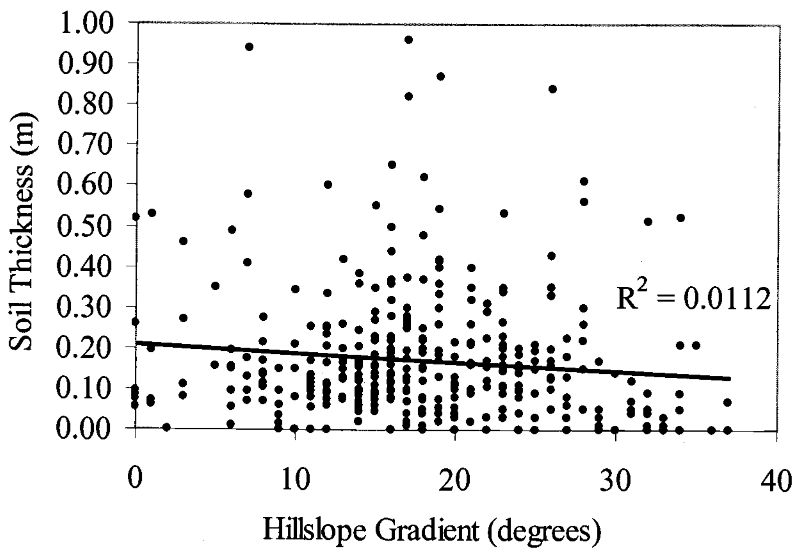

Figure 3.4(c) Regression test of correlation between slope gradient and soil thickness.

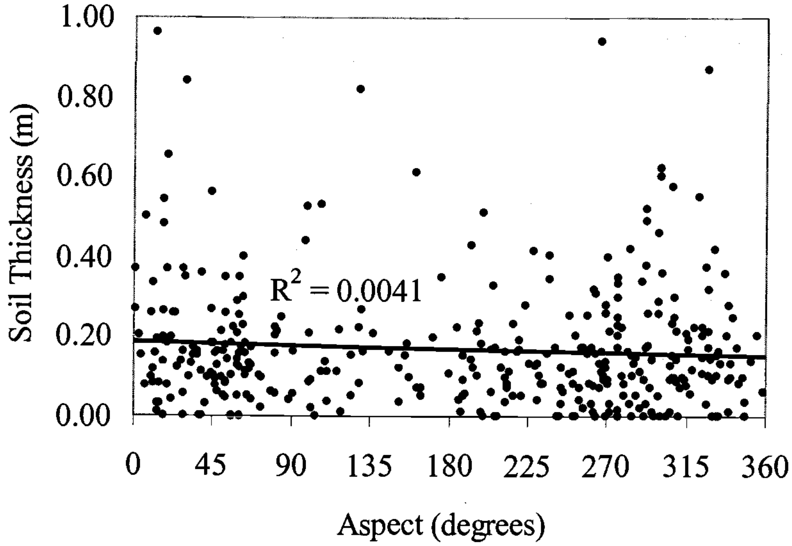

Figure 3.4(d) Regression test of correlation between aspect and soil thickness, showing high degree of soil variability.

Initial comparison of mean soil thickness between aspect classes reveals apparently thinner soils on south-facing slopes (Table 3.3), however, analysis of variance

Table 3.3. Relationship between aspect and soil thickness (m).

	E	*NE*	*N*	*NW*	*W*	*SW*	*S*	*SE*
Mean soil depth	0.20	0.17	0.16	0.18	0.16	0.13	0.15	0.20
n	50	76	25	16	25	39	68	68
Std. dev. (s)	0.186	0.130	0.147	0.184	0.158	0.107	0.145	0.180
Variance (s^2)	0.035	0.017	0.021	0.034	0.025	0.011	0.021	0.032

reveals that these apparent differences are not significant (p-value = 0.260). Soil thickness was also compared between different lithologies using fixed effects analysis of variance (Table 3.4). Differences in mean soil thickness for the three represented rock types in the study area were found to be highly significant, with a p-value well below 0.0001. Soil depths were thickest for plagiogranites and thinnest for rocks of the sheeted dike and diabase complex (Table 3.5). A similar

Table 3.4. One-way ANOVA of soil thickness between substratum lithologies.

	d.f.	**Sum of Sqrs**	**Mean Sqr**	***F*-statistic**	***p*-value**
Lithology	2	0.728	0.364	16.369	<<0.0001
Residuals	364	8.100	0.022		
Residual Std Err:	0.149				

Table 3.5. Variation of soil thickness with bedrock lithology.

	Basal Group	**Plagiogranite**	**Sheeted Dike Complex**
Mean soil depth (m)	0.18	0.31	0.15
n	58	30	279
Std Deviation (s)	0.088	0.216	0.151
Variance (s^2)	0.008	0.047	0.023
SE Mean	0.012	0.039	0.009

comparison was made of soil depths between watersheds. A box plot of soil thickness data grouped by watershed (Figure 3.5) reveals similar mean soil thickness values, but different variances, between classes. The large number of

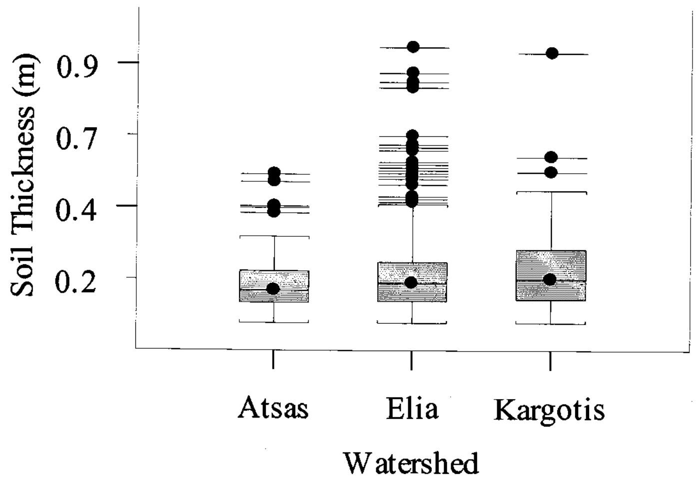

Figure 3.5. Box plot of soil thickness variability between watersheds. The Elia is the largest watershed, whereas the Atsas is the smallest.

outliers in the Elia watershed most likely reflects the greater number of samples (n=270) in the Elia as compared to the Atsas (n= 61) and Kargotis (n=36). Alternatively, the range of outliers may reflect watershed size - there exists greater probability of high outliers when the measurement area is large. One-way analysis of variance among soil sites grouped by watershed suggests that variation of soil thickness between watersheds is not statistically significant given the p-value of 0.247 (Table 3.6). The findings suggest that of the traditional pedogenetic variables

Table 3.6. One-way ANOVA of soil thickness between watersheds.

	d.f.	**Sum of Sqrs**	**Mean Sqr**	***F*-statistic**	***p*-value**
Watershed	2	0.068	0.034	1.405	0.247
Residuals	364	8.761	0.024		
Resid. Std. Err:	0.155				

addressed in this study, only lithology can be said to exhibit a statistically detectable effect on soil development. None of the pedogenetic variables exhibit a clear relationship, causal or otherwise, with soil thickness in the Troodos Mountains.

Because single-variable statistical analyses may not be able to detect partial contributions by individual variables in complex geomorphologic systems, however, a multivariate linear regression analysis was employed to attempt to model pedogenetic relationships in the study area. The best-fit model found was:

$$Y = \beta_1*(\text{slope factor}) + \beta_2*(\text{precipitation factor}).$$

The significance of the pedogenetic variables and the multiple coefficient of correlation value for the regression model are displayed in Table 3.7. *P*-values

Table 3.7. Results of multivariate linear regression model.

Variable	**Value**	**Std. Error**	***t*-value**	***p*-value**
(Intercept)	0.026	0.031	0.829	0.4079
slope gradient	-0.004	0.001	-3.769	0.0002
M.A.P.	0.000	0.000	7.395	0.0000
Multiple R-Squared:	0.1404			
F-statistic	29.71 (on 2 and 364 degrees of freedom, p-value <<0.0001)			

calculated within this model suggest a high significance of detected correlation (p-value < 0.0001). However, the low multivariate correlation coefficient, $R^2 = 0.1404$, suggests that this model does not accurately describe soil-thickness variance within the study area. The model presented here represents the most successful of several richer multivariate regression models tested, suggesting that pedogenesis cannot be described solely on the basis of traditional geomorphologic and pedogenetic landscape attributes.

Topography Revisited: Hill Slope Position

Buffer-derived classification of hill slope position

A preliminary review of the data suggests a trend of downslope-thickening soil profiles consistent with qualitative field observations and hill slope pedogenesis models. To better describe how soil thickness varies across landforms, the hill slope position of soil measurement sites were classified in the GIS based on their proximity to ridgelines and summits. Three buffer widths of 10 meters, 15 meters, and 25 meters were explored. Table 3.8 illustrates the effect of varying buffer width on soil toposequence analysis. It is thought that the 15-meter buffer best models the narrow morphology of ridges and landforms in the study area,

Table 3.8. Comparison of results for varied buffer width.

	Summit 10m	**Summit 15m**	**Summit 20m**
mean soil thickness (m)	0.14	0.13	0.15
n	30	49	74
Std Deviation (*s*)	0.096	0.078	0.110
Variance (s^2)	0.009	0.006	0.012

moreover, the sample variance was least for samples identified using this buffer width. Table 3.9 illustrates general trends for classes established via the automated, 15-meter buffer classification method. The mean depth to the soil-bedrock contact

Table 3.9. Summary of buffer-derived hill slope classes.

	Footslope	**Backslope**	**Summit**
mean soil thickness (m)	0.19	0.17	0.13
n	53	263	49
Std Deviation (*s*)	0.189	0.158	0.078
Variance (s^2)	0.036	0.025	0.006
SE Mean	0.026	0.010	0.011

Table 3.10. ANOVA of mean soil thickness between buffer-derived hill slope classes.

	d.f.	**Sum of Squares**	**Mean Sq**	***F*-Statistic**	***p*-value**
Hill Slope Class	3	0.151	0.503	2.106	0.0991
Residuals	363	8.677	0.024		
Residual Std Error	0.155				

was 13 centimeters along ridges, 17 centimeters along backslopes, and 19 centimeters along footslopes. This trend corroborates field observations of a downslope-thickening soil profile; however, a fixed-effects one-way analysis of variance of mean soil depth between hill slope classes under a null hypothesis of no difference (Table 3.10), suggests that the differences in mean thickness of soil between hill slope positions are not statistically significant (p-value >>0.05).

Analysis of data from the 10-meter and 25-meter buffers yields similar results. In this way, the data are weakly suggestive but statistically inconclusive. Therefore, more detailed means of classifying soil hill slope position using the full five classes proposed by Ruhe and Walker (1968) must be employed to accurately model pedogenesis within the Troodos Mountains.

Slope-derived classification of hill slope position

Topographic cross-sections of the seven transects - individual landforms of which were investigated in detail - are presented in Figure 3.6, below. The toposequences investigated in all but Transect 7 are apparent toposequences only, because they are constructed from profiles from a "random walk" along forestry roads. This method is most appropriate where hill slopes less than approximately one hundred meters in length are being investigated. Longer subdivisions of transects are more likely to include discontinuous landforms. The apparent toposequences described here are thought representative of hill slopes throughout the study area. Transect 7 consists entirely of field soil-bedrock profiles, dug at approximately 20-meter intervals along the axis of a single rectilinear landform. In total, 32 toposequences comprising 149 data points were identified. Each toposequence was classified as rectilinear, curvilinear-convex, or curvi-linear concave according to slope-profile characteristics. Slope profiles of individual

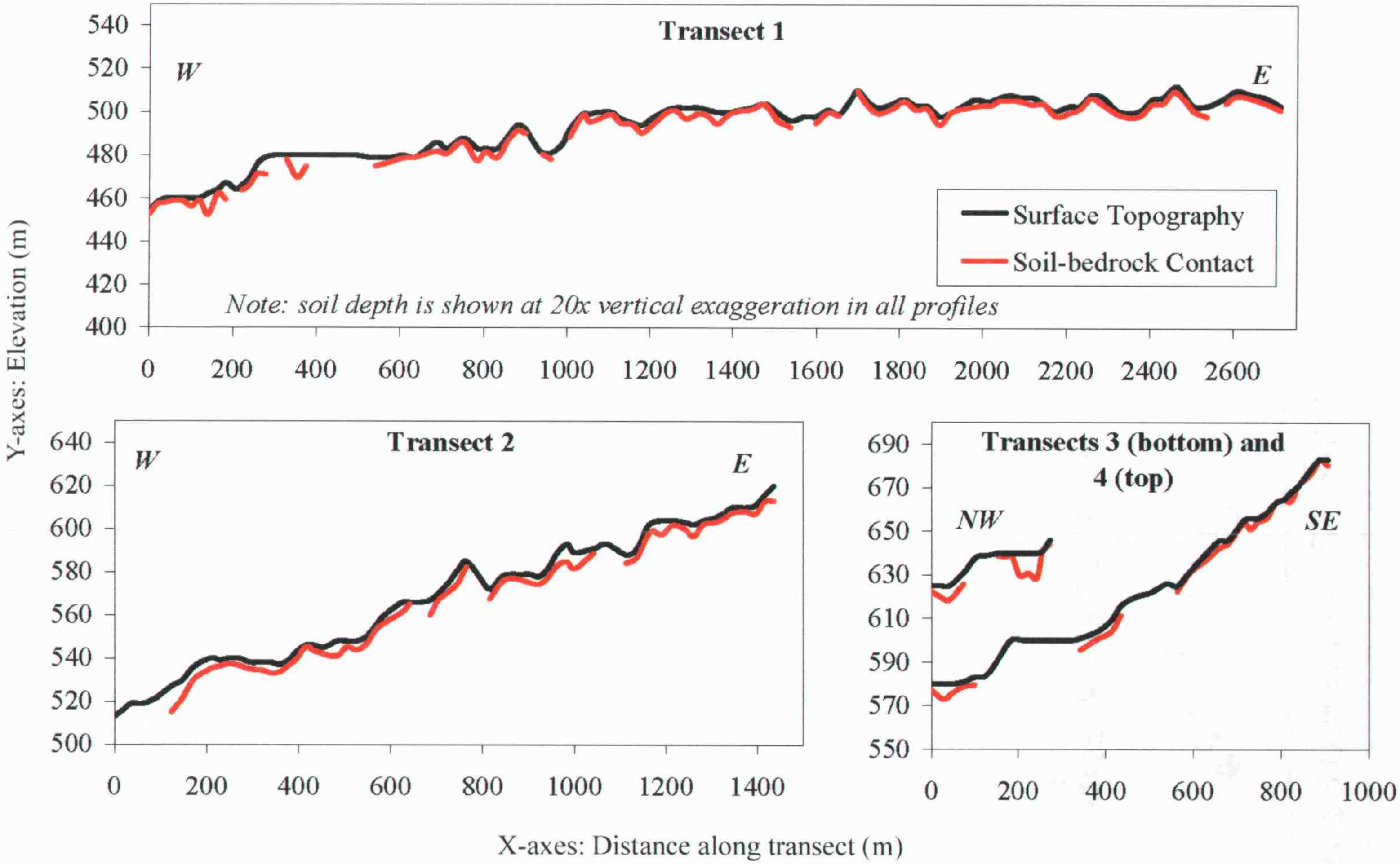

Figure 3.6. Generalized topographic and solum profiles.

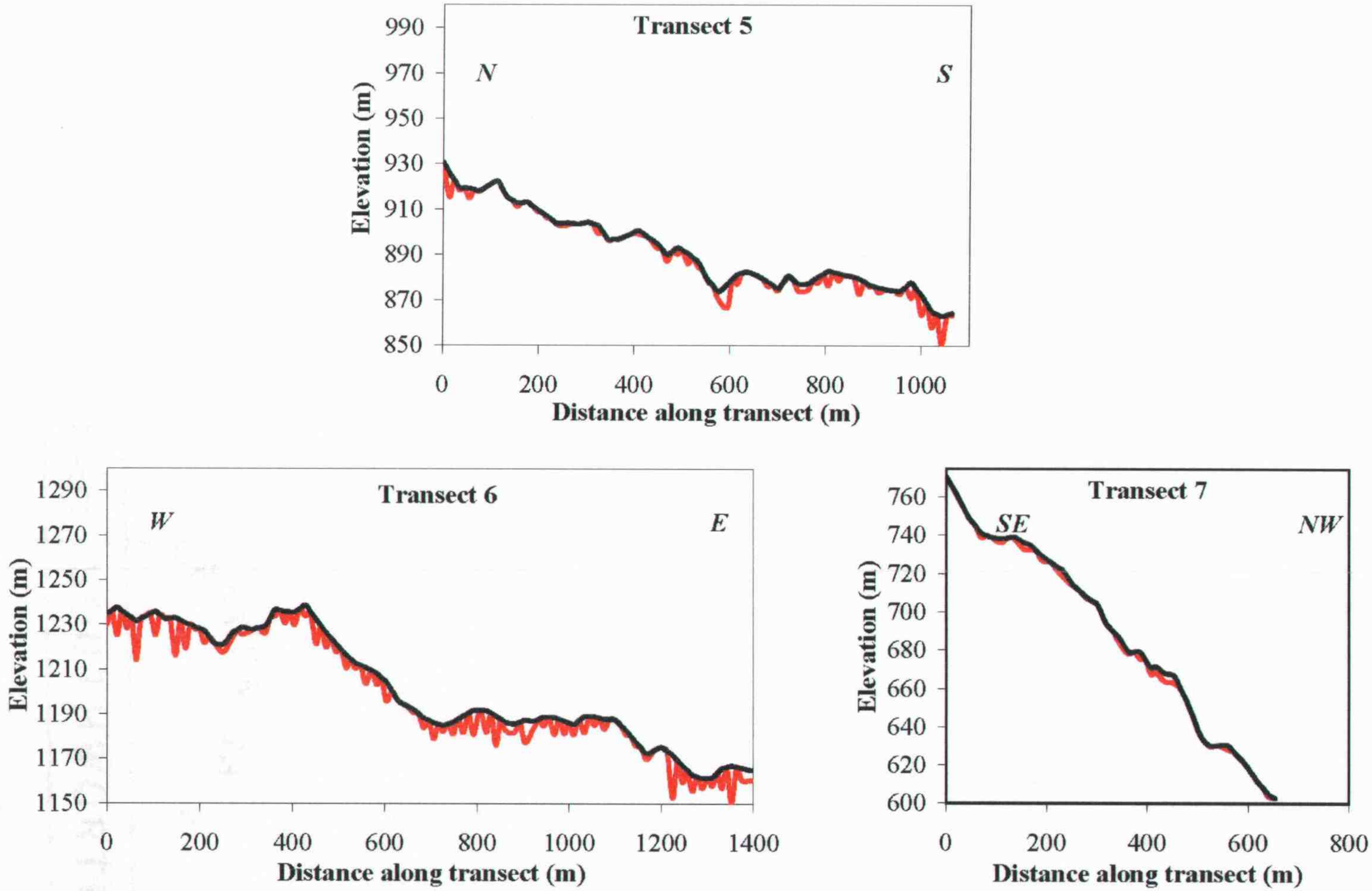

Figure 3.6 (continued). Generalized topographic and solum profiles.

toposequences for each morphological class may be compared in Figures 3.7(a), 3.7(b) and 3.7(c).

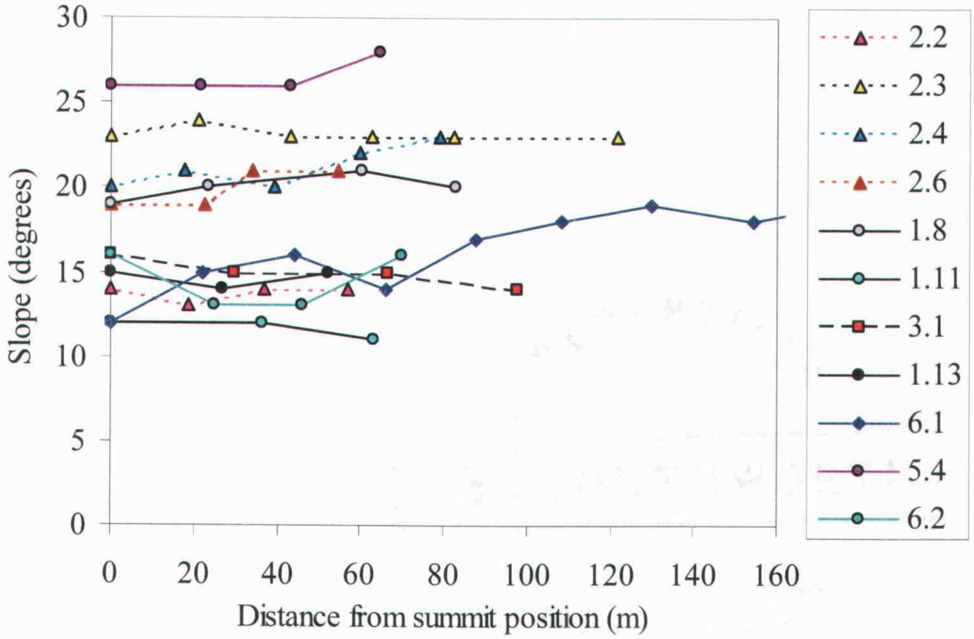

Figure 3.7 (a). Slope characteristics of rectilinear hill slope morphology classes.

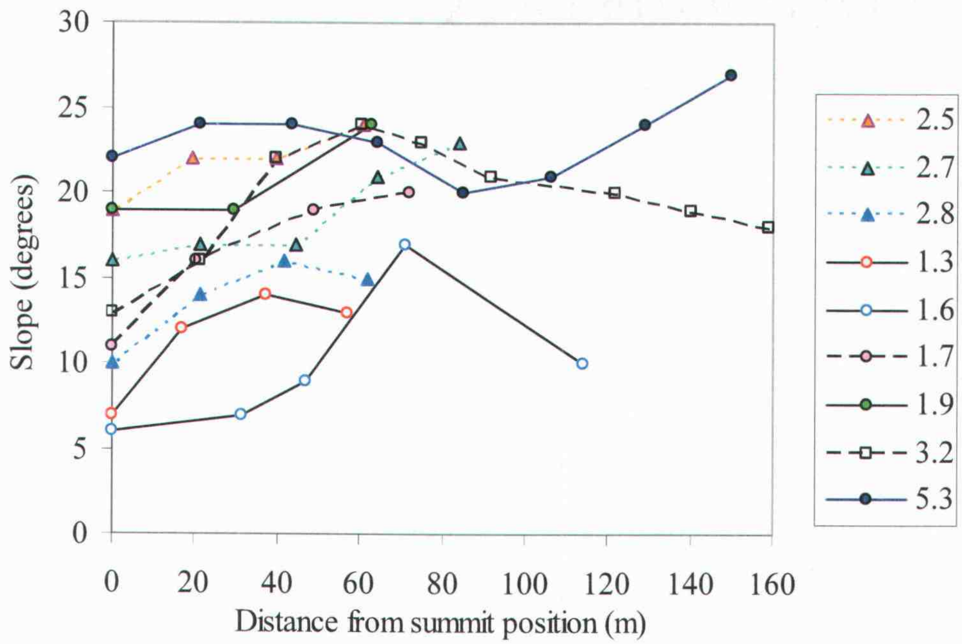

Figure 3.7 (b) Slope characteristics of curvilinear-convex hill slope morphology classes.

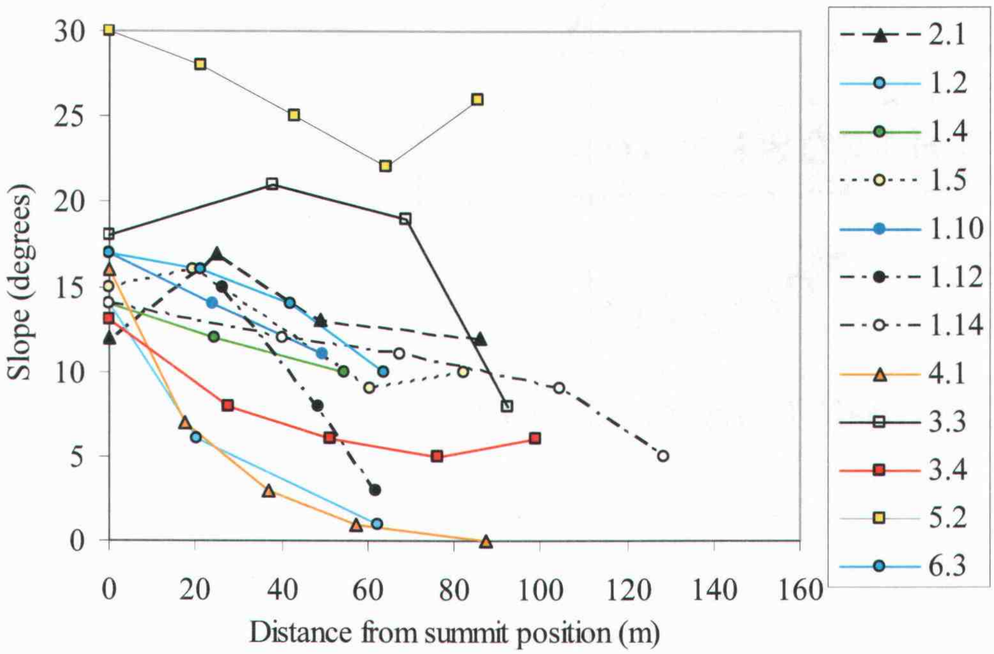

Figure 3.7 (c). Slope characteristics of curvilinear-concave hill slope morphology classes.

If pedogenesis in the Troodos mountains is chiefly a function of hill slope morphology then soil thickness should vary with hill slope position in a closely similar manner for all landforms of similar geomorphological classification. Analysis of soil thickness in the 32 toposequences in this study, however, produces wide scatter within each of the three distinct landform morphology classes (Figure 3.8(a), (b) and (c)). This scatter suggests that pedogenesis does not vary consistently with slope morphology across the study area.

Soil thickness for rectilinear hill slopes was expected to remain relatively constant along backslopes but to increase in footslope and toeslope positions, however, the data suggest that alternate models must be developed. Several toposequences show decreases in soil thickness with distance downslope (*e.g.*, hill slope 2.6), or stochastic oscillation (*e.g.* hill slopes 2.3, 6.1). Soils for curvilinear-

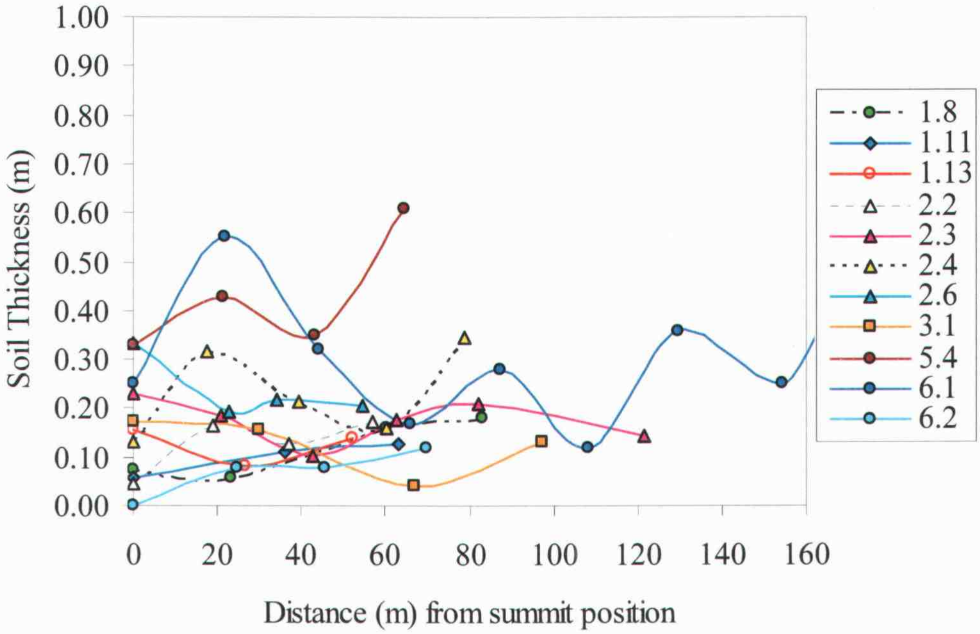

Figure 3.8(a). Soil depth trends for rectilinear hill slope toposequences.

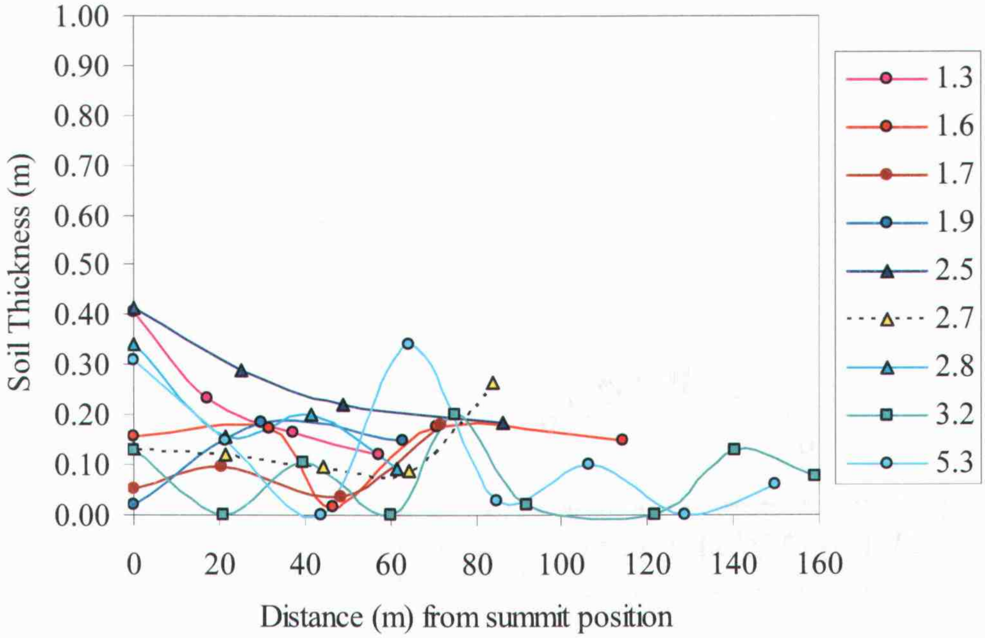

Figure 3.8(b). Soil depth trends for curvilinear-convex hill slope toposequences.

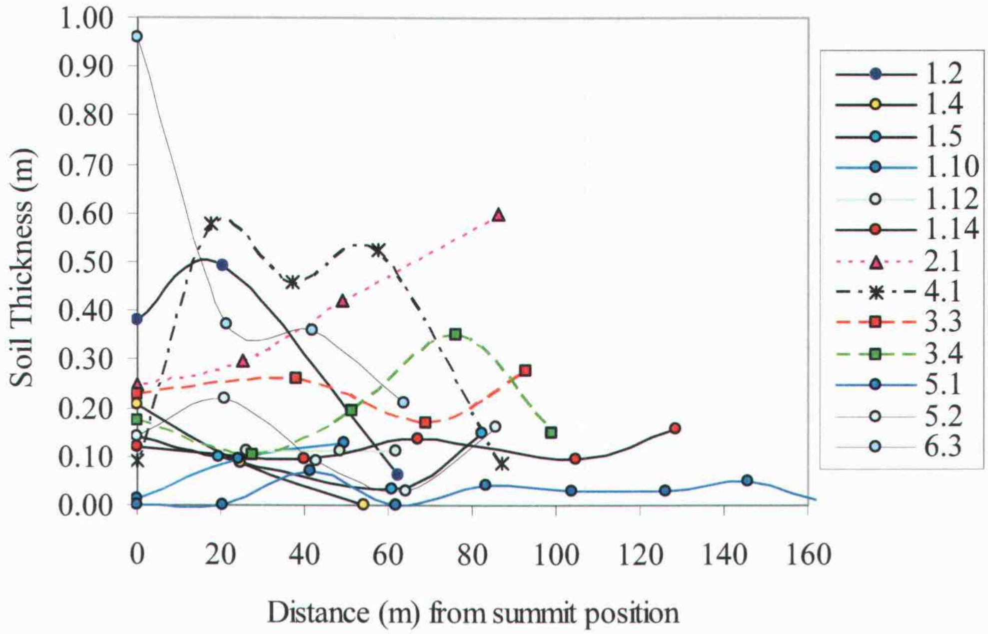

Figure 3.8(c). Soil depth trends for curvilinear-concave hill slope toposequences.

convex toposequences were predicted to be thinnest on backslopes, with sharply deeper soils in footslope and toeslope positions. However, only three sites conform to this model (hill slopes 1.3, 2.5, and 2.7) while others exhibit apparently stochastic soil depth variability (*e.g.* hill slopes 1.7, 3.2, and 5.7). Soil thickness for curvilinear-concave hill slopes was hypothesized to increase with distance downslope, with generally shallower soils in the backslope positions. As with the other landform morphologies, however, the data exhibit apparently stochastic soil depth variability and cannot be described by a single trend.

From Figure 3.8(a), (b), and (c) it may be noted that longer hill slopes often exhibit greater variability in soil thickness than shorter hill slopes. In some instances this results from the discontinuity of the "apparent" toposequences, however, other sites indicate that such variability represents natural hill slope soil patterns. For example, soil depth to bedrock was measured in the field at 20-meter intervals along the axis of the 650 meter-long, continuous toposequence of Transect 7, and was found to be quite variable (Figure 3.9). Concurrent with the

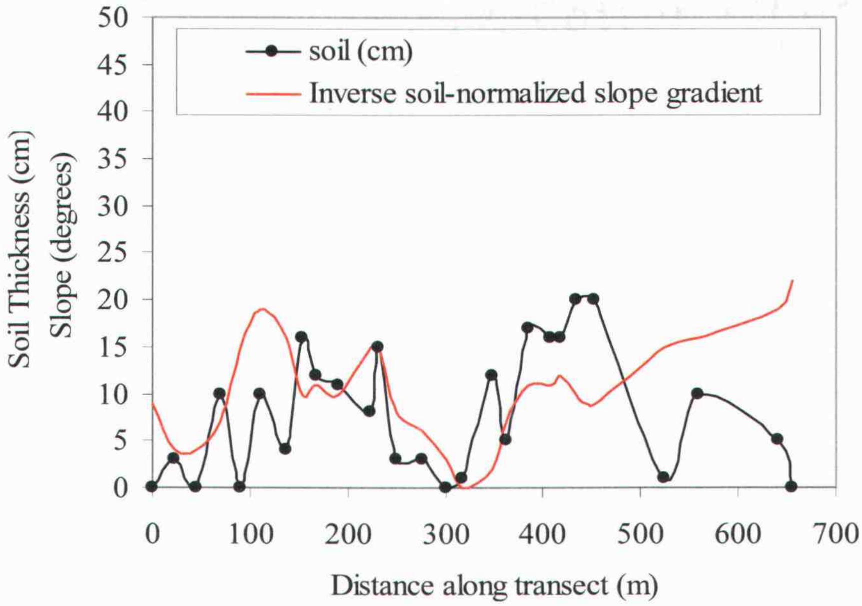

Figure 3.9. Stochastic variability in slope and solum profiles for transect 7.1, and varying solum-slope relationships along toposequence. Inverse soil normalized slope gradient was used to better compare amplitudes of variability.

variability in soil thickness are changes, in the relationship, from inverse to positive, of soil thickness to hill slope gradient. Slope values for measurement sites along the transect were derived from the 25-m DEM in the GIS.

Scaling effects also bear consideration when reviewing these soil data. Given the narrow morphology of mountain spurs and ridgelines in the Troodos, slope morphology may be considered at a broader geomorphologic scale. Thus, rectilinear slopes are the backslopes of larger mountain spurs, curvilinear-convex slopes represent mountain shoulders, and curvilinear-concave landforms comprise the footslopes. Initial comparison of group means reveals that footslopes exhibit the greatest mean soil depth while backslopes have intermediate soil depths, and shoulder positions exhibit the smallest mean soil depth (Table 3.11). One-way

Table 3.11. Summary of distinct hill slope morphology classes.

	Concave (footslope)	**Rectilinear (backslope)**	**Convex (shoulder)**
mean soil thickness (m)	0.18	0.16	0.14
n	61	81	46
Std Deviation (*s*)	0.183	0.123	0.108
Variance (s^2)	0.033	0.015	0.012
SE Mean	0.023	0.014	0.016

ANOVA between the three hill slope morphology classes reveals, however, that these apparent differences are not statistically different given the high p-value of 0.4013.

Similar suggestive, but statistically insignificant, trends result when all slope-derived hill slope position data are compared independent of specific toposequences. Comparison of mean soil depths for the five traditional hill slope classes corroborates field observations of a general soil pattern in the northern Troodos (Table 3.12). Soils are generally thinnest on summits and deepest along

Table 3.12. Summary statistics for toposequence analysis hill slope classes.

	Toeslope	**Footslope**	**Backslope**	**Shoulder**	**Summit**
mean soil depth (m)	0.22	0.17	0.17	0.19	0.18
n	17	83	150	48	39
Std Deviation (*s*)	0.242	0.131	0.163	0.137	0.179
Variance (s^2)	0.059	0.017	0.027	0.019	0.032
SE Mean	0.059	0.014	0.013	0.020	0.029

toeslopes, and there exists a greater range of variability among footslope, backslope, and shoulder soils. As with previous analyses, however, the results of one-way

ANOVA of mean soil depth for each of the five hill slope classes (p-value > 0.05) strongly suggests that apparent differences in mean soil thickness between classes are not statistically significant (Table 3.13). No one model explored here accurately

Table 3.13. ANOVA of mean soil thickness between toposequence classes.

	d.f.	**Sum of Sq**	**Mean Sq**	***F*-Statistic**	***p*-value**
Hill slope Class	5	0.213	0.043	1.788	0.1145
Residuals	361	8.615	0.024		
Residual Std Error	0.154				

describes relationships between slope processes and pedogenetic factors within the Troodos in sufficient detail to predict toposequence patterns across the sites or scale of study.

Predictive Soil Models

Predictive mapping through external slope stability models

The hydrologic-slope stability predictions from the SHALSTAB model were compared to soil thickness measurements using a simple linear regression. No detectable linear relationship exists between the two, given the correlation coefficient $R^2 \ll 1.0$ (Figure 3.10). A map of SHALSTAB-predicted landscape stability is presented in Figure 3.11 below. The predominance of landforms classified as "stable" suggested by the model contradicts field observations of severely eroded, rocky slopes even within areas of low relief, especially near the measured soil sites.

Alternative tests of the model explored variations of soil cohesion and soil thickness values but failed to produce results realistic for the Troodos. In some cases, values of high stability ($q/T \approx 10.0$) defined up to 95% of the output grid area.

Based on these data, neither the default nor the user-defined parameters of the SHALSTAB model adequately characterize hill slope stability within the field area.

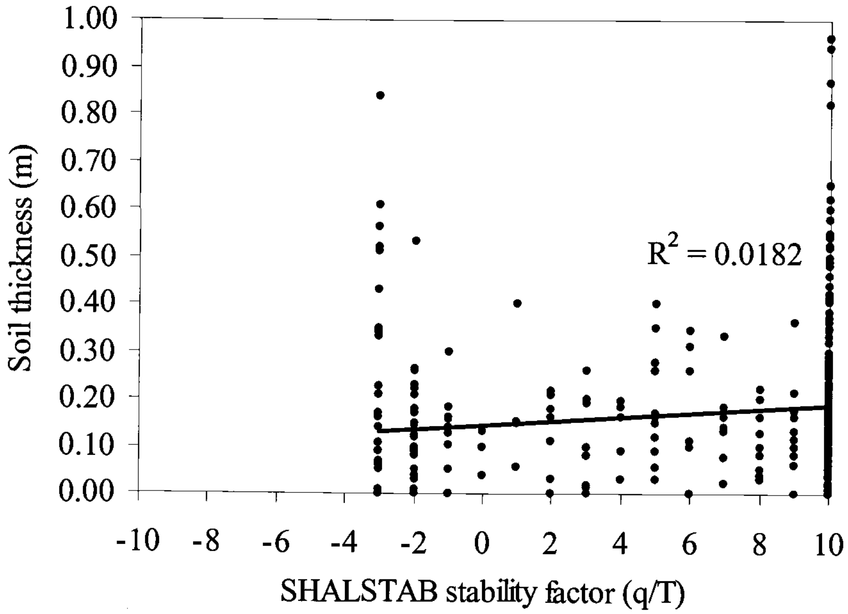

Figure 3.10. Comparison of SHALSTAB stability to soil development.

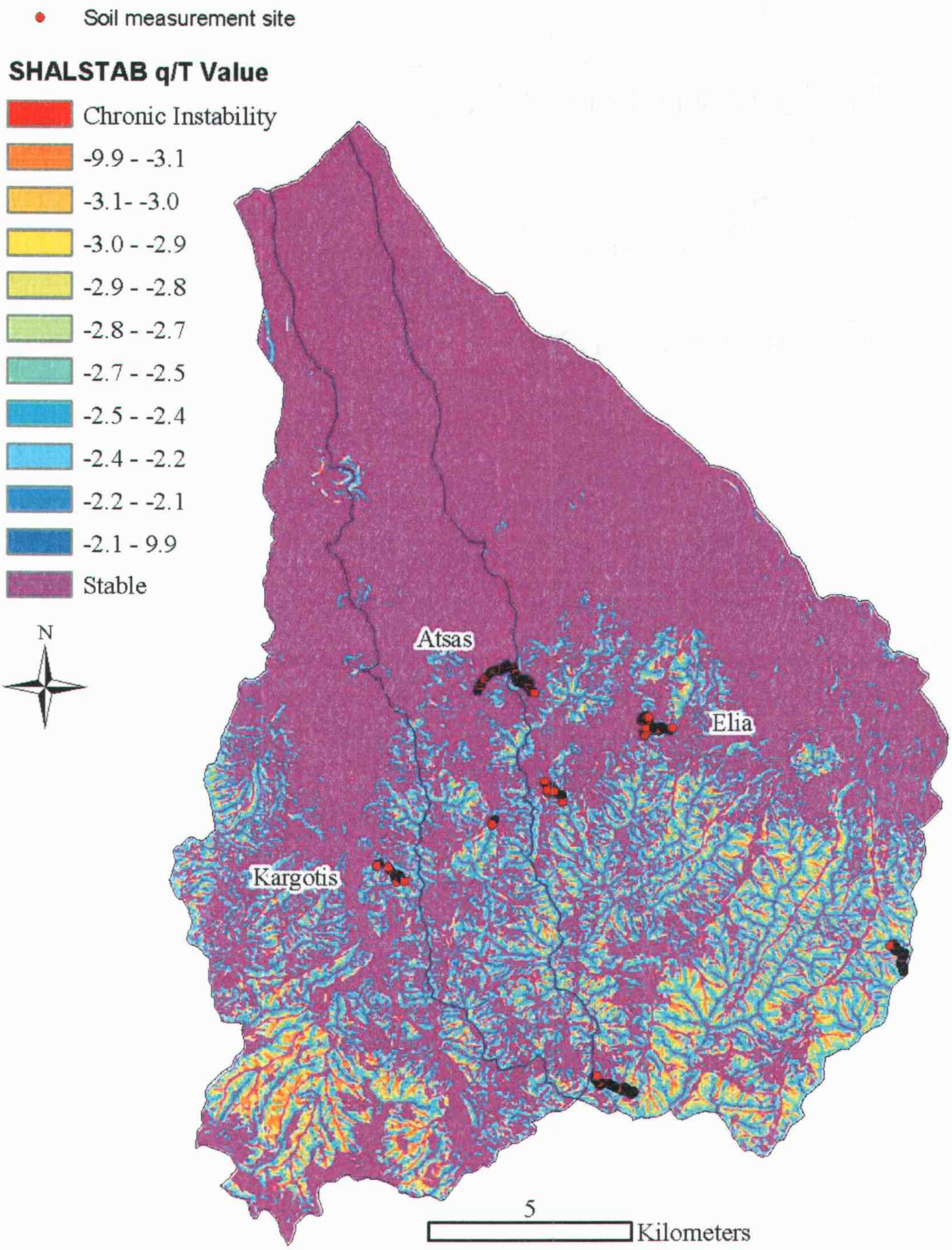

Figure 3.11. SHALSTAB stability map of the Kargotis, Atsas, and Elia watersheds.

Predictive mapping through analysis of northern Troodos data

Given the low-magnitude coefficients of correlation produced by the rich and simple linear regression models, accurate predictive mapping based on soil and landscape attribute data from this study did not prove feasible. Soils within the Troodos are thin and exhibit high degrees of variability that cannot be accounted for based on hill slope position, slope, precipitation, or other measured landscape attributes. High variability within individual toposequences also precludes spatial interpolation of soil thickness across landform or catchment boundaries for these reasons. Furthermore, correlation between soil thickness and bedrock fracture characteristics prevent any soil depth prediction based on lithologic characteristics across the study area. The results presented here suggest that accurate modelling of soil landscape patterns in the Troodos, may require a finer scale and better-tailored methods of soil-landscape attribute analysis.

DISCUSSION

Soil-Profile Thickness

Troodos soils have been described by many authors as thin, parched, and rocky, a by-product of centuries of timber harvesting by humans and grazing by domesticated goats. To put the thin Troodos soils into proper geomorphologic and pedologic context, a comparison to soils from similar geomorphologic settings around the world is presented here. Similar seasonal soil moisture patterns, substratum lithology, geomorphology, and land use make studies of landscape pedology in regions such as the western coast of North America ideal for comparison to the Troodos. Soil thickness, mean annual precipitation (MAP), and elevation are compared in Table 4.1 (below) between hill slope, colluvial soils from Oregon, California, and Cyprus.

It is noteworthy that the two thickest soils occur under extremely high MAP values, and that a highly suggestive, inverse trend exists between soil thickness and elevation (if the Felcher series is excluded). Although no statistically significant patterns were detected in the Troodos data presented above, one general observation may be made. The upper envelope of the data exhibit a general trend consistent with traditional pedogenetic models: greater soil thickness values appear more likely to occur at higher elevation and MAP levels, and at lower slope gradient values. Such an observation does not permit precise, predictive mapping of soil thickness, however, the general, upper-envelope trend and greater variability at high elevation and MAP values are consistent with expectations of a weathering-

Table 4.1. Comparing soil depths among xeric soil series formed in colluvium derived from weathered, fractured, basic igneous rocks (*e.g.*, basalt, serpentinite) in distinct total mean annual precipitation (MAP) regimes.

Series	Location	Soil Depth (cm)	MAP (mm)	Slope (°)	Avg. Elevation (m)	Soil Taxonomy
Dixonville*	Benton Co., OR	127	1270	15	236	Ultic Argixeroll
Felcher**	Lake Co., OR	61	279	30	1646	Xeric Haplocambid
Gilroy***	Solano Co., CA	76	572	10	305	Typic Argixeroll
Henneke°	San Luis Obispo Co., CA	48	635	20	610	Lithic Argixeroll
Obispo°	San Luis Obispo Co., CA	51	635	20	610	Lithic Haploxeroll
Price**	Benton Co., OR	127	1270	20	335	Dystric Xerochrept
Trimmer***	Solano Co., CA	79	572	10	335	Mollic Haploxeralf
Troodos"	N. Troodos, Cyprus	*17*	*490*	*20*	*720*	Lithic Xerorthent

* Soil Survey Staff, 1975

** Soil Survey Staff, 2002

*** Soil Survey Staff, 1977

° Soil Survey Staff, 1983

" Average values for all Troodos data obtained in this research limited geomorphological system. Isolated hill slopes that remain undisturbed by erosional events for longer-than-average time periods will exhibit greater soil development and will appear less stochastic. The resulting soil prediction model holds, therefore, that there should exist greater numbers of moderately-well-developed soils in stable areas of high precipitation and low slope gradient.

Implications of Correlation with Traditional Soil-forming Factors

It has already been noted that the five broad factors of pedogenesis are often so intricately related that fully independent analysis of each can prove meaningless (Hugget, 1998). Certainly, the results of the linear regression and ANOVA analyses presented above suggest that such may be the case for soil genesis in the Troodos. Nevertheless, implications of the individual correlation tests for climate, slope, elevation, aspect, and lithology do require further discussion.

Climate analysis in this research involved a simple comparison of MAP to soil thickness, because increased soil moisture levels are known to facilitate biological activity, chemical weathering of parent minerals, and the translocation of clays and soil nutrients. On the other hand, increased precipitation may promote soil erosion, especially in steep terrain. Climate factors such as temperature and MAP in mountainous regions such as the Troodos are largely orographic, so pedogenetic measures may be dominated by topographic rather than climatic signatures. For these reasons, lack of conclusive linear correlations in the comparison of soil thickness to MAP is not surprising. Increased soil thickness variability and greater numbers of thicker profiles in regions of high MAP may reflect strong storm effects on weathering-limited hill slope soils. Combined analysis of high-resolution storm intensity and rainfall erosivity data, and other landscape attribute data might more precisely constrain dominant pedogenetic and geomorphologic processes.

Statistically inconclusive slope correlation tests were more surprising, especially given qualitative impressions of downslope-thickening soil profiles imparted through field observations in the Troodos. However, slope does not always correlate closely with pedogenesis. Other researchers (*e.g.* King *et al.*, 1983) have found that neither slope length nor slope gradient showed a persuasive or consistent relationship to soil development in their study. Alternatively, lack of correlation between soil development and slope angle may suggest that the thin soils of the Troodos fall below some depth threshold at which slope angle is no longer influential. Such a scenario might also account for discrepancies between soil thickness data and SHALSTAB hydrologic-slope stability estimates. These possibilities will be discussed in more detail below.

Elevation signatures in soil thickness data may reflect concurrent changes in related pedogenetic factors such as climate (temperature, moisture, rainfall erosivity) and topography (slope gradient, slope length) and for that reason elevation data should serve as a simpler, alternate pattern indicator in multivariate regression analyses. The lack of correlation between elevation and soil thickness further suggests that rock-to-regolith conversion is independent of climate and relief.

Lack of significant trends among aspect classes is also not surprising, given that slope aspect is an amalgamation of climatic and topographic variables. In the northern hemisphere, southwest-facing slopes generally experience higher temperature ranges and drier conditions than slopes facing northeast, and also exhibit vegetative differences as a result (Birkeland, 1999). However, in weathering-limited regimes where soils are thin and weakly developed, aspect should not be expected to promote major differences in soil thickness given relatively greater importance of more specific variables such as temperature or slope gradient.

Lithology was the only factor found to have a significant relationship with changing soil-profile thickness. As mentioned above, multivariate linear regression models detected no trends in association with MAP and elevation; however, the possibility of concurrent orographic contributions cannot be entirely discounted given that the volcanic-intrusive-plutonic lithologic succession of the northern Troodos occurs in tandem with topographic and climatological gradations. That is, the three identified lithologic classes occupy different topoclimatic positions. If the small but significant soil thickness variation between lithologic classes does indicate an influence on pedogenesis by parent material, then the results from the bedrock fracture analysis are indeed intriguing. Lack of linearity in plots of bedrock fracture density against soil thickness suggests that slope processes in the Troodos are weathering-limited. Therefore, the anticipated positive correlation between soil thickness and rock fracture density does not occur because weathering products are eroded soon after their genesis.

Lithologic controls of Troodos soils are corroborated by other authors. For example, the rocks of the diabase unit crumble easily and yield sandy, gray soils, whereas the pillow lavas present at lower elevations erode rapidly and typically generate immature soil-profiles of thin, gravelly sandy loam texture along topographic lows (Christodoulou, 1959). Where soils are thin and weakly developed, bedrock comprises an integral part of the forest substrate. This is the case for xeric soil moisture regimes in the mountains of other Mediterranean areas (Noller, Personal Communication) and in California, where weathered bedrock stores plant-available water along fracture zones (Hubbert *et al.*, 2001). In dry Mediterranean climates, moisture may drain rapidly into fractured soil-bedrock profiles, leaving the upper profile dry and rendering weathering processes ineffective (Taylor and Eggleton, 2001).

Relict Topography and Soil Inheritance

Narrow temporal scope is one of the chief limitations of pattern-based approaches to landscape analysis. Present-day soil properties are typically compared to present-day landscape properties, but such an approach is not necessarily valid. Landscapes can retain topographic characteristics from past periods of rapid geomorphologic change that have yet to reach equilibrium with present-day conditions (Hunt & Wu, 2004). Similarly, Phillips (1999) cites several studies in which landform soil profile variations unrelated to observed variations in contemporary topography, parent material, drainage, and vegetation, in fact resulted from the lasting effects of tree throw in ancient, vanished forests. The pedologic effects of tree throw comprise just one example of soil memory or inheritance (Phillips, 1999). Such patterns that take decades or hundreds of years to evolve are stabilizing functions of ecosystems that may also help them recover from disturbance or to resist stressors (Thomas, 2001). Moreover, it is often difficult to prove that present-day soil properties are in steady state with the current form of the hill slope (Park & Burt, 2002). Hence, the concepts of relict topography and inherited soil properties must be addressed by process-based studies.

Temporal components of the Troodos landscape were integrated into this study through observation of Quaternary geomorphologic units, archaeological units, and hill slope stability throughout the study area. Incised Pleistocene channel gravels indicate episodes of relatively rapid geomorphologic change in the distant past, while archaeological finds, including medieval pottery sherds and intact, centuries-old, stone check dams, indicate relative stability of toeslopes and coarse surface material, respectively, during the Late Holocene (Given *et al.*, 2003).

Dynamics of Geomorphological Systems

Flights of uplifted marine terraces, deeply incised stream channels, and thin, weakly developed soils of the Troodos Mountains indicate that the landscape of Cyprus continues to experience tectonic uplift and corresponding geomorphologic change. High uplift or erosion rates, or both, typically yield soils that are thin or absent (Anderson *et al.*, 2002). Fracture flow limits both the contact time and surface contact area of rock minerals with water, leading to low chemical denudation rates associated with bedrock weathering (Anderson *et al.*, 2002).

Estimates of erosion rates have been calculated for catchments near this study area and are compared to rates from the more humid North American West Coast in Table 4.2. The Kalavasos Reservoir catchment, which exhibits similar

Table 4.2. Average erosion rates published for distinct geomorphological locales.

Source	*Average Erosion Rate (mm/yr)*	*Site Location*
Dörflinger, 2003	0.17 mm/yr	Kalavasos Reservoir Catchment, Cyprus
Burdon (*cited in* Christodoulou, 1959)	0.05 mm/yr	Lightly forested foothills of the Troodos Mts., Cyprus
Heimsath *et al.*, 2001	0.117 mm/yr	Oregon Coast Range
Reneau & Dietrich, 1991	0.057 mm/yr	Sierra Nevada

lithologies, is located approximately 20-25 kilometers southeast of this study area. Erosion rates put forth by Burdon apply to lightly forested foothills of the Troodos Mountains above elevations of 150 meters (Christodoulou, 1959). Dörflinger (2003) notes that the average value reported for the greater catchment of the Kalavasos reservoir is based on a sediment delivery ratio and therefore includes an inherent degree of uncertainty. It is also noted that sediment yields in neighboring watersheds may be an order of magnitude higher, due to potential differences in soil type, lithology, vegetative cover, and land use (Dörflinger, 2003).

By comparison, the implication of these studies (Table 4.1) is that high erosion rates in the steeper mid-ranges of the Troodos may be too high, and rock weathering rates too low, to permit soil development – the geomorphological balance is limited by sediment supply. Although not statistically significant on an individual case basis, the factors of pedogenesis in aggregate support a weathering-limited geomorphologic system. For example, the hint at such a system is seen in the data for fracture density (compare Figure 1.1(a) with Figures. 3.2 and 3.3), though unsupported.

Hill Slope Models and Soil Prediction

Lack of statistically significant correlation between the hydrologic-slope stability model and measured soil thickness is best addressed within the geomorphologic context of a weathering-limited system, because soil memory is transient or of short duration. The inability of SHALSTAB to accurately characterize Troodos hill slopes is due to differences between modelled and real properties of the soil-bedrock profile. SHALSTAB is not designed for regions dominated by rocky outcrops or cliffs. The Troodos do exhibit stripped and rocky slopes, but slopes mantled by thin, gravelly colluvium are more typical. In any case, testing the utility of the SHALSTAB model in the Troodos was deemed worthwhile given the similarity between hypothesized soil spatial patterns of this research and soil spatial characteristics assumed by the model. Specifically, SHALSTAB is designed to predict correctly the observed tendency for soils to be thick in valleys and thin on ridges, and it models the soil mantle as a mobile layer of colluvium atop fractured bedrock (Dietrich & Montgomery, 1998). Such a model considers ridges relatively stable except during unusually heavy storms, while steep valley axes require only minor rainfall events to fail. Therefore, soil thickness is expected to vary across the landscape in a systematic manner (Dietrich & Montgomery, 1998).

Comparing SHALSTAB stability values to soil-thickness data reveals that the model does not suit hill slope surface mechanics in the Troodos. Authors of the SHALSTAB model strongly recommend that any predictions be compared to actual landslide data, which can help determine if failed correlations result from poorly defined parameters or, instead, inapplicability of the model to field site geomorphology (Dietrich & Montgomery, 1998). One shortfall of this research, however, is its lack of mapped landslide data for the Troodos. Without this data, the true reasons for the utility or inapplicability of the SHALSTAB model cannot be identified precisely.

Scale

Given the lack of trends not only among the SHALSTAB data, but also among landscape attribute data, the scale of surface process variability merits discussion. The soil processes that promote important morphological distinctions within and between distinct soil series occur at microscopic scales as well as macroscopic. Research has demonstrated that the rate of mass loss is approximately three times greater in soil than in parent bedrock; this mass loss, viz-a-viz the degree of weathering which occurs at the top of the weathered rock profile, varies significantly throughout catchments (Anderson *et al.*, 2002). Study of soil morphological variability must address downward and lateral variability at extremely fine scales before the interactions and results of soil surface processes may be predicted across landforms. Soil variability in the Troodos might better be understood, therefore, through detailed chemical analysis of complete soil, regolith, and rock profiles.

Conversely, a landscape scale may be most appropriate for studies of landscape sensitivity. Whereas no landscape property has yet been found to be an effective guide in all cases, research has not yet fully linked watersheds, slope changes, or ecotones to the scales of spatial variability in regolith, soil, or water movement (Thomas, 2001). Still it is suggested that a grasp of wide-scale factors such as stream sediment capacity, uplift rates, stream incision rates, climate limits, and landsliding are necessary before fine-scale soil variability can be fully understood in complex, semi-arid landscapes.

Because of the connectivity within environmental systems, soil spatial variation must be regarded as dynamic (Phillips, 1999). Thus, the methods employed in this research were inadequate to achieve stated objectives. To realistically model natural soil landscape patterns in the Troodos, a mixed temporal- and spatial- scale approach is recommended. Soils, however thin, of a complex landscape such as the Troodos must be understood as products of gradual, geological scale processes (tectonics) further imprinted with millenia- and annual-scale signatures (climate, regolith production).

CONCLUSION

This research comprised a pattern-based approach at an intermediate scale that strove to: 1) identify the controls of soil genesis and landscape stability within the Troodos Mountains of Cyprus; 2) compare field measurements to expected soil thickness trends from traditional models of soil toposequences prevalent in current scientific literature; and 3) develop a predictive model for hillslope pedogenesis based on measured soil properties within the field area.

Definitive pedogenetic controls could not be constrained based on the results of this study. Expected correlations between soil thickness and MAP, slope, elevation, aspect, and watershed were not found. Soil thickness values were found to vary with rock type, however, additional chemical and mineralogical data might better define lithologic effects on pedogenesis. Soil spatial patterns were not found to vary consistently along hill slopes, nor, unexpectedly, were significant differences in soil thickness detected between hill slope segments of different morphology. Differences between measured soil data and values predicted by an external landscape stability model suggest that the Troodos are best described only within the context of a weathering-limited geomorphological system. For that reason, predictive maps of soil thickness are likely feasible with greater and more comprehensive soil and landscape information, or development of appropriate models.

Given the results and analysis of this study, the view presented here considers that 5,000 years of potentially adverse human land use practices did not promote insidious and severe soil erosion in the Troodos because development of mature soil-profiles may never have been possible. Exceptions to this low pedogenetic potential include isolated hill slopes in which erosional events did not transpire with the normal frequency, and the margins of large-order streams with stable alluvial terraces. Typical, weathering-limited hill slopes of the Troodos are characterized by a geomorphologically rapid loss of any fine sediments produced through weathering of the igneous bedrock. Short-term disruptive processes such as forest fire, land sliding, tree throw, and raindrop impact, combined with long-term processes such as tectonic uplift and stream incision, are the most likely driving forces behind the net erosion of hill slope sediments. Barring large-magnitude climate fluctuations akin to the Little Ice Age, pedogenetic rates seem unlikely to increase within the next 500 or even 5,000 years.

The complex soil, geological, hydrological, and cultural systems of the Troodos Mountains of Cyprus present an ideal opportunity for further, integrated soil geomorphologic research. Future research into geomorphologic and pedologic processes in the Troodos would benefit enormously from chemical and mass-balance analysis of rock or mineral weathering rates similar to those employed by Anderson *et al.* (2002) for small catchments in western Oregon. Alternatively, sediment delivery models might be developed for Holocene and Pleistocene river systems within the Troodos, with the aim of constraining better soil erosion estimates. Better hill slope models for the Troodos might be established through the application of more refined algorithms of topographic position to the DEM through GIS analysis. In addition, the rich cultural resources of forests in the Troodos Mountains should not be overlooked. Millenia of human land use practices have introduced archaeological features of determinable age that are indicative of past environmental conditions. Therefore, there exists great potential for illuminating soil-geoarchaeological research into the dynamic human and environmental past of the Troodos Mountains of Cyprus.

REFERENCES

Anderson, S. P., Dietrich, W.E. & Brimhall, G.H. Jr. 2002. Weathering profiles, mass-balance analysis, and rates of solute loss: Linkages between weathering and erosion in a small, steep catchment. *Geological Society of America Bulletin*, **114(9)**, 1143 1158.

Birkeland, P. W. 1999. *Soils and Geomorphology*. Oxford University Press Inc., New York.

Birkeland, P.W., Shroba, R.R., Burns, S.F., Price, A.B., Tonkin, P.J. 2003. Integrating soils and geomorphology in mountains - an example from the Front Range of Colorado. *Geomorphology*, **55**, 329 344.

Braun, J., Heimsath, A.M. & Chappell, J. 2001. Sediment transport mechanisms on soil-mantled hillslopes. *Geology*, **29(8)**, 683 686.

Christodoulou, D. 1959. *The evolution of the rural land use pattern in Cyprus*. World Land Use Survey Monograph 2: Cyprus. Geographical Publications Limited, England.

Coops, N., Ryan, P., Loughhead, A., Mackey, B., Gallant, J., Mullen, I. & Austin, M. 1998. *Developing and testing procedures to predict topographic position from digital elevation models (DEM) for species mapping (Phase 1)*. CSIRO Forestry and Forest Products: Client Report No. 271.

Dietrich, W.E., Bellugi, D., Sklar, L., Stock, J. D., Heimsath, A. M., & Roering, J. J. 2003. *Geomorphic transport laws for predicting landscape form and dynamics*. Prediction in Geomorphology, Geophysical Monograph 135, American Geophysical Union.

Dietrich, W.E. & Montgomery, D.R. 1998. *Shalstab: a digital terrain model for mapping shallow landslide potential*. http://socrates.berkeley.edu/~geomorph/shalstab.

D'Odorico, P. 2000. A possible bi-stable evolution of soil thickness. *Journal of Geophysical Research*, **105 (B11)**, 25927 25935.

Dörflinger, G. 2003. *Assessment of sedimentation and erosion: Kalavasos Reservoir and catchment, Cyprus*. MSc dissertation, University of Wales, Bangor.

Ehlen, J. 2002. Some effects of weathering on joints in granitic rocks. *Catena* **49**, 91 109.

Flanagan, D.C. & Nearing, M.A. 1995. *USDA - Water Erosion Prediction Project: Hillslope profile and watershed model documentation*. NSERL Report No. 10. USDA-ARS National Soil Erosion Research Laboratory.

Frazier, C.S., & Graham, R.C. 2000. Pedogenic transformation of fractured granitic bedrock, Southern California. *Soil Science Society of America Journal*, **64**, 2057 2069.

Gabet, E.J., Reichman, O.J. & Eric W. Seabloom, 2003. The effects of bioturbation on soil processes and sediment transport. *Annual Review of Earth and Planetary Science* **31**, 249 273.

Gama-Castro, J.E., Flores-Roman, D., Solleiro-Rebolledo, E., Jasso-Castañeda,C., Vallejo-Gómez, E., Rocha-Torrallardona, A.M., & Villalpando-González, J.L. 2004. Neosols, relict paleosols, and alterites in the Transmexican Volcanic Belt, Morelos state: Characterization and regional spatial distribution. *Revista Mexicana de Ciencias Geológicas,* **21(1)**, 160 174.

Gass, I.G. 1975. The Troodos massif: Its role in the unravelling of the ophiolite problem and its significance in the understanding of constructive plate margin processes, *In*: *Ophiolites: Proceedings of the International Ophiolite Symposium Cyprus 1979*. Panayiotou, A., Ministry of Agriculture and Natural Resources, Nicosia, Cyprus.

Geological Survey Department. 1995. *Geological Map of Cyprus*. Ministry of Agriculture, Natural Resources and Environment, Government of Cyprus, Nicosia, Cyprus.

Gessler, P.E., Chadwick, O.A., Chamran, F., Althouse, L. & Holmes, K. 2000. Modeling soil-landscape and ecosystem properties using terrain attributes. *Soil Science Society of America Journal*, **64,** 2046 2056.

Given, M., Boutin, A., Blankespoor, B., Corley, H., Digney, S., Gibson, E., Graham, A., Horowitz, M., Kassianidou, V., Knapp, A.B., Lufafa, A., McCartney, C., Noller, J., Robins, C., Slevin, S., Sollars, L., Tselios, T., & Jacobson, K.W. 2003. *Troodos Archaeological and Environmental Survey Project: Report on the Fourth Season, July-August 2003*. University of Glasgow, http://www.taesp.arts.gla.ac.uk.

Heimsath, A.M., Dietrich, W.E., Nishiizumi, K. & Finkel, R.C. 1997. The soil production function and landscape equilibrium. *Nature*, **388**, 358 361.

Heimsath, A.M., Dietrich, W.E., Nishiizumi, K. & Finkel, R.C. 1999. Cosmogenic nuclides, topography, and the spatial variation of soil depth. *Geomorphology*, **27**, 151 172.

Heimsath, A.M., Dietrich, W.E., Nishiizumi, K. & Finkel, R.C. 2001. Stochastic processes of soil production and transport: erosion rates, topographic variation and cosmogenic nuclides in the Oregon Coast Range. *Earth Surface Processes and Landforms*, **26**, 531 552.

Hubbert, K. R., Graham, R.C. & Anderson, M.A. 2001. Soil and weathered bedrock: components of a jeffrey pine plantation substrate. *Soil Science Society of America Journal*, **65**, 1255 1262.

Hugget, R.J. 1998. Soil chronosequences, soil development, and soil evolution: A critical review. *Catena*, **32**, 155 172.

Hunt, A.G. & Wu, J.Q. 2004. Climatic influences on Holocene variations in soil erosion rates on a small hill in the Mojave Desert. *Geomorphology*, **58**, 263 289.

Jenny, H. 1941. *Factors of soil formation; a system of quantitative pedology.* McGraw Hill Publications, New York.

Keefe, EK., Cover, W.W., Giloane, W., Moore, J.M. Jr., Teleki, S. & White, E.T. 1971. *Area Handbook for Cyprus.* DA Pam 550-22, Foreign Area Studies of the American University, Washington D.C.

King, G.J., Acton, D.F. & St. Arnaud, R.J. 1983. Soil-landscape analysis in relation to soil distribution and mapping at a site within the Weyburn Association. *Canadian Journal of Soil Science,* **63(4)**, 657 670.

McBratney, A., Mendoça Santos, M.L. & Minasny, B. 2003. On digital soil mapping. *Geoderma*, **117**, 3 52.

Migoń, P. & Lidmar-Bergström, K. 2001. Weathering mantles and their significance for geomorphological evolution of central and northern Europe since the Mesozoic. *Earth-Science Reviews,* **56**, 285 324.

Moore, I.D., Gessler, P.E., Nielsen, G.A. & Peterson, G.A. 1993. Soil Attribute Prediction Using Terrain Analysis. *Soil Science Society of America Journal*, **57**, 443 452.

Morris, A. 1996. A review of palaeomagnetic research in the Troodos ophiolite, Cyprus. In: *Paleomagnetism and Tectonics of the Mediterranean Region*, Morris, A. and D.H. Tarling. 1996. Geological Society Special Publication No. 105, The Geological Society, London.

Noller, Jay Stratton. 2003. Personal communication. Oregon State University.

Norton, J.B., Sandor, J.A., & White, C.S. 2003. Hillslope soils and organic matter dynamics within a Native American agroecosystem on the Colorado Plateau. *Soil Science Society of America Journal*, **67**, 225 234.

Park, S.J. & Burt, T.P. 2002. Identification and Characterization of Pedogeomorphological Processes on a Hillslope. *Soil Science Society of America Journal*, **66**, 1897 1910.

Phillips, J.D. 1999. *Earth Surface Systems: Complexity, Order and Scale.* Blackwell Publishers, Malden, Massachusetts.

Reneau, S.L. & Dietrich, W.E. 1991. Erosion rates in the southern Oregon Coast Range: Evidence for an equilibrium between hillslope erosion and sediment yield. *Earth Surface Processes and Landforms,* **16**, 307 322.

Robertson, A.H.F. & Woodcock, N.H. 1979. Tectonic setting of the Troodos massif in the east Mediterranean. In: *Ophiolites: Proceedings of the International Ophiolite Symposium Cyprus 1979.* Panayiotou, A., Ministry of Agriculture and Natural Resources, Nicosia, Cyprus.

Roering, J.J., Almond, P., Tonkin, P., & McKean, J. 2002. Soil transport driven by biological processes over millenial time scales. *Geology*, **30(12)**, 1115-1118.

Ruhe, R.V. & Walker, P.H. 1968. Hillslope models and soil formation: I. Open systems. *Trans. 9th International Congress of Soil Science,* **4**, 551 560.

Secretariat of the United Nations Convention to Combat Desertification. 2002. Addendum 2: Cyprus. In: *Compilation of summaries of reports submitted by Northern Mediterranean, Central and Eastern European and other country parties*, pp. 32 33, United Nations, http://www.unccd.int/.

Soil Survey Staff. 1975. *Soil Survey of Benton County area, Oregon.* United States Department of Agriculture Soil Conservation Service, Washington D.C.

Soil Survey Staff. 1977. *Soil Survey of Solano County, California.* United States Department of Agriculture Soil Conservation Service, Washington D.C.

Soil Survey Staff. 1983. *Soil Survey of San Luis Obispo County, California: Coastal Part.* United States Department of Agriculture Soil Conservation Service, Washington D.C.

Soil Survey Staff. 2002. *Soil Survey of Lake County, Oregon: Southern Part.* United States Department of Agriculture Soil Conservation Service, Washington D.C.

Soil Survey Staff. 2003. *Keys to Soil Taxonomy, Ninth Edition.* United States Department of Agriculture Natural Resources Conservation Service.

Tarboton, D.G. 2002. *TauDEM version 2.0.* Utah State University, http://www.engineering.usu.edu/cee/faculty/dtarb/.

Taylor, G. & Eggleton, R.A. 2001. *Regolith Geology and Geomorphology.* John Wiley & Sons Limited, England.

Thirgood, J.V. 1987. *Cyprus: a chronicle of its forests, land, and people.* University of British Columbia Press, Vancouver.

Thomas, Michael F., 2001. Landscape sensitivity in time and space - an introduction. *Catena*, **42**, 83 98.

Tsai, C.C., Chen, Z.S., Duh, C.T., & Horng, F.W. 2001. Prediction of soil depth using a soil-landscape regression model: a case study on forest soils in southern Taiwan. *Proceedings of the National Science Council*, **25(1)**, 34 39.

Walker, P.H. & Ruhe, R.V. 1968. Hillslope models and soil formation: II. Closed systems. *Trans. 9th International Congress of Soil Science*, **4**, 561 568.

Weitkamp, W.A., Graham, R.C., Anderson, M.A. & Amrhein, C. 1996. Pedogenesis of a vernal pool entisol-alfisol-vertisol catena in southern California. *Soil Science Society of America Journal*, **60**, 316 323.

Weiss, A. D. 2001, Topographic Positions and Landforms Analysis (Conference Poster). ESRI International User Conference, San Diego, California.

Wischmeier, W.H. 1976. Use and misuse of the universal soil loss equation. *Journal of Soil and Water Conservation*, **31(1)**, 5 9.

APPENDICES

Appendix A - Image Analysis of Fractures

Table A1. Data from soil-fracture correlation test in classified filtered images

Image ID	Sub-sample ID	Profile Depth (pixels)	Profile Width (pixels)	Soil Depth (pixels)	Total # Fracture Pixels	Fracture % of Tot. Area	Soil Depth (cm)
1773	x	1006	183	73	8347	4.88	10.9
2974	1	421	118	82	4294	5.50	12.3
2974	2	436	108	32	2666	6.11	4.8
2986	2	679	122	50	3944	5.15	7.5
2986	1	750	122	92	6053	6.62	13.8
2986	3	750	122	27	6234	6.27	4.0
2987	1	935	153	33	7188	5.21	4.9
2987	2	932	153	12	7679	5.46	1.8
2990	3	559	141	40	3119	4.22	6.0
2990	2	538	128	105	2540	4.59	15.7
2990	1	597	142	35	4619	5.45	5.2
3008	1	804	159	31	7046	5.73	4.6
3008	2	804	159	50	7615	6.35	7.5

Table A2. Data from soil-fracture correlation test in classified raw images

Image ID	Sub-sample ID	Profile Depth (pixels)	Profile Width (pixels)	Soil Depth (pixels)	Total # Fracture Pixels	Fracture % of Tot. Area	Soil Depth (cm)
2974	1	421	118	82	3615	9.06	12.3
1773	x	1006	183	73	23755	13.90	10.9
2974	2	436	108	32	6648	15.24	4.8
2986	2	679	122	50	8569	11.18	7.5
2986	1	750	122	92	10796	11.80	13.8
2986	3	777	122	27	7626	7.67	4.0
2987	1	935	153	33	15319	11.10	4.9
2987	2	932	153	12	20340	14.45	1.8
2990	2	538	128	105	4443	8.03	15.7
2990	1	597	142	35	6552	7.73	5.2
3008	1	804	159	31	14126	11.49	4.6
3008	2	804	159	50	20926	17.45	7.5

Table A3. Data from manual delineation of bedrock fractures in GIS.

Explanation of column headings	
Image ID	Unique photograph identifier used in all analyses.
Length	Total length, in meters, of all delineated fractures in each image.
Rock Area	Total area, in meters^2, of rock below the soil-bedrock contact.
Fracture	Total area-normalized fracture length, meters of fracture per meters rock outcrop, per image.
Soil Area	Total area, in meters^2, of soil profile above soil-bedrock contact.
Soil Depth	Thickness of soil profile in meters from surface to bedrock contact.

Image ID	Length	Rock Area	Fracture	Soil Area	Soil Depth
2977	33.34	8.99	3.71	0.70	0.13
2978	62.44	9.62	6.49	0.90	0.17
2986	77.88	9.58	8.12	0.70	0.13
2987	33.80	12.74	2.65	0.90	0.16
2990	30.54	7.66	3.99	0.90	0.16
3010	39.77	12.55	3.17	1.10	0.20
3016	66.00	12.76	5.17	0.60	0.11
3017	98.52	10.61	9.29	1.10	0.19
3043	51.39	6.93	7.42	0.60	0.11
3044	33.05	6.99	4.73	0.30	0.05
3046	21.41	6.85	3.13	1.10	0.19
3051	17.58	6.94	2.53	0.70	0.12
3059	20.28	4.81	4.22	0.40	0.08
3062	22.56	8.77	2.57	1.10	0.21
3063	13.25	6.42	2.07	0.50	0.09
3069	29.90	7.11	4.21	0.50	0.09
3070	27.10	7.15	3.79	1.50	0.28
3074	48.97	7.16	6.84	0.70	0.14
3080	29.19	6.77	4.31	0.90	0.17
3081	33.91	6.16	5.51	0.80	0.15
3082	39.88	7.11	5.61	0.30	0.05
3083	72.35	9.03	8.02	0.50	0.10
3086	44.77	10.54	4.25	0.90	0.16
3092	25.24	13.72	1.84	1.40	0.27
3098	47.72	7.37	6.48	0.80	0.15
3100	61.05	10.29	5.93	0.30	0.06
3107	31.22	8.04	3.88	0.50	0.09
3108	42.37	8.12	5.22	0.40	0.08

Table A3 (Continued)

Image ID	Length	Rock Area	Fracture	Soil Area	Soil Depth
3117	40.23	8.68	4.64	0.50	0.09
3119	43.99	10.15	4.33	0.00	0.00
3120	36.51	8.27	4.42	0.30	0.06
3134	21.55	7.94	2.71	0.60	0.12
3162	3.59	5.62	0.64	1.30	0.25
3163	13.21	7.38	1.79	0.70	0.13
3165	55.28	10.82	5.11	0.80	0.16
3171	15.33	6.27	2.45	0.60	0.13
3172	50.41	9.27	5.44	0.00	0.00
3173	29.25	4.69	6.23	0.10	0.02
3205	49.58	12.34	4.02	1.40	0.26

Appendix B - Field Data and Soil-Depth Analyses

Table B1. Data from: 1) Image analysis of photographed soil-bedrock outcrops; and 2) field auger, shovel, and outcrop sites.

	Explanation of column headings
Site ID	Individual record identifier; photograph site identifiers begin with a number (e.g. 1010037). Field excavation site identifiers begin with a letter (e.g. A1).
Easting, Northing	GPS UTM coordinates of photographed roadcut outcrops or pit sites.
Min, Max	Minimum and maximum depths of soil, measured in photographed soil profiles.
Area	Total soil profile area, measured in photographed soil profiles.
Width	Total straight-line distance between lower right and lower left corners of photographed soil profiles.
Mean	Average soil depth, in meters, for image sites, calculated as Area/Width. Field-measured depth for pit sites.

Site ID	Easting	Northing	Min	Max	Area	Width	Mean
2970	497672	3877705	0.25	0.30	3.00	5.00	0.60
2972	497696	3877712	0.10	0.80	2.10	5.00	0.42
2973	497719	3877718	0.10	0.40	1.50	5.02	0.30
2974	497732	3877753	0.00	0.05	0.65	2.60	0.25
2976	497722	3877769	0.02	0.20	0.70	5.06	0.14
2977	497720	3877788	0.05	0.30	0.70	5.36	0.13
2978	497729	3877808	0.07	0.40	0.90	5.33	0.17
2982	497745	3877825	0.04	0.50	0.80	5.28	0.15
2983	497769	3877834	0.02	0.30	1.00	5.78	0.17
2984	497789	3877838	0.30	0.20	1.30	5.28	0.25
2985	497808	3877835	0.08	0.30	0.90	5.18	0.17
2986	497816	3877818	0.00	0.20	0.70	5.57	0.13
2987	497814	3877800	0.00	0.30	0.90	5.53	0.16
2988	497815	3877780	0.00	0.40	0.22	5.00	0.04
2989	497823	3877764	0.02	0.30	0.70	5.52	0.13
2990	497836	3877747	0.00	0.40	0.90	5.77	0.16
2991	497844	3877719	0.10	0.70	1.90	5.43	0.35
2992	497854	3877701	0.03	0.30	0.80	5.58	0.14
2993	497865	3877683	0.10	0.30	1.10	5.26	0.21
2994	497871	3877662	0.10	0.40	1.00	5.65	0.18

Table B1 (continued).

Site ID	Easting	Northing	Min	Max	Area	Width	Mean
2995	497876	3877643	0.00	0.40	0.60	5.88	0.10
2996	497881	3877624	0.00	0.50	1.10	5.99	0.18
2997	497894	3877587	0.10	0.40	1.30	5.67	0.23
2998	497901	3877574	0.03	0.60	0.20	5.00	0.04
2999	497911	3877530	0.10	0.50	2.00	5.77	0.35
3000	497915	3877513	0.00	0.30	0.90	5.63	0.16
3001	497924	3877493	0.00	0.00	1.06	5.00	0.21
3003	497938	3877478	0.10	0.60	1.70	5.35	0.32
3004	497955	3877470	0.00	0.30	0.70	5.39	0.13
3005	497978	3877515	0.05	0.50	1.20	5.34	0.22
3007	498004	3877523	0.06	0.30	0.70	5.41	0.13
3008	498022	3877530	0.00	0.20	0.50	5.34	0.09
3009	498041	3877530	0.00	0.30	0.70	5.71	0.12
3010	498060	3877521	0.10	0.40	1.10	5.60	0.20
3011	498079	3877510	0.10	0.40	1.00	5.45	0.18
3012	498090	3877494	0.10	0.40	1.30	5.86	0.22
3013	498097	3877475	0.20	0.50	1.50	5.18	0.29
3014	498110	3877458	0.30	0.60	2.10	5.09	0.41
3015	498124	3877467	0.30	0.50	2.00	5.38	0.37
3016	498148	3877501	0.10	0.20	0.60	5.52	0.11
3017	498181	3877563	0.10	0.40	1.10	5.64	0.19
3020	498196	3877545	0.00	0.50	1.20	5.80	0.21
3021	498211	3877528	0.10	0.40	1.20	5.55	0.22
3022	498218	3877519	0.00	0.10	0.96	5.00	0.19
3026	498237	3877511	0.00	0.50	1.80	5.43	0.33
3030	498260	3877506	0.00	0.20	0.60	5.18	0.12
3031	498286	3877507	0.00	0.30	0.90	5.80	0.16
3032	498306	3877505	0.20	0.40	1.40	5.28	0.26
3033	498323	3877492	0.00	0.40	0.50	5.65	0.09
3034	498342	3877479	0.00	0.20	0.50	5.29	0.09
3035	498359	3877469	0.00	0.40	0.70	5.84	0.12
3036	498377	3877461	0.00	0.30	0.70	5.26	0.13
3037	498401	3877478	0.00	0.20	0.50	5.36	0.09
3038	498415	3877494	0.10	1.10	1.20	5.98	0.20
3039	498426	3877511	0.10	0.50	0.90	5.73	0.16
3040	498433	3877530	0.10	0.80	1.90	5.54	0.34
3041	493630	3878449	0.00	0.30	0.40	5.60	0.07
3042	493634	3878467	0.00	0.10	0.20	5.42	0.04

Table **B1** (continued).

Site ID	Easting	Northing	Min	Max	Area	Width	Mean
3043	493634	3878487	0.10	0.20	0.60	5.47	0.11
3044	493636	3878506	0.00	0.10	0.30	5.69	0.05
3045	493636	3878528	0.00	0.20	0.40	5.70	0.07
3046	493635	3878549	0.10	0.30	1.10	5.66	0.19
3047	493649	3878562	0.00	0.20	0.40	6.45	0.06
3048	493669	3878566	0.50	0.80	2.46	5.02	0.49
3050	493709	3878579	0.50	0.60	2.00	5.25	0.38
3051	493711	3878617	0.05	0.30	0.70	5.73	0.12
3052	493712	3878634	0.10	0.30	0.90	5.41	0.17
3053	493723	3878651	0.00	0.50	1.30	5.56	0.23
3054	493736	3878666	0.20	0.90	2.30	5.67	0.41
3056	493760	3878710	0.00	0.20	0.50	5.16	0.10
3057	493769	3878733	0.40	0.60	2.60	5.02	0.52
3058	493782	3878751	0.20	0.40	1.30	5.00	0.26
3059	493817	3878793	0.00	0.20	0.40	5.28	0.08
3060	493867	3878832	0.00	0.00	0.00	5.00	0.00
3062	493906	3878857	0.00	0.20	1.10	5.19	0.21
3063	493939	3878881	0.00	0.20	0.50	5.32	0.09
3064	493958	3878896	0.00	0.20	0.40	5.59	0.07
3065	493979	3878915	0.00	0.00	0.00	5.00	0.00
3066	494002	3878924	0.00	0.30	0.50	5.67	0.09
3067	494030	3878934	0.00	0.50	1.10	5.33	0.21
3068	494042	3878955	0.00	0.30	0.60	5.27	0.11
3069	494079	3878965	0.10	0.30	0.50	5.47	0.09
3070	494103	3878988	0.20	0.50	1.50	5.40	0.28
3071	494123	3878991	0.00	0.20	0.40	5.49	0.07
3072	494150	3878981	0.10	0.40	1.10	5.37	0.20
3073	494167	3878962	0.00	0.20	0.60	5.59	0.11
3074	494185	3878948	0.00	0.30	0.70	5.04	0.14
3075	494201	3878959	0.00	0.20	0.50	5.10	0.10
3076	494211	3878999	0.00	0.20	0.20	5.70	0.04
3077	494232	3879003	0.00	0.20	0.80	5.43	0.15
3078	494274	3878992	0.00	0.50	1.00	5.70	0.18
3079	494304	3879002	0.00	0.05	0.08	5.03	0.02
3080	494301	3879017	0.00	0.30	0.90	5.22	0.17
3081	494298	3879041	0.10	0.30	0.80	5.16	0.15
3082	494298	3879071	0.00	0.20	0.30	5.60	0.05

Table B1 (continued).

Site ID	Easting	Northing	Min	Max	Area	Width	Mean
3083	494308	3879089	0.00	0.20	0.50	5.21	0.10
3084	494334	3879100	0.00	0.10	0.20	5.32	0.04
3085	494357	3879096	0.04	0.40	1.00	5.52	0.18
3086	494377	3879084	0.04	0.40	0.90	5.57	0.16
3087	494400	3879055	0.00	0.20	0.30	5.39	0.06
3088	494417	3879040	0.00	0.20	0.40	5.34	0.07
3089	494440	3879035	0.00	0.60	1.40	5.43	0.26
3090	494469	3879033	0.02	0.20	0.70	4.98	0.14
3091	494492	3879029	0.00	0.30	0.70	5.12	0.14
3092	494514	3879023	0.10	0.40	1.40	5.21	0.27
3093	494522	3878996	0.00	0.30	0.30	5.31	0.06
3094	494520	3878970	0.00	0.10	0.10	5.54	0.02
3095	494521	3878941	0.00	0.20	0.20	5.21	0.04
3096	494517	3878911	0.00	0.20	0.10	5.47	0.02
3097	494540	3878892	0.10	0.30	1.00	5.43	0.18
3098	494572	3878883	0.10	0.20	0.80	5.36	0.15
3099	494610	3878837	0.00	0.40	0.80	5.11	0.16
3100	494614	3878808	0.00	0.20	0.30	5.25	0.06
3101	494607	3878783	0.00	0.10	0.20	5.28	0.04
3102	494564	3878769	0.00	0.10	0.06	5.17	0.01
3103	494565	3878745	0.00	0.20	0.50	5.37	0.09
3104	494584	3878728	0.00	0.40	0.70	5.54	0.13
3105	494588	3878692	0.00	0.30	0.60	5.31	0.11
3106	494607	3878673	0.00	0.10	0.30	5.21	0.06
3107	494629	3878690	0.00	0.20	0.50	5.31	0.09
3108	494652	3878705	0.00	0.10	0.40	5.25	0.08
3109	494680	3878713	0.00	0.30	1.00	5.36	0.19
3110	494700	3878693	0.00	0.00	0.00	5.01	0.00
3111	494695	3878656	0.00	0.20	0.40	3.75	0.11
3112	494702	3878637	0.00	0.10	0.63	3.85	0.16
3113	494726	3878640	0.00	0.00	0.40	4.98	0.08
3114	494739	3878645	0.00	0.20	0.50	5.57	0.09
3115	494760	3878652	0.00	0.10	0.40	5.21	0.08
3116	494777	3878670	0.00	0.20	0.60	4.76	0.13
3117	494788	3878690	0.02	0.20	0.50	5.32	0.09
3118	494803	3878716	0.02	0.30	0.90	5.38	0.17
3119	494803	3878742	0.00	0.00	0.00	5.00	0.00
3120	494814	3878759	0.00	0.15	0.30	5.10	0.06

Table B1 (continued).

Site ID	Easting	Northing	Min	Max	Area	Width	Mean
3121	494830	3878753	0.05	0.20	0.40	2.68	0.15
3122	494850	3878735	0.06	0.20	0.80	5.17	0.15
3123	494862	3878715	0.00	0.20	0.40	5.20	0.08
3124	494866	3878688	0.00	0.10	0.30	4.93	0.06
3125	494884	3878668	0.10	0.30	0.90	5.27	0.17
3126	494916	3878658	0.00	0.20	0.40	5.02	0.08
3127	494929	3878629	0.00	0.40	0.60	5.40	0.11
3128	494904	3878620	0.00	0.30	0.60	5.31	0.11
3129	494882	3878607	0.00	0.40	0.60	5.38	0.11
3130	494865	3878587	0.00	0.35	0.69	5.00	0.14
3131	494846	3878575	0.00	0.20	0.20	2.38	0.08
3132	494845	3878562	0.00	0.30	0.80	5.07	0.16
3133	494865	3878558	0.03	0.20	0.50	5.27	0.09
3134	494882	3878552	0.00	0.20	0.60	5.15	0.12
3135	494898	3878524	0.10	0.40	1.30	5.17	0.25
3136	494907	3878480	0.03	0.30	0.70	4.97	0.14
3137	494910	3878454	0.00	0.20	0.30	2.50	0.12
3138	494939	3878426	0.00	0.20	0.50	5.25	0.10
3139	494966	3878423	0.00	0.20	0.70	5.13	0.14
3140	495003	3878419	0.03	0.10	0.50	5.30	0.09
3141	495027	3878417	0.10	0.30	0.80	5.14	0.16
3142	495033	3878406	0.00	0.20	0.50	5.24	0.10
3143	491671	3873825	0.00	0.10	0.32	4.62	0.07
3144	491670	3873825	0.70	0.60	4.70	5.00	0.94
3145	491657	3873817	0.00	0.20	0.40	4.93	0.08
3146	491644	3873809	0.00	0.30	0.40	4.64	0.09
3150	491631	3873797	0.90	0.30	2.70	5.14	0.53
3151	491620	3873781	0.30	0.70	2.30	5.00	0.46
3152	491624	3873761	0.00	0.00	1.50	2.60	0.58
3158	491638	3873735	0.00	0.30	0.40	4.31	0.09
3160	491606	3873864	0.00	0.40	1.40	5.42	0.26
3161	491585	3873888	0.00	0.70	1.70	5.12	0.33
3162	491580	3873910	0.10	0.40	1.30	5.11	0.25
3163	491571	3873927	0.04	0.30	0.70	5.29	0.13
3164	491600	3873933	0.00	0.10	0.20	4.71	0.04
3165	491637	3873933	0.00	0.30	0.80	5.14	0.16
3166	491667	3873926	0.10	0.60	0.90	5.22	0.17
3167	491671	3873907	0.00	0.25	0.40	4.85	0.08

Table B1 (continued).

Site ID	Easting	Northing	Min	Max	Area	Width	Mean
3168	491705	3873898	0.00	0.25	0.35	5.00	0.07
3169	491712	3873884	0.10	0.30	1.30	5.20	0.25
3170	491715	3873867	0.00	0.30	0.40	5.36	0.07
3171	491724	3873848	0.00	0.30	0.60	4.61	0.13
3172	491738	3873836	0.00	0.00	0.00	5.00	0.00
3173	491748	3873818	0.00	0.10	0.10	5.17	0.02
3174	491759	3873808	0.00	0.30	1.10	5.47	0.20
3175	491771	3873796	0.00	0.00	0.00	5.00	0.00
3176	491794	3873777	0.00	0.20	0.50	4.79	0.10
3177	491808	3873765	0.00	0.00	0.00	5.00	0.00
3178	491824	3873755	0.00	0.30	0.70	5.49	0.13
3204	491478	3874015	0.00	0.50	0.73	3.24	0.23
3205	491467	3874036	0.00	0.50	1.40	5.38	0.26
3206	491454	3874064	0.10	0.30	0.90	5.26	0.17
3207	491423	3874086	0.20	0.40	1.40	5.07	0.28
3208	491207	3874198	0.06	0.30	0.90	5.17	0.17
3209	491187	3874187	0.00	0.25	0.36	3.42	0.11
3210	491169	3874170	0.10	0.30	1.00	5.17	0.19
3211	491160	3874148	0.00	0.60	0.71	2.03	0.35
3212	491141	3874128	0.00	0.30	0.74	5.00	0.15
1010037	504160	3871517	0.00	0.12	0.17	5.11	0.03
1010039	504157	3871529	0.00	1.13	2.64	5.10	0.52
1010040	504155	3871550	0.00	0.28	0.26	5.11	0.05
1010041	504159	3871570	0.00	0.99	1.11	5.17	0.21
1010042	504158	3871590	0.00	0.19	0.05	5.10	0.01
1010044	504151	3871627	0.00	0.10	0.01	5.29	0.00
1010045	504134	3871638	0.00	0.00	0.00	5.11	0.00
1010046	504122	3871655	0.00	0.40	0.34	5.13	0.07
1010047	504115	3871674	0.00	0.00	0.00	5.07	0.00
1010048	504103	3871691	0.00	0.17	0.22	5.08	0.04
1010049	504092	3871708	0.00	0.18	0.17	5.09	0.03
1010050	504085	3871729	0.00	0.46	0.17	5.09	0.03
1010053	504094	3871746	0.00	0.32	0.23	5.09	0.05
1010054	504106	3871764	0.00	0.00	0.00	5.10	0.00
1010062	504119	3871782	0.00	0.00	0.00	5.09	0.00
1010063	504112	3871801	0.00	0.30	0.85	5.08	0.17
1010064	504107	3871822	0.00	0.10	0.05	5.11	0.01
1010068	504121	3871839	0.00	0.15	0.06	5.14	0.01

Table B1 (continued).

Site ID	Easting	Northing	Min	Max	Area	Width	Mean
1010070	504147	3871870	0.00	0.27	0.15	2.26	0.07
1010073	504158	3871907	0.00	0.27	0.45	5.07	0.09
1010074	504168	3871925	0.00	0.26	0.72	5.15	0.14
1010075	504185	3871938	0.00	0.24	0.64	4.45	0.14
1010079	504185	3871959	0.00	0.50	1.10	5.09	0.22
1010080	504180	3871980	0.00	0.40	0.46	5.09	0.09
1010081	504160	3871986	0.00	0.28	0.17	5.09	0.03
1010082	504139	3871989	0.00	0.35	0.83	5.09	0.16
1010083	504123	3871999	0.00	0.52	0.84	1.66	0.51
1010084	504106	3872010	0.00	0.36	1.05	5.09	0.21
1010085	504088	3872019	0.00	0.00	0.00	5.09	0.00
1010086	504067	3872025	0.00	0.12	0.03	5.09	0.01
1010087	504046	3872024	0.00	0.27	0.48	5.09	0.09
1010088	504025	3872022	0.00	0.25	0.18	5.09	0.04
1010089	504007	3872033	0.00	0.30	0.26	5.20	0.05
1010090	503986	3872029	0.00	0.40	0.49	3.33	0.15
1010091	503967	3872031	0.00	0.32	0.72	5.09	0.14
1010092	503953	3872047	0.00	0.35	0.65	5.13	0.13
1010094	503953	3872068	0.00	0.65	1.59	5.10	0.31
1010095	503955	3872089	0.00	0.33	0.74	5.09	0.15
1010096	503962	3872110	0.00	0.00	0.00	5.09	0.00
1010097	503966	3872130	0.00	0.75	1.72	5.10	0.34
1010098	503969	3872150	0.00	0.16	0.13	4.70	0.03
1010099	503958	3872168	0.00	0.34	0.52	5.02	0.10
1010100	503937	3872176	0.00	0.00	0.00	5.09	0.00
1010101	503917	3872181	0.00	0.36	0.28	5.09	0.06
1010102	503902	3872198	0.00	0.60	1.24	3.75	0.33
1010103	503881	3872196	0.00	0.52	2.21	5.10	0.43
1010104	503863	3872184	0.10	0.56	1.79	5.09	0.35
1010105	503845	3872173	0.30	0.75	3.10	5.09	0.61
1010106	503825	3872167	0.00	0.25	0.25	5.09	0.05
1010179	497498	3868572	0.14	0.32	1.17	5.11	0.23
1010180	497498	3868551	0.33	0.84	3.21	5.18	0.62
1010181	497481	3868538	0.13	0.47	1.53	5.09	0.30
1010183	497463	3868529	0.00	1.44	4.44	5.12	0.87
1010184	497446	3868517	0.00	0.00	0.00	5.09	0.00
1010188	497426	3868514	0.43	0.61	2.72	5.16	0.53
1010189	497409	3868526	0.00	0.00	0.00	2.63	0.00

Table B1 (continued).

Site ID	Easting	Northing	Min	Max	Area	Width	Mean
1010190	497388	3868533	0.51	0.89	2.79	3.32	0.84
1010191	497374	3868550	0.36	0.66	1.66	2.95	0.56
1010192	497364	3868568	0.00	0.30	0.26	5.09	0.05
1010193	497355	3868586	0.00	0.50	1.32	5.09	0.26
1010194	497352	3868608	0.00	0.00	0.00	5.09	0.00
1010195	497341	3868624	0.00	0.33	0.94	5.11	0.18
1010196	497324	3868634	0.00	0.28	0.52	5.08	0.10
1010197	497308	3868648	0.00	0.29	0.63	3.92	0.16
1010198	497298	3868664	0.00	0.08	0.16	5.13	0.03
1010199	497268	3868670	0.00	0.32	0.83	5.11	0.16
1010200	497263	3868649	0.00	0.26	0.73	5.12	0.14
1010201	497256	3868629	0.07	0.64	1.36	5.15	0.26
1010202	497249	3868610	0.19	0.41	1.50	5.09	0.29
1010203	497245	3868586	0.11	0.38	1.26	5.13	0.25
1010204	497224	3868593	0.28	0.79	2.80	5.08	0.55
1010205	497209	3868609	0.05	0.61	1.61	5.07	0.32
1010206	497193	3868624	0.08	0.29	0.84	5.07	0.17
1010207	497175	3868636	0.22	0.40	1.44	5.09	0.28
1010208	497156	3868644	0.00	0.25	0.61	5.08	0.12
1010209	497135	3868649	0.18	0.51	1.82	5.09	0.36
1010210	497111	3868654	0.00	0.50	1.28	5.13	0.25
1010211	497091	3868658	0.28	0.57	1.18	2.84	0.42
1010214	497034	3868677	0.00	0.15	0.32	5.06	0.06
1010215	497023	3868695	0.00	0.42	0.82	3.65	0.22
1010216	497009	3868712	0.16	0.64	1.81	5.14	0.35
1010217	496994	3868726	0.05	0.20	0.64	5.09	0.13
1010218	496974	3868735	0.00	0.52	1.33	5.11	0.26
1010219	496952	3868733	0.19	0.56	1.62	4.40	0.37
1010220	496930	3868731	0.32	0.62	2.72	5.08	0.54
1010221	496903	3868739	0.34	0.54	1.08	2.24	0.48
1010222	496888	3868753	0.32	1.07	3.30	5.11	0.65
1010223	496875	3868769	0.00	0.33	0.91	5.09	0.18
1010225	496857	3868777	0.12	0.26	0.97	5.12	0.19
1010226	496834	3868775	0.39	0.64	1.09	2.17	0.50
1020001	496815	3868777	0.07	0.28	0.78	5.08	0.15
1020002	496794	3868774	0.05	0.47	1.04	5.12	0.20
1020003	496771	3868775	0.12	0.61	1.89	5.07	0.37
1020004	496750	3868780	0.18	0.35	1.15	4.26	0.27

Table B1 (continued).

Site ID	Easting	Northing	Min	Max	Area	Width	Mean
1020005	496730	3868785	0.09	0.40	1.00	4.27	0.23
1020006	496712	3868770	0.16	0.43	1.19	3.28	0.36
1020007	496695	3868756	0.05	0.42	1.00	5.21	0.19
1020008	496678	3868743	0.03	0.45	1.11	5.10	0.22
1020009	496661	3868729	0.00	0.00	0.00	1.95	0.00
1020010	496642	3868745	0.00	0.23	0.42	5.10	0.08
1020011	496641	3868766	0.00	0.26	0.41	5.09	0.08
1020012	496637	3868790	0.00	0.30	0.59	5.13	0.12
1020014	496592	3868824	0.81	1.10	4.54	4.72	0.96
1020015	496578	3868840	0.23	0.50	1.88	5.06	0.37
1020016	496572	3868860	0.12	0.51	1.87	5.18	0.36
1020017	496563	3868880	0.04	0.32	1.05	5.08	0.21
1020018	496548	3868897	0.00	0.43	1.01	5.09	0.20
1020019	496532	3868910	0.00	0.65	2.35	5.29	0.44
1020020	496540	3868929	0.58	0.99	2.70	3.28	0.82
1020021	496559	3868942	0.13	0.52	1.39	5.09	0.27
1020022	496575	3868953	0.00	0.59	1.12	5.11	0.22
P1	497719	3877449	n/a	n/a	n/a	n/a	0.20
P2	497742	3877393	n/a	n/a	n/a	n/a	0.17
P3	497760	3877370	n/a	n/a	n/a	n/a	0.08
P4	497752	3877340	n/a	n/a	n/a	n/a	0.08
P6	497795	3877460	n/a	n/a	n/a	n/a	0.21
P7	497802	3877460	n/a	n/a	n/a	n/a	0.15
P8	497790	3877524	n/a	n/a	n/a	n/a	0.40
P10	497846	3877792	n/a	n/a	n/a	n/a	0.22
Astart	495502	3876008	n/a	n/a	n/a	n/a	0.08
A1	495493	3876001	n/a	n/a	n/a	n/a	0.10
A2	495479	3875986	n/a	n/a	n/a	n/a	0.10
A3	495479	3875989	n/a	n/a	n/a	n/a	0.08
A4	495478	3875987	n/a	n/a	n/a	n/a	0.16
A5	495463	3875983	n/a	n/a	n/a	n/a	0.02
A6	495449	3875987	n/a	n/a	n/a	n/a	0.08
A7	495433	3875982	n/a	n/a	n/a	n/a	0.09
A8	495421	3875970	n/a	n/a	n/a	n/a	0.11
A9	495421	3875974	n/a	n/a	n/a	n/a	0.10
A10	495411	3875961	n/a	n/a	n/a	n/a	0.16
A11	495394	3875944	n/a	n/a	n/a	n/a	0.00
A12	495384	3875943	n/a	n/a	n/a	n/a	0.01

Table B1 (continued).

Site ID	Easting	Northing	Min	Max	Area	Width	Mean
S01	495726	3875879	n/a	n/a	n/a	n/a	0.00
S02	495722	3875722	n/a	n/a	n/a	n/a	0.18
S03	495704	3875887	n/a	n/a	n/a	n/a	0.03
S04	495685	3875896	n/a	n/a	n/a	n/a	0.00
S05	495663	3875909	n/a	n/a	n/a	n/a	0.10
S06	495643	3875907	n/a	n/a	n/a	n/a	0.00
S07	495624	3875912	n/a	n/a	n/a	n/a	0.10
S08	495600	3875923	n/a	n/a	n/a	n/a	0.04
S09	495587	3875935	n/a	n/a	n/a	n/a	0.16
S10	495573	3875939	n/a	n/a	n/a	n/a	0.12
S11	495553	3875950	n/a	n/a	n/a	n/a	0.11
S12	495525	3875963	n/a	n/a	n/a	n/a	0.08
S13	495519	3875971	n/a	n/a	n/a	n/a	0.15
S14	495526	3875987	n/a	n/a	n/a	n/a	0.03
S15	495506	3876006	n/a	n/a	n/a	n/a	0.03
S16	495488	3876022	n/a	n/a	n/a	n/a	0.00
S17	495483	3876038	n/a	n/a	n/a	n/a	0.01
S18	495459	3876054	n/a	n/a	n/a	n/a	0.12
S19	495452	3876068	n/a	n/a	n/a	n/a	0.05
S20	495429	3876070	n/a	n/a	n/a	n/a	0.17
S21	495429	3876092	n/a	n/a	n/a	n/a	0.16
S22	495420	3876089	n/a	n/a	n/a	n/a	0.16
S23	495404	3876095	n/a	n/a	n/a	n/a	0.20
S24	495386	3876090	n/a	n/a	n/a	n/a	0.20
S25	495361	3876156	n/a	n/a	n/a	n/a	0.01
S26	495329	3876140	n/a	n/a	n/a	n/a	0.10
S27	495286	3876209	n/a	n/a	n/a	n/a	0.05
S28	495284	3876222	n/a	n/a	n/a	n/a	0.00
RD1	495358	3875951	n/a	n/a	n/a	n/a	0.10
RD2	495341	3875996	n/a	n/a	n/a	n/a	0.05
RD3	493992	3875152	n/a	n/a	n/a	n/a	0.30
N1	495530	3875966	n/a	n/a	n/a	n/a	0.10
K001	494060	3875277	n/a	n/a	n/a	n/a	0.01
K002	494056	3875272	n/a	n/a	n/a	n/a	0.15
K003	494044	3875256	n/a	n/a	n/a	n/a	0.11
K004	494033	3875252	n/a	n/a	n/a	n/a	0.40
K006	494022	3875252	n/a	n/a	n/a	n/a	0.00
A13	495374	3875934	n/a	n/a	n/a	n/a	0.00

Table B1 (continued).

Site ID	Easting	Northing	Min	Max	Area	Width	Mean
K007	494023	3875236	n/a	n/a	n/a	n/a	0.13
K008	494016	3875235	n/a	n/a	n/a	n/a	0.05
K009	494009	3875230	n/a	n/a	n/a	n/a	0.18
K010	494001	3875225	n/a	n/a	n/a	n/a	0.17
K011	493992	3875214	n/a	n/a	n/a	n/a	0.05
K012	493978	3875185	n/a	n/a	n/a	n/a	0.00

Table B.2. Landscape attribute data obtained through GIS analysis of soil profiles.

	Explanation of column headings
Site ID	Individual record identifier; photograph site identifiers begin with a number (e.g. 1010037). Field excavation site identifiers begin with a letter (e.g.A1).
Elev	Elevation (meters above mean sea level) obtained from DEM overlay of soil sites.
Slope	Slope (degrees) obtained from overlay of DEM-derived slope grid with soil sites.
Aspect	Aspect (degrees) obtained from overlay of DEM-derived aspect grid with soil sites.
MAP	Total mean annual precipitation (mm) obtained from shapefile-derived grid overlay of rainfall data with mapped soil profiles.
Lithology	Substratum lithology, obtained from overlay of 1:250,000 geological map with mapped soil profiles.
Wtrshd	Watershed in which soil profile is located, determined from 1:50,000 stream maps.

Site ID	Elev	Slope	Aspect	MAP	Lithology	Wtrshd
2970	527	12	301	387	Sheeted Dikes (Diabase)	Elia
2972	530	13	283	387	Sheeted Dikes (Diabase)	Elia
2973	536	17	276	387	Basal Group	Elia
2974	540	12	277	387	Basal Group	Elia
2976	539	8	270	387	Basal Group	Elia
2977	540	7	286	386	Basal Group	Elia
2978	540	8	316	386	Basal Group	Elia
2982	538	13	332	386	Basal Group	Elia
2983	538	14	344	386	Basal Group	Elia
2984	538	14	84	386	Basal Group	Elia
2985	537	14	34	386	Basal Group	Elia
2986	539	14	48	386	Basal Group	Elia
2987	543	13	51	386	Basal Group	Elia
2988	546	14	53	387	Basal Group	Elia
2989	546	17	59	387	Basal Group	Elia
2990	545	18	61	387	Basal Group	Elia
2991	548	21	61	387	Basal Group	Elia
2992	548	23	59	388	Basal Group	Elia

Table B.2 (continued).

Site ID	Elev	Slope	Aspect	MAP	Lithology	Wtrshd
2993	548	23	59	388	Basal Group	Elia
2994	550	23	52	388	Basal Group	Elia
2995	555	23	46	388	Basal Group	Elia
2996	560	24	46	389	Basal Group	Elia
2997	566	23	63	389	Basal Group	Elia
2998	566	24	67	389	Basal Group	Elia
2999	567	23	53	390	Basal Group	Elia
3000	570	22	36	390	Basal Group	Elia
3001	575	20	82	390	Basal Group	Elia
3003	581	21	263	391	Basal Group	Elia
3004	585	20	335	391	Basal Group	Elia
3005	572	27	325	390	Basal Group	Elia
3007	578	26	335	390	Basal Group	Elia
3008	579	24	313	390	Basal Group	Elia
3009	579	26	60	390	Basal Group	Elia
3010	579	25	22	390	Basal Group	Elia
3011	578	24	156	390	Basal Group	Elia
3012	582	22	185	390	Basal Group	Elia
3013	589	22	59	390	Basal Group	Elia
3014	593	19	228	391	Basal Group	Elia
3015	589	17	327	391	Basal Group	Elia
3016	591	20	289	390	Basal Group	Elia
3017	588	17	17	389	Basal Group	Elia
3020	591	21	137	389	Basal Group	Elia
3021	601	21	118	390	Basal Group	Elia
3022	603	19	19	390	Basal Group	Elia
3026	604	19	11	390	Basal Group	Elia
3030	604	20	11	390	Basal Group	Elia
3031	603	23	12	390	Basal Group	Elia
3032	602	23	17	390	Basal Group	Elia
3033	604	21	47	390	Basal Group	Elia
3034	605	17	10	390	Basal Group	Elia
3035	607	17	210	390	Basal Group	Elia
3036	610	16	340	391	Basal Group	Elia
3037	610	15	306	390	Basal Group	Elia
3038	611	16	277	390	Basal Group	Elia
3039	616	14	259	390	Basal Group	Elia
3040	620	10	238	390	Basal Group	Elia

Table B.2 (continued).

Site ID	Elev	Slope	Aspect	MAP	Lithology	Wtrshd
3041	454	14	214	379	Sheeted Dikes (Diabase)	Atsas
3042	458	9	213	379	Sheeted Dikes (Diabase)	Atsas
3043	460	3	215	379	Sheeted Dikes (Diabase)	Atsas
3044	460	0	222	379	Sheeted Dikes (Diabase)	Atsas
3045	460	1	165	378	Sheeted Dikes (Diabase)	Atsas
3046	460	1	171	378	Sheeted Dikes (Diabase)	Atsas
3047	460	1	246	378	Sheeted Dikes (Diabase)	Atsas
3048	462	6	293	378	Sheeted Dikes (Diabase)	Atsas
3050	467	14	293	377	Sheeted Dikes (Diabase)	Atsas
3051	466	13	245	377	Sheeted Dikes (Diabase)	Atsas
3052	469	14	221	377	Sheeted Dikes (Diabase)	Atsas
3053	476	12	217	376	Sheeted Dikes (Diabase)	Atsas
3054	479	7	238	376	Sheeted Dikes (Diabase)	Atsas
3056	480	0	158	376	Sheeted Dikes (Diabase)	Atsas
3057	480	0	-1	375	Sheeted Dikes (Diabase)	Atsas
3058	480	0	23	375	Sheeted Dikes (Diabase)	Atsas
3059	480	0	-1	374	Sheeted Dikes (Diabase)	Atsas
3060	480	2	304	374	Sheeted Dikes (Diabase)	Atsas
3062	479	8	328	373	Sheeted Dikes (Diabase)	Atsas
3063	479	7	308	373	Sheeted Dikes (Diabase)	Atsas
3064	480	8	312	373	Sheeted Dikes (Diabase)	Atsas
3065	479	10	311	372	Sheeted Dikes (Diabase)	Atsas
3066	482	12	310	372	Sheeted Dikes (Diabase)	Atsas
3067	486	14	315	372	Sheeted Dikes (Diabase)	Atsas
3068	483	16	319	372	Sheeted Dikes (Diabase)	Atsas
3069	488	15	339	372	Sheeted Dikes (Diabase)	Atsas
3070	483	16	270	371	Sheeted Dikes (Diabase)	Atsas
3071	483	16	162	371	Sheeted Dikes (Diabase)	Atsas
3072	483	12	101	371	Sheeted Dikes (Diabase)	Atsas
3073	489	15	324	371	Sheeted Dikes (Diabase)	Atsas
3074	494	15	352	371	Sheeted Dikes (Diabase)	Atsas
3075	492	16	347	371	Sheeted Dikes (Diabase)	Atsas
3076	481	9	349	371	Sheeted Dikes (Diabase)	Atsas
3077	481	10	324	371	Sheeted Dikes (Diabase)	Atsas
3078	492	17	294	371	Sheeted Dikes (Diabase)	Atsas
3079	499	9	277	370	Sheeted Dikes (Diabase)	Atsas
3080	499	7	257	370	Sheeted Dikes (Diabase)	Atsas
3081	500	6	264	370	Sheeted Dikes (Diabase)	Atsas

Table B.2 (continued).

Site ID	Elev	Slope	Aspect	MAP	Lithology	Wtrshd
3082	500	11	318	370	Sheeted Dikes (Diabase)	Atsas
3083	497	16	341	369	Sheeted Dikes (Diabase)	Atsas
3084	495	19	152	369	Sheeted Dikes (Diabase)	Atsas
3085	494	20	19	369	Sheeted Dikes (Diabase)	Atsas
3086	497	21	28	369	Sheeted Dikes (Diabase)	Atsas
3087	501	20	28	370	Sheeted Dikes (Diabase)	Atsas
3088	502	19	19	370	Sheeted Dikes (Diabase)	Atsas
3089	502	19	10	370	Sheeted Dikes (Diabase)	Atsas
3090	502	16	54	370	Sheeted Dikes (Diabase)	Atsas
3091	501	8	17	370	Sheeted Dikes (Diabase)	Atsas
3092	500	3	44	370	Sheeted Dikes (Diabase)	Atsas
3093	500	6	81	370	Sheeted Dikes (Diabase)	Elia
3094	501	14	102	370	Sheeted Dikes (Diabase)	Elia
3095	502	20	89	371	Sheeted Dikes (Diabase)	Elia
3096	504	19	73	371	Sheeted Dikes (Diabase)	Elia
3097	500	19	45	371	Sheeted Dikes (Diabase)	Elia
3098	496	24	37	371	Sheeted Dikes (Diabase)	Elia
3099	498	22	64	372	Sheeted Dikes (Diabase)	Elia
3100	501	19	91	372	Sheeted Dikes (Diabase)	Elia
3101	499	18	111	372	Sheeted Dikes (Diabase)	Elia
3102	510	17	119	373	Sheeted Dikes (Diabase)	Elia
3103	505	14	102	373	Sheeted Dikes (Diabase)	Elia
3104	502	11	67	373	Sheeted Dikes (Diabase)	Elia
3105	504	12	39	374	Sheeted Dikes (Diabase)	Elia
3106	506	12	190	374	Sheeted Dikes (Diabase)	Elia
3107	503	11	212	374	Sheeted Dikes (Diabase)	Elia
3108	503	12	7	373	Sheeted Dikes (Diabase)	Elia
3109	498	15	17	373	Sheeted Dikes (Diabase)	Elia
3110	500	9	28	373	Sheeted Dikes (Diabase)	Elia
3111	504	11	45	374	Sheeted Dikes (Diabase)	Elia
3112	506	12	131	374	Sheeted Dikes (Diabase)	Elia
3113	505	11	345	374	Sheeted Dikes (Diabase)	Elia
3114	505	12	330	374	Sheeted Dikes (Diabase)	Elia
3115	507	13	315	374	Sheeted Dikes (Diabase)	Elia
3116	508	14	306	374	Sheeted Dikes (Diabase)	Elia
3117	507	14	307	373	Sheeted Dikes (Diabase)	Elia
3118	507	11	204	373	Sheeted Dikes (Diabase)	Elia
3119	504	12	207	373	Sheeted Dikes (Diabase)	Elia

Table B.2 (continued).

Site ID	Elev	Slope	Aspect	MAP	Lithology	Wtrshd
3120	501	9	79	372	Sheeted Dikes (Diabase)	Elia
3121	501	9	34	372	Sheeted Dikes (Diabase)	Elia
3122	503	14	47	373	Sheeted Dikes (Diabase)	Elia
3123	503	15	47	373	Sheeted Dikes (Diabase)	Elia
3124	508	15	48	373	Sheeted Dikes (Diabase)	Elia
3125	507	16	67	373	Sheeted Dikes (Diabase)	Elia
3126	501	10	53	374	Sheeted Dikes (Diabase)	Elia
3127	500	3	107	374	Sheeted Dikes (Diabase)	Elia
3128	501	8	116	374	Sheeted Dikes (Diabase)	Elia
3129	506	15	111	374	Sheeted Dikes (Diabase)	Elia
3130	507	15	110	374	Sheeted Dikes (Diabase)	Elia
3131	511	14	101	375	Sheeted Dikes (Diabase)	Elia
3132	512	15	81	375	Sheeted Dikes (Diabase)	Elia
3133	507	14	73	375	Sheeted Dikes (Diabase)	Elia
3134	503	11	66	375	Sheeted Dikes (Diabase)	Elia
3135	503	11	60	375	Sheeted Dikes (Diabase)	Elia
3136	507	15	59	376	Sheeted Dikes (Diabase)	Elia
3137	510	14	60	376	Sheeted Dikes (Diabase)	Elia
3138	508	12	32	376	Sheeted Dikes (Diabase)	Elia
3139	507	11	27	376	Sheeted Dikes (Diabase)	Elia
3140	503	9	42	376	Sheeted Dikes (Diabase)	Elia
3141	500	5	47	376	Sheeted Dikes (Diabase)	Elia
3142	501	6	50	377	Sheeted Dikes (Diabase)	Elia
3143	640	7	266	538	Sheeted Dikes (Diabase)	Kargotis
3144	640	7	266	538	Sheeted Dikes (Diabase)	Kargotis
3145	640	3	214	538	Sheeted Dikes (Diabase)	Kargotis
3146	640	0	53	539	Sheeted Dikes (Diabase)	Kargotis
3150	640	1	99	539	Sheeted Dikes (Diabase)	Kargotis
3151	640	3	299	540	Sheeted Dikes (Diabase)	Kargotis
3152	640	7	307	541	Sheeted Dikes (Diabase)	Kargotis
3158	646	16	291	542	Sheeted Dikes (Diabase)	Kargotis
3160	631	13	299	536	Sheeted Dikes (Diabase)	Kargotis
3161	625	12	276	535	Sheeted Dikes (Diabase)	Kargotis
3162	625	12	249	534	Sheeted Dikes (Diabase)	Kargotis
3163	625	14	226	534	Sheeted Dikes (Diabase)	Kargotis
3164	632	15	231	533	Sheeted Dikes (Diabase)	Kargotis
3165	640	15	236	533	Sheeted Dikes (Diabase)	Kargotis
3166	646	16	241	533	Sheeted Dikes (Diabase)	Kargotis

Table B.2 (continued).

Site ID	Elev	Slope	Aspect	MAP	Lithology	Wtrshd
3167	646	15	251	534	Sheeted Dikes (Diabase)	Kargotis
3168	655	17	255	534	Sheeted Dikes (Diabase)	Kargotis
3169	656	17	259	534	Sheeted Dikes (Diabase)	Kargotis
3170	656	18	263	535	Sheeted Dikes (Diabase)	Kargotis
3171	659	19	266	536	Sheeted Dikes (Diabase)	Kargotis
3172	663	20	264	536	Sheeted Dikes (Diabase)	Kargotis
3173	665	21	257	537	Sheeted Dikes (Diabase)	Kargotis
3174	668	23	252	537	Sheeted Dikes (Diabase)	Kargotis
3175	671	24	253	538	Sheeted Dikes (Diabase)	Kargotis
3176	679	22	249	538	Sheeted Dikes (Diabase)	Kargotis
3177	683	16	242	539	Sheeted Dikes (Diabase)	Kargotis
3178	683	13	230	539	Sheeted Dikes (Diabase)	Kargotis
3204	616	18	276	530	Sheeted Dikes (Diabase)	Kargotis
3205	609	21	270	529	Sheeted Dikes (Diabase)	Kargotis
3206	604	19	256	528	Sheeted Dikes (Diabase)	Kargotis
3207	601	8	224	527	Sheeted Dikes (Diabase)	Kargotis
3208	583	13	207	524	Sheeted Dikes (Diabase)	Kargotis
3209	581	8	180	525	Sheeted Dikes (Diabase)	Kargotis
3210	580	6	220	526	Sheeted Dikes (Diabase)	Kargotis
3211	580	5	276	527	Sheeted Dikes (Diabase)	Kargotis
3212	580	6	287	528	Sheeted Dikes (Diabase)	Kargotis
1010037	931	33	293	570	Sheeted Dikes (Diabase)	Elia
1010039	926	34	293	569	Sheeted Dikes (Diabase)	Elia
1010040	920	34	287	568	Sheeted Dikes (Diabase)	Elia
1010041	924	35	272	568	Sheeted Dikes (Diabase)	Elia
1010042	918	33	263	567	Sheeted Dikes (Diabase)	Elia
1010044	923	37	242	566	Sheeted Dikes (Diabase)	Elia
1010045	916	37	243	566	Sheeted Dikes (Diabase)	Elia
1010046	913	37	245	565	Sheeted Dikes (Diabase)	Elia
1010047	913	36	251	565	Sheeted Dikes (Diabase)	Elia
1010048	910	31	255	564	Sheeted Dikes (Diabase)	Elia
1010049	907	27	262	564	Sheeted Dikes (Diabase)	Elia
1010050	904	27	283	563	Sheeted Dikes (Diabase)	Elia
1010053	904	32	299	562	Sheeted Dikes (Diabase)	Elia
1010054	904	33	297	561	Sheeted Dikes (Diabase)	Elia
1010062	904	32	285	561	Sheeted Dikes (Diabase)	Elia
1010063	903	29	277	560	Sheeted Dikes (Diabase)	Elia
1010064	897	29	296	559	Sheeted Dikes (Diabase)	Elia

Table B.2 (continued).

Site ID	Elev	Slope	Aspect	MAP	Lithology	Wtrshd
1010068	897	29	306	558	Sheeted Dikes (Diabase)	Elia
1010070	901	31	295	557	Sheeted Dikes (Diabase)	Elia
1010073	895	34	314	555	Sheeted Dikes (Diabase)	Elia
1010074	890	30	310	555	Sheeted Dikes (Diabase)	Elia
1010075	893	30	296	554	Sheeted Dikes (Diabase)	Elia
1010079	891	28	279	553	Sheeted Dikes (Diabase)	Elia
1010080	887	25	269	552	Sheeted Dikes (Diabase)	Elia
1010081	879	22	244	552	Sheeted Dikes (Diabase)	Elia
1010082	874	26	219	553	Sheeted Dikes (Diabase)	Elia
1010083	877	32	200	553	Sheeted Dikes (Diabase)	Elia
1010084	881	34	196	552	Sheeted Dikes (Diabase)	Elia
1010085	883	34	200	552	Sheeted Dikes (Diabase)	Elia
1010086	881	32	199	552	Sheeted Dikes (Diabase)	Elia
1010087	878	32	189	552	Sheeted Dikes (Diabase)	Elia
1010088	875	32	186	553	Sheeted Dikes (Diabase)	Elia
1010089	881	29	188	553	Sheeted Dikes (Diabase)	Elia
1010090	877	28	188	553	Sheeted Dikes (Diabase)	Elia
1010091	877	24	193	553	Sheeted Dikes (Diabase)	Elia
1010092	880	20	231	553	Sheeted Dikes (Diabase)	Elia
1010094	883	22	264	552	Sheeted Dikes (Diabase)	Elia
1010095	882	24	284	551	Sheeted Dikes (Diabase)	Elia
1010096	881	24	291	550	Sheeted Dikes (Diabase)	Elia
1010097	880	23	290	549	Sheeted Dikes (Diabase)	Elia
1010098	877	20	272	548	Basal Group	Elia
1010099	876	21	232	548	Basal Group	Elia
1010100	875	24	208	548	Basal Group	Elia
1010101	874	27	204	548	Sheeted Dikes (Diabase)	Elia
1010102	878	26	206	547	Sheeted Dikes (Diabase)	Elia
1010103	872	26	193	548	Sheeted Dikes (Diabase)	Elia
1010104	865	26	176	548	Sheeted Dikes (Diabase)	Elia
1010105	863	28	161	549	Sheeted Dikes (Diabase)	Elia
1010106	864	31	164	550	Sheeted Dikes (Diabase)	Elia
1010179	1235	16	307	739	Sheeted Dikes (Diabase)	Elia
1010180	1238	18	301	740	Sheeted Dikes (Diabase)	Elia
1010181	1234	19	308	740	Sheeted Dikes (Diabase)	Elia
1010183	1232	19	327	740	Sheeted Dikes (Diabase)	Elia
1010184	1234	22	348	741	Sheeted Dikes (Diabase)	Elia
1010188	1236	23	107	741	Sheeted Dikes (Diabase)	Elia

Table B.2 (continued).

Site ID	Elev	Slope	Aspect	MAP	Lithology	Wtrshd
1010189	1233	24	17	740	Sheeted Dikes (Diabase)	Elia
1010190	1233	26	30	740	Sheeted Dikes (Diabase)	Elia
1010191	1231	28	45	740	Sheeted Dikes (Diabase)	Elia
1010192	1229	28	51	740	Sheeted Dikes (Diabase)	Elia
1010193	1227	28	53	740	Sheeted Dikes (Diabase)	Elia
1010194	1221	27	56	740	Sheeted Dikes (Diabase)	Elia
1010195	1221	27	56	739	Sheeted Dikes (Diabase)	Elia
1010196	1226	26	56	739	Sheeted Dikes (Diabase)	Elia
1010197	1229	24	48	739	Sheeted Dikes (Diabase)	Elia
1010198	1228	23	41	739	Sheeted Dikes (Diabase)	Elia
1010199	1229	16	146	740	Sheeted Dikes (Diabase)	Elia
1010200	1237	15	329	740	Sheeted Dikes (Diabase)	Elia
1010201	1236	13	294	741	Sheeted Dikes (Diabase)	Elia
1010202	1236	15	299	741	Sheeted Dikes (Diabase)	Elia
1010203	1239	12	308	741	Sheeted Dikes (Diabase)	Elia
1010204	1232	15	322	742	Sheeted Dikes (Diabase)	Elia
1010205	1226	16	328	742	Sheeted Dikes (Diabase)	Elia
1010206	1221	14	328	742	Sheeted Dikes (Diabase)	Elia
1010207	1216	17	339	741	Sheeted Dikes (Diabase)	Elia
1010208	1213	18	270	741	Sheeted Dikes (Diabase)	Elia
1010209	1211	19	302	741	Sheeted Dikes (Diabase)	Elia
1010210	1208	18	342	741	Sheeted Dikes (Diabase)	Elia
1010211	1204	19	331	741	Sheeted Dikes (Diabase)	Elia
1010214	1190	14	359	741	Sheeted Dikes (Diabase)	Elia
1010215	1188	16	81	740	Sheeted Dikes (Diabase)	Elia
1010216	1186	15	30	740	Sheeted Dikes (Diabase)	Elia
1010217	1185	15	33	739	Plagiogranite	Elia
1010218	1186	17	24	739	Plagiogranite	Elia
1010219	1189	18	19	739	Plagiogranite	Elia
1010220	1192	19	17	739	Plagiogranite	Elia
1010221	1192	18	17	739	Plagiogranite	Elia
1010222	1189	16	19	739	Plagiogranite	Elia
1010223	1186	16	19	739	Plagiogranite	Elia
1010225	1186	16	14	738	Plagiogranite	Elia
1010226	1187	16	7	738	Plagiogranite	Elia
1020001	1187	17	4	738	Plagiogranite	Elia
1020002	1189	18	3	739	Plagiogranite	Elia
1020003	1189	18	1	739	Plagiogranite	Elia

Table B.2 (continued).

Site ID	Elev	Slope	Aspect	MAP	Lithology	Wtrshd
1020004	1187	17	1	739	Plagiogranite	Elia
1020005	1186	15	198	738	Plagiogranite	Elia
1020006	1189	16	337	739	Plagiogranite	Elia
1020007	1189	18	316	739	Plagiogranite	Elia
1020008	1188	18	320	740	Plagiogranite	Elia
1020009	1188	16	334	740	Plagiogranite	Elia
1020010	1183	13	129	740	Plagiogranite	Elia
1020011	1178	13	11	740	Plagiogranite	Elia
1020012	1172	16	25	740	Plagiogranite	Elia
1020014	1172	17	13	739	Plagiogranite	Elia
1020015	1167	16	28	738	Plagiogranite	Elia
1020016	1163	14	39	738	Plagiogranite	Elia
1020017	1161	10	50	737	Plagiogranite	Elia
1020018	1162	13	81	737	Plagiogranite	Elia
1020019	1166	16	98	736	Plagiogranite	Elia
1020020	1167	17	129	736	Plagiogranite	Elia
1020021	1166	15	130	735	Plagiogranite	Elia
1020022	1165	15	129	735	Plagiogranite	Elia
P1	576	26	355	391	Sheeted Dikes (Diabase)	Elia
P2	606	25	293	392	Sheeted Dikes (Diabase)	Elia
P3	606	24	261	392	Sheeted Dikes (Diabase)	Elia
P4	597	24	234	392	Sheeted Dikes (Diabase)	Elia
P6	586	25	310	391	Sheeted Dikes (Diabase)	Elia
P7	586	25	307	391	Sheeted Dikes (Diabase)	Elia
P8	585	21	271	390	Sheeted Dikes (Diabase)	Elia
P10	536	15	57	386	Basal Group	Elia
Astart	708	27	15	423	Sheeted Dikes (Diabase)	Elia
A1	712	21	72	424	Sheeted Dikes (Diabase)	Elia
A2	716	16	284	424	Sheeted Dikes (Diabase)	Elia
A3	715	16	271	424	Sheeted Dikes (Diabase)	Elia
A4	716	16	282	424	Sheeted Dikes (Diabase)	Elia
A5	713	17	289	424	Sheeted Dikes (Diabase)	Elia
A6	708	20	280	424	Sheeted Dikes (Diabase)	Elia
A7	701	23	271	425	Sheeted Dikes (Diabase)	Elia
A8	695	24	267	425	Sheeted Dikes (Diabase)	Elia
A9	695	24	269	425	Sheeted Dikes (Diabase)	Elia
A10	690	22	267	425	Sheeted Dikes (Diabase)	Elia
A11	684	18	270	426	Sheeted Dikes (Diabase)	Elia

Table B.2 (continued).

Site ID	Elev	Slope	Aspect	MAP	Lithology	Wtrshd
A12	681	17	272	426	Sheeted Dikes (Diabase)	Elia
A13	678	16	276	427	Sheeted Dikes (Diabase)	Elia
S01	771	24	330	429	Sheeted Dikes (Diabase)	Elia
S02	754	23	199	435	Sheeted Dikes (Diabase)	Elia
S03	760	29	327	428	Sheeted Dikes (Diabase)	Elia
S04	750	29	332	428	Sheeted Dikes (Diabase)	Elia
S05	741	26	332	427	Sheeted Dikes (Diabase)	Elia
S06	739	18	300	427	Sheeted Dikes (Diabase)	Elia
S07	738	14	64	427	Sheeted Dikes (Diabase)	Elia
S08	739	17	22	427	Sheeted Dikes (Diabase)	Elia
S09	736	23	91	426	Sheeted Dikes (Diabase)	Elia
S10	735	22	194	426	Sheeted Dikes (Diabase)	Elia
S11	729	23	251	426	Sheeted Dikes (Diabase)	Elia
S12	723	18	233	425	Sheeted Dikes (Diabase)	Elia
S13	722	18	125	425	Sheeted Dikes (Diabase)	Elia
S14	715	25	14	424	Sheeted Dikes (Diabase)	Elia
S15	708	27	15	423	Sheeted Dikes (Diabase)	Elia
S16	704	30	38	423	Sheeted Dikes (Diabase)	Elia
S17	694	33	14	422	Sheeted Dikes (Diabase)	Elia
S18	686	31	152	421	Sheeted Dikes (Diabase)	Elia
S19	679	26	125	421	Sheeted Dikes (Diabase)	Elia
S20	679	22	262	421	Sheeted Dikes (Diabase)	Elia
S21	671	22	213	420	Sheeted Dikes (Diabase)	Elia
S22	672	21	334	420	Sheeted Dikes (Diabase)	Elia
S23	668	23	338	420	Sheeted Dikes (Diabase)	Elia
S24	667	24	324	420	Sheeted Dikes (Diabase)	Elia
S25	630	18	339	417	Sheeted Dikes (Diabase)	Elia
S26	630	17	328	418	Sheeted Dikes (Diabase)	Elia
S27	605	14	217	415	Sheeted Dikes (Diabase)	Elia
S28	603	11	104	414	Sheeted Dikes (Diabase)	Elia
RD1	673	17	279	426	Sheeted Dikes (Diabase)	Elia
RD2	665	18	280	424	Sheeted Dikes (Diabase)	Elia
RD3	582	28	63	464	Sheeted Dikes (Diabase)	Atsas
N1	722	20	196	425	Sheeted Dikes (Diabase)	Elia
K001	540	6	187	458	Sheeted Dikes (Diabase)	Atsas
K002	540	6	155	458	Sheeted Dikes (Diabase)	Atsas
K003	540	12	64	459	Sheeted Dikes (Diabase)	Atsas
K004	545	19	63	459	Sheeted Dikes (Diabase)	Atsas

Table B.2 (continued).

Site ID	Elev	Slope	Aspect	MAP	Lithology	Wtrshd
K006	549	25	61	459	Sheeted Dikes (Diabase)	Atsas
K007	553	27	66	460	Sheeted Dikes (Diabase)	Atsas
K008	557	28	65	460	Sheeted Dikes (Diabase)	Atsas
K009	562	27	64	460	Sheeted Dikes (Diabase)	Atsas
K010	567	26	62	461	Sheeted Dikes (Diabase)	Atsas
K011	573	23	59	461	Sheeted Dikes (Diabase)	Atsas
K012	581	16	39	462	Sheeted Dikes (Diabase)	Atsas

Table B3. Toposequence and hillslope stability data obtained through transect and GIS analysis of soil profiles.

	Explanation of column headings
Site ID	Individual record identifier; photograph site identifiers begin with a number (e.g. 1010037). Field excavation site identifiers begin with a
Soil Tax.	General soil classification, based on profile descriptions and depth characteristics.
Posit 15	Relative hillslope position determined through the 15-meter buffer analysis. Three classes: footslope, backslope, and summit.
Posit Topo	Hillslope position determined through visual interpretation of site position along transect topographic profiles. Five classes. Sites off-transect were not classified.
Topo ID	Identifier assigned to soil profiles along apparent toposequences.
q/T	SHALSTAB hydrologic-slope stability value, derived from parameter-defined analysis of the 25-meter DEM.

Site ID	Soil Tax.	Posit 15	Posit Topo	Topo ID	q/T
2970	Typic Xerorthent	Backslope	Backslope	2.1	10
2972	Lithic Xerorthent	Backslope	Backslope	2.1	10
2973	Lithic Xerorthent	Backslope	Backslope	2.1	10
2974	Lithic Xerorthent	Backslope	Shoulder	2.1	10
2976	Lithic Xerorthent	Backslope	Footslope	-	10
2977	Lithic Xerorthent	Backslope	Shoulder	-	10
2978	Lithic Xerorthent	Summit	Shoulder	-	10
2982	Lithic Xerorthent	Backslope	Footslope	-	10
2983	Lithic Xerorthent	Backslope	Summit	-	10
2984	Lithic Xerorthent	Summit	Shoulder	-	10
2985	Lithic Xerorthent	Summit	Footslope	2.2	10
2986	Lithic Xerorthent	Backslope	Backslope	2.2	10
2987	Lithic Xerorthent	Summit	Backslope	2.2	10
2988	Lithic Xerorthent	Summit	Backslope	2.2	10
2989	Lithic Xerorthent	Backslope	Shoulder	-	10
2990	Lithic Xerorthent	Backslope	Footslope	-	10
2991	Lithic Xerorthent	Backslope	Shoulder	-	5
2992	Lithic Xerorthent	Backslope	Shoulder	2.3	-2
2993	Lithic Xerorthent	Backslope	Footslope	2.3	-2
2994	Lithic Xerorthent	Backslope	Backslope	2.3	-2
2995	Lithic Xerorthent	Backslope	Backslope	2.3	-1
2996	Lithic Xerorthent	Backslope	Backslope	2.3	-1

Table B3 (continued)

Site ID	Soil Tax.	Posit 15	Posit Topo	Topo ID	q/T
2997	Lithic Xerorthent	Backslope	Shoulder	2.3	-2
2998	Lithic Xerorthent	Backslope	Footslope	-	-2
2999	Lithic Xerorthent	Backslope	Footslope	2.4	6
3000	Lithic Xerorthent	Backslope	Backslope	2.4	8
3001	Lithic Xerorthent	Backslope	Backslope	2.4	9
3003	Lithic Xerorthent	Backslope	Backslope	2.4	10
3004	Lithic Xerorthent	Footslope	Summit	2.4	7
3005	Lithic Xerorthent	Backslope	Footslope	-	-3
3007	Lithic Xerorthent	Backslope	Backslope	-	-1
3008	Lithic Xerorthent	Summit	Shoulder	-	-2
3009	Lithic Xerorthent	Backslope	Footslope	-	-2
3010	Lithic Xerorthent	Backslope	Footslope	-	3
3011	Lithic Xerorthent	Backslope	Footslope	2.5	4
3012	Lithic Xerorthent	Backslope	Backslope	2.5	8
3013	Lithic Xerorthent	Backslope	Backslope	2.5	10
3014	Lithic Xerorthent	Footslope	Summit	2.5	10
3015	Lithic Xerorthent	Footslope	Footslope	-	10
3016	Lithic Xerorthent	Backslope	Backslope	-	10
3017	Lithic Xerorthent	Summit	Footslope	-	4
3020	Lithic Xerorthent	Summit	Backslope	2.6	2
3021	Lithic Xerorthent	Summit	Backslope	2.6	2
3022	Lithic Xerorthent	Backslope	Shoulder	2.6	3
3026	Lithic Xerorthent	Backslope	Shoulder	2.6	7
3030	Lithic Xerorthent	Backslope	Shoulder	-	9
3031	Lithic Xerorthent	Backslope	Footslope	-	1
3032	Lithic Xerorthent	Backslope	Footslope	2.7	-2
3033	Lithic Xerorthent	Backslope	Backslope	2.7	5
3034	Lithic Xerorthent	Backslope	Backslope	2.7	10
3035	Lithic Xerorthent	Backslope	Backslope	2.7	10
3036	Lithic Xerorthent	Footslope	Shoulder	2.7	10
3037	Lithic Xerorthent	Backslope	Footslope	2.8	10
3038	Lithic Xerorthent	Backslope	Backslope	2.8	10
3039	Lithic Xerorthent	Summit	Backslope	2.8	10
3040	Lithic Xerorthent	Summit	Backslope	2.8	10
3041	Lithic Xerorthent	Backslope	Backslope	-	10
3042	Lithic Xerorthent	Backslope	Backslope	-	10
3043	Lithic Xerorthent	Backslope	Shoulder	-	10
3044	Lithic Xerorthent	Backslope	Toeslope	-	10

Table B3 (continued)

Site ID	Soil Tax.	Posit 15	Posit Topo	Topo ID	q/T
3045	Lithic Xerorthent	Backslope	Toeslope	-	10
3046	Lithic Xerorthent	Backslope	Toeslope	-	10
3047	Lithic Xerorthent	Backslope	Footslope	1.2	10
3048	Lithic Xerorthent	Footslope	Backslope	1.2	10
3050	Lithic Xerorthent	Backslope	Summit	1.2	10
3051	Lithic Xerorthent	Backslope	Backslope	1.3	10
3052	Lithic Xerorthent	Footslope	Backslope	1.3	10
3053	Lithic Xerorthent	Footslope	Backslope	1.3	10
3054	Lithic Xerorthent	Backslope	Shoulder	1.3	10
3056	Lithic Xerorthent	Backslope	Toeslope	-	10
3057	Typic Xerorthent	Backslope	Toeslope	-	10
3058	Lithic Xerorthent	Summit	Toeslope	-	10
3059	Lithic Xerorthent	Backslope	Toeslope	-	10
3060	Lithic Xerorthent	Backslope	Toeslope	-	10
3062	Lithic Xerorthent	Footslope	Footslope	-	10
3063	Lithic Xerorthent	Backslope	Footslope	-	10
3064	Lithic Xerorthent	Backslope	Shoulder	-	10
3065	Lithic Xerorthent	n/a Overlap	Footslope	1.4	10
3066	Lithic Xerorthent	n/a Overlap	Backslope	1.4	10
3067	Lithic Xerorthent	Backslope	Summit	1.4	10
3068	Lithic Xerorthent	Footslope	Footslope	-	10
3069	Lithic Xerorthent	Summit	Summit	-	10
3070	Lithic Xerorthent	Backslope	Footslope	-	10
3071	Lithic Xerorthent	Backslope	Summit	-	10
3072	Lithic Xerorthent	Footslope	Backslope	-	10
3073	Lithic Xerorthent	Footslope	Backslope	-	10
3074	Lithic Xerorthent	Footslope	Shoulder	1.5	10
3075	Lithic Xerorthent	Backslope	Backslope	1.5	10
3076	Lithic Xerorthent	Backslope	Backslope	1.5	10
3077	Lithic Xerorthent	Backslope	Footslope	1.5	10
3078	Lithic Xerorthent	Footslope	Backslope	1.6	10
3079	Lithic Xerorthent	Backslope	Backslope	1.6	10
3080	Lithic Xerorthent	Backslope	Shoulder	1.6	10
3081	Lithic Xerorthent	Summit	Shoulder	1.6	10
3082	Lithic Xerorthent	Summit	Shoulder	1.7	10
3083	Lithic Xerorthent	Summit	Backslope	1.7	10
3084	Lithic Xerorthent	Backslope	Backslope	1.7	8
3085	Lithic Xerorthent	Summit	Footslope	1.7,1.8	4

Table B3 (continued)

Site ID	Soil Tax.	Posit 15	Posit Topo	Topo ID	q/T
3086	Lithic Xerorthent	Backslope	Backslope	1.8	2
3087	Lithic Xerorthent	Backslope	Backslope	1.8	5
3088	Lithic Xerorthent	Backslope	Summit	1.8	7
3089	Lithic Xerorthent	Backslope	Toeslope	-	5
3090	Lithic Xerorthent	Summit	Shoulder	-	7
3091	Lithic Xerorthent	Summit	Backslope	-	10
3092	Lithic Xerorthent	Backslope	Footslope	-	10
3093	Lithic Xerorthent	Summit	Footslope	-	10
3094	Lithic Xerorthent	Backslope	Summit	-	10
3095	Lithic Xerorthent	Backslope	Footslope	-	10
3096	Lithic Xerorthent	Backslope	Summit	1.9	3
3097	Lithic Xerorthent	Backslope	Backslope	1.9	7
3098	Lithic Xerorthent	Backslope	Footslope	1.9	5
3099	Lithic Xerorthent	Summit	Footslope	-	-1
3100	Lithic Xerorthent	Summit	Summit	-	1
3101	Lithic Xerorthent	Backslope	Footslope	-	0
3102	Lithic Xerorthent	Backslope	Summit	1.10	3
3103	Lithic Xerorthent	Footslope	Backslope	1.10	10
3104	Lithic Xerorthent	Backslope	Footslope	1.10,1.11	10
3105	Lithic Xerorthent	Footslope	Backslope	1.11	10
3106	Lithic Xerorthent	Backslope	Shoulder	1.11	10
3107	Lithic Xerorthent	Backslope	Footslope	-	10
3108	Lithic Xerorthent	Backslope	Backslope	-	10
3109	Lithic Xerorthent	Backslope	Footslope	-	10
3110	Lithic Xerorthent	Backslope	Backslope	-	10
3111	Lithic Xerorthent	Backslope	Backslope	-	10
3112	Lithic Xerorthent	Backslope	Summit	-	10
3113	Lithic Xerorthent	Footslope	Footslope	-	10
3114	Lithic Xerorthent	Footslope	Backslope	-	10
3115	Lithic Xerorthent	Footslope	Backslope	-	10
3116	Lithic Xerorthent	Backslope	Summit	-	10
3117	Lithic Xerorthent	Backslope	Toeslope	-	10
3118	Lithic Xerorthent	Summit	Shoulder	-	10
3119	Lithic Xerorthent	Summit	Backslope	-	10
3120	Lithic Xerorthent	Summit	Footslope	-	10
3121	Lithic Xerorthent	Backslope	Footslope	-	10
3122	Lithic Xerorthent	Backslope	Summit	-	10
3123	Lithic Xerorthent	Backslope	Footslope	-	10

Table B3 (continued)					
Site ID	Soil Tax.	Posit 15	Posit Topo	Topo ID	q/T
3124	Lithic Xerorthent	Backslope	Backslope	-	10
3125	Lithic Xerorthent	Summit	Backslope	-	10
3126	Lithic Xerorthent	Backslope	Backslope	-	10
3127	Lithic Xerorthent	Backslope	Footslope	1.12	10
3128	Lithic Xerorthent	Backslope	Backslope	1.12	10
3129	Lithic Xerorthent	Backslope	Backslope	1.12	10
3130	Lithic Xerorthent	Backslope	Footslope	1.12	10
3131	Lithic Xerorthent	Footslope	Backslope	1.12	10
3132	Lithic Xerorthent	Footslope	Shoulder	1.12	10
3133	Lithic Xerorthent	Footslope	Backslope	-	10
3134	Lithic Xerorthent	Backslope	Footslope	-	10
3135	Lithic Xerorthent	Backslope	Footslope	-	10
3136	Lithic Xerorthent	Backslope	Backslope	-	10
3137	Lithic Xerorthent	Backslope	Summit	1.13	10
3138	Lithic Xerorthent	Footslope	Backslope	1.13	10
3139	Lithic Xerorthent	Backslope	Backslope	1.13	10
3140	Lithic Xerorthent	Backslope	Backslope	1.13	10
3141	Lithic Xerorthent	Backslope	Footslope	1.13	10
3142	Lithic Xerorthent	Backslope	Footslope	-	10
3143	Lithic Xerorthent	Backslope	Toeslope	-	10
3144	Typic Xerorthent	Backslope	Toeslope	-	10
3145	Lithic Xerorthent	Footslope	Toeslope	4.1	10
3146	Lithic Xerorthent	Footslope	Toeslope	4.1	10
3150	Typic Xerorthent	Footslope	Toeslope	4.1	10
3151	Lithic Xerorthent	Backslope	Footslope	4.1	10
3152	Typic Xerorthent	Backslope	Backslope	4.1	10
3158	Lithic Xerorthent	Backslope	Backslope	4.1	10
3160	Lithic Xerorthent	Backslope	Backslope	-	3
3161	Lithic Xerorthent	Backslope	Footslope	-	10
3162	Lithic Xerorthent	Footslope	Shoulder	-	10
3163	Lithic Xerorthent	Backslope	Footslope	3.1	10
3164	Lithic Xerorthent	Backslope	Backslope	3.1	10
3165	Lithic Xerorthent	Backslope	Backslope	3.1	10
3166	Lithic Xerorthent	Footslope	Summit	3.1	10
3167	Lithic Xerorthent	Backslope	Footslope	-	10
3168	Lithic Xerorthent	Backslope	Backslope	-	10
3169	Lithic Xerorthent	Footslope	Shoulder	-	10
3170	Lithic Xerorthent	Footslope	Footslope	3.2	10

Table B3 (continued)

Site ID	Soil Tax.	Posit 15	Posit Topo	Topo ID	q/T
3171	Lithic Xerorthent	Backslope	Backslope	3.2	10
3172	Lithic Xerorthent	Backslope	Shoulder	3.2	10
3173	Lithic Xerorthent	Backslope	Backslope	3.2	10
3174	Lithic Xerorthent	Backslope	Backslope	3.2	8
3175	Lithic Xerorthent	Backslope	Backslope	3.2	2
3176	Lithic Xerorthent	Backslope	Backslope	3.2	-3
3177	Lithic Xerorthent	Backslope	Shoulder	3.2	-1
3178	Lithic Xerorthent	Backslope	Summit	3.2	8
3204	Lithic Xerorthent	Backslope	Backslope	3.3	10
3205	Lithic Xerorthent	Backslope	Backslope	3.3	6
3206	Lithic Xerorthent	Backslope	Footslope	3.3	-3
3207	Lithic Xerorthent	Backslope	Footslope	3.3	5
3208	Lithic Xerorthent	Backslope	Summit	3.4	9
3209	Lithic Xerorthent	Backslope	Footslope	3.4	10
3210	Lithic Xerorthent	Footslope	Footslope	3.4	10
3211	Lithic Xerorthent	Footslope	Toeslope	3.4	10
3212	Lithic Xerorthent	Footslope	Toeslope	3.4	10
1010037	Lithic Xerorthent	Footslope	Backslope	-	-2
1010039	Typic Xerorthent	Backslope	Backslope	-	-3
1010040	Lithic Xerorthent	Backslope	Footslope	-	-3
1010041	Lithic Xerorthent	Backslope	Footslope	-	-3
1010042	Lithic Xerorthent	Backslope	Footslope	-	-3
1010044	Lithic Xerorthent	Backslope	Summit	5.1	-3
1010045	Lithic Xerorthent	Backslope	Backslope	5.1	-3
1010046	Lithic Xerorthent	Backslope	Backslope	5.1	-3
1010047	Lithic Xerorthent	Summit	Backslope	5.1	-3
1010048	Lithic Xerorthent	Summit	Backslope	5.1	-2
1010049	Lithic Xerorthent	Summit	Backslope	5.1	-2
1010050	Lithic Xerorthent	Summit	Backslope	5.1	-2
1010053	Lithic Xerorthent	Backslope	Backslope	5.1	-2
1010054	Lithic Xerorthent	Footslope	Backslope	5.1	-3
1010062	Lithic Xerorthent	Backslope	Backslope	5.1	-3
1010063	Lithic Xerorthent	Backslope	Backslope	5.1	-3
1010064	Lithic Xerorthent	Backslope	Backslope	5.1	-2
1010068	Lithic Xerorthent	Backslope	Backslope	5.1	-3
1010070	Lithic Xerorthent	Backslope	Summit	-	-3
1010073	Lithic Xerorthent	Backslope	Backslope	-	-3
1010074	Lithic Xerorthent	Backslope	Footslope	-	-3

Table B3 (continued)

Site ID	**Soil Tax.**	**Posit 15**	**Posit Topo**	**Topo ID**	**q/T**
1010075	Lithic Xerorthent	Backslope	Summit	5.2	-3
1010079	Lithic Xerorthent	Backslope	Backslope	5.2	-2
1010080	Lithic Xerorthent	Footslope	Backslope	5.2	4
1010081	Lithic Xerorthent	Backslope	Backslope	5.2	5
1010082	Lithic Xerorthent	Backslope	Footslope	5.2	-3
1010083	Typic Xerorthent	Backslope	Backslope	-	-3
1010084	Lithic Xerorthent	Backslope	Backslope	-	-3
1010085	Lithic Xerorthent	Backslope	Summit	-	-3
1010086	Lithic Xerorthent	Backslope	Shoulder	-	-3
1010087	Lithic Xerorthent	Backslope	Backslope	-	-3
1010088	Lithic Xerorthent	Footslope	Footslope	-	-2
1010089	Lithic Xerorthent	Footslope	Summit	-	-2
1010090	Lithic Xerorthent	Backslope	Footslope	-	-2
1010091	Lithic Xerorthent	Backslope	Footslope	-	-1
1010092	Lithic Xerorthent	Summit	Backslope	-	9
1010094	Lithic Xerorthent	Summit	Summit	5.3	6
1010095	Lithic Xerorthent	Backslope	Backslope	5.3	1
1010096	Lithic Xerorthent	Backslope	Backslope	5.3	-2
1010097	Lithic Xerorthent	Footslope	Backslope	5.3	-3
1010098	Lithic Xerorthent	Footslope	Backslope	5.3	8
1010099	Lithic Xerorthent	Backslope	Backslope	5.3	3
1010100	Lithic Xerorthent	Backslope	Backslope	5.3	-1
1010101	Lithic Xerorthent	Backslope	Footslope	5.3	-3
1010102	Lithic Xerorthent	Backslope	Summit	5.4	-3
1010103	Lithic Xerorthent	Backslope	Backslope	5.4	-3
1010104	Lithic Xerorthent	Backslope	Footslope	5.4	-3
1010105	Typic Xerorthent	Backslope	Footslope	5.4	-3
1010106	Lithic Xerorthent	Backslope	Footslope	-	-2
1010179	Lithic Xerorthent	Backslope	Backslope	-	10
1010180	Typic Xerorthent	Backslope	Summit	-	10
1010181	Lithic Xerorthent	Backslope	Backslope	-	10
1010183	Typic Xerorthent	Backslope	Footslope	-	10
1010184	Lithic Xerorthent	Backslope	Backslope	-	3
1010188	Typic Xerorthent	Backslope	Summit	-	-2
1010189	Lithic Xerorthent	Backslope	Backslope	-	-3
1010190	Typic Xerorthent	Backslope	Backslope	-	-3
1010191	Typic Xerorthent	Backslope	Backslope	-	-3
1010192	Lithic Xerorthent	Backslope	Backslope	-	-3

Site ID	Soil Tax.	Posit 15	Posit Topo	Topo ID	q/T
Table B3 (continued)					
1010193	Lithic Xerorthent	Backslope	Backslope	-	-2
1010194	Lithic Xerorthent	Backslope	Footslope	-	-2
1010195	Lithic Xerorthent	Backslope	Footslope	-	-2
1010196	Lithic Xerorthent	Backslope	Backslope	-	-2
1010197	Lithic Xerorthent	Backslope	Summit	-	-1
1010198	Lithic Xerorthent	Backslope	Shoulder	-	2
1010199	Lithic Xerorthent	Summit	Shoulder	-	10
1010200	Lithic Xerorthent	Summit	Summit	-	10
1010201	Lithic Xerorthent	Backslope	Summit	-	10
1010202	Lithic Xerorthent	Footslope	Summit	-	10
1010203	Lithic Xerorthent	Footslope	Summit	6.1	10
1010204	Typic Xerorthent	Backslope	Backslope	6.1	10
1010205	Lithic Xerorthent	Backslope	Backslope	6.1	10
1010206	Lithic Xerorthent	Backslope	Backslope	6.1	10
1010207	Lithic Xerorthent	Backslope	Backslope	6.1	10
1010208	Lithic Xerorthent	Backslope	Backslope	6.1	10
1010209	Lithic Xerorthent	Backslope	Backslope	6.1	9
1010210	Lithic Xerorthent	Backslope	Backslope	6.1	10
1010211	Lithic Xerorthent	Backslope	Backslope	6.1	10
1010214	Lithic Xerorthent	Backslope	Backslope	6.1	9
1010215	Lithic Xerorthent	Backslope	Backslope	6.1	10
1010216	Lithic Xerorthent	Backslope	Footslope	6.1	10
1010217	Lithic Xerorthent	Backslope	Footslope	6.1	10
1010218	Lithic Xerorthent	Backslope	Footslope	-	10
1010219	Lithic Xerorthent	Backslope	Backslope	-	10
1010220	Typic Xerorthent	Backslope	Shoulder	-	10
1010221	Lithic Xerorthent	Backslope	Shoulder	-	10
1010222	Typic Xerorthent	Backslope	Backslope	-	10
1010223	Lithic Xerorthent	Summit	Footslope	-	10
1010225	Lithic Xerorthent	Summit	Footslope	-	10
1010226	Typic Xerorthent	Backslope	Shoulder	-	10
1020001	Lithic Xerorthent	Backslope	Shoulder	-	10
1020002	Lithic Xerorthent	Backslope	Summit	-	10
1020003	Lithic Xerorthent	Backslope	Shoulder	-	10
1020004	Lithic Xerorthent	Backslope	Shoulder	-	10
1020005	Lithic Xerorthent	Backslope	Footslope	-	10
1020006	Lithic Xerorthent	Backslope	Shoulder	-	10
1020007	Lithic Xerorthent	Backslope	Shoulder	-	10

Table B3 (continued)

Site ID	Soil Tax.	Posit 15	Posit Topo	Topo ID	q/T
1020008	Lithic Xerorthent	Backslope	Shoulder	-	10
1020009	Lithic Xerorthent	Footslope	Shoulder	6.2	10
1020010	Lithic Xerorthent	Footslope	Backslope	6.2	10
1020011	Lithic Xerorthent	Backslope	Backslope	6.2	10
1020012	Lithic Xerorthent	Backslope	Footslope	6.2	10
1020014	Typic Xerorthent	Footslope	Backslope	6.3	10
1020015	Lithic Xerorthent	Footslope	Backslope	6.3	10
1020016	Lithic Xerorthent	Backslope	Backslope	6.3	10
1020017	Lithic Xerorthent	Backslope	Footslope	6.3	10
1020018	Lithic Xerorthent	Backslope	Footslope	-	10
1020019	Lithic Xerorthent	Footslope	Shoulder	-	10
1020020	Typic Xerorthent	Footslope	Summit	-	10
1020021	Lithic Xerorthent	Backslope	Shoulder	-	10
1020022	Lithic Xerorthent	Backslope	Shoulder	-	10
P1	Lithic Xerorthent	Backslope	Backslope	-	10
P2	Lithic Xerorthent	Summit	Shoulder	-	-2
P3	Lithic Xerorthent	Summit	Backslope	-	10
P4	Lithic Xerorthent	Backslope	Backslope	-	10
P6	Lithic Xerorthent	Footslope	Footslope	-	10
P7	Lithic Xerorthent	Backslope	Footslope	-	-2
P8	Lithic Xerorthent	Backslope	Backslope	-	1
P10	Lithic Xerorthent	Backslope	Footslope	-	10
Astart	Lithic Xerorthent	Backslope	n/a	n/a	-2
A1	Lithic Xerorthent	Backslope	n/a	n/a	0
A2	Lithic Xerorthent	Summit	n/a	n/a	9
A3	Lithic Xerorthent	Summit	n/a	n/a	8
A4	Lithic Xerorthent	Summit	n/a	n/a	9
A5	Lithic Xerorthent	Summit	n/a	n/a	7
A6	Lithic Xerorthent	Backslope	n/a	n/a	3
A7	Lithic Xerorthent	Backslope	n/a	n/a	-2
A8	Lithic Xerorthent	Backslope	n/a	n/a	2
A9	Lithic Xerorthent	Backslope	n/a	n/a	0
A10	Lithic Xerorthent	Backslope	n/a	n/a	8
A11	Lithic Xerorthent	Backslope	n/a	n/a	10
A12	Lithic Xerorthent	Backslope	n/a	n/a	10
A13	Lithic Xerorthent	Footslope	n/a	n/a	10
S01	Lithic Xerorthent	Backslope	Summit	7.1	2
S02	Lithic Xerorthent	Footslope	n/a	n/a	2

Table B3 (continued)

Site ID	Soil Tax.	Posit 15	Posit Topo	Topo ID	q/T
S03	Lithic Xerorthent	Backslope	Summit	7.1	-2
S04	Lithic Xerorthent	Backslope	Summit	7.1	-2
S05	Lithic Xerorthent	Backslope	Summit	7.1	0
S06	Lithic Xerorthent	Backslope	Shoulder	7.1	9
S07	Lithic Xerorthent	Backslope	Shoulder	7.1	6
S08	Lithic Xerorthent	Summit	Shoulder	7.1	8
S09	Lithic Xerorthent	Summit	Backslope	7.1	7
S10	Lithic Xerorthent	Summit	Backslope	7.1	5
S11	Lithic Xerorthent	Backslope	Backslope	7.1	6
S12	Lithic Xerorthent	Summit	Backslope	7.1	9
S13	Lithic Xerorthent	Summit	Backslope	7.1	10
S14	Lithic Xerorthent	Backslope	Backslope	7.1	4
S15	Lithic Xerorthent	Backslope	Backslope	7.1	-2
S16	Lithic Xerorthent	Backslope	Backslope	7.1	-1
S17	Lithic Xerorthent	Backslope	Backslope	7.1	-2
S18	Lithic Xerorthent	Backslope	Backslope	7.1	-2
S19	Lithic Xerorthent	Backslope	Backslope	7.1	-2
S20	Lithic Xerorthent	Backslope	Backslope	7.1	5
S21	Lithic Xerorthent	Backslope	Backslope	7.1	4
S22	Lithic Xerorthent	Backslope	Backslope	7.1	5
S23	Lithic Xerorthent	Backslope	Backslope	7.1	3
S24	Lithic Xerorthent	Backslope	Backslope	7.1	3
S25	Lithic Xerorthent	Backslope	Footslope	7.1	10
S26	Lithic Xerorthent	Backslope	Footslope	7.1	10
S27	Lithic Xerorthent	Footslope	Footslope	7.1	10
S28	Lithic Xerorthent	Backslope	Footslope	7.1	10
RD1	Lithic Xerorthent	Footslope	n/a	n/a	10
RD2	Lithic Xerorthent	Backslope	n/a	n/a	8
RD3	Lithic Xerorthent	Backslope	n/a	n/a	-1
N1	Lithic Xerorthent	Summit	n/a	n/a	8
K001	Lithic Xerorthent	Footslope	n/a	n/a	10
K002	Lithic Xerorthent	Backslope	n/a	n/a	10
K003	Lithic Xerorthent	Backslope	n/a	n/a	10
K004	Lithic Xerorthent	Backslope	n/a	n/a	5
K006	Lithic Xerorthent	Backslope	n/a	n/a	-1
K007	Lithic Xerorthent	Backslope	n/a	n/a	0
K008	Lithic Xerorthent	Backslope	n/a	n/a	-2
K009	Lithic Xerorthent	Backslope	n/a	n/a	-2

Table B3 (continued)

Site ID	Soil Tax.	Posit 15	Posit Topo	Topo ID	q/T
K010	Lithic Xerorthent	Backslope	n/a	n/a	-2
K011	Lithic Xerorthent	Backslope	n/a	n/a	-1
K012	Lithic Xerorthent	Summit	n/a	n/a	6

Appendix C - Soil Profile Descriptions

The following are simple soil profile descriptions of two Entisols representative of regional soil profile characteristics. Soil colors are moist except where noted. No chemical data are available.

Site P1

Slope =	26 degrees
Aspect =	N
Landform =	Colluvial hillslope (Backslope position)
Vegetation =	*Pinus brutia*, *Cistus sp.*
Soil Cover =	100% pine litter, moss, cistus litter, cistus plants, and pine trees.
Location =	E0497719, N3877449: Forest roadcut; elevation 576m;

O -- 10 to 0 cm; (min thickness = 3cm; max thickness = 20cm). Moss and lichen, decomposing pine needles and twigs.

A -- 0 to 7 cm; dark yellow brown (10YR 4/4) silty clay loam, 10YR6/4 dry; moderate, fine granular structure; hard; friable; slightly-sticky, slightly plastic; many (5) very fine to medium roots throughout; many very fine pores throughout; no redoximorphic features; 2% fine, weathered, basalt gravel; white fungal mycorrhizae throughout; clear wavy boundary.

A2 -- 7 to 15 cm; dark yellow brown (10YR 3/4) silty clay loam, 2.5Y 6/4 dry; weak fine to medium granular structure; slightly hard, friable; nonsticky, non-plastic; no redox features; common fine to very fine roots (3/cm^2); few (1) fine to medium (4mm) pores; <2% fine basalt fragments; gradual wavy boundary.

C -- 15 to 20 cm; dark yellow brown (10YR 3/4) gravelly silty clay loam; massive; hard; friable; nonsticky, non-plastic; gradual irregular boundary.

2R -- 20cm to 200cm+ hydrothermically weathered Basal Group rocks (sheeted diabase dikes and pillow lavas); highly fractured.

Site P6

Slope =	25 degrees
Aspect =	N
Landform =	Active gully – colluvial alluvial slope (footslope position).
Vegetation =	*Cistus sp.*, domesticated olive, *Pinus brutia*, and others.
Soil Cover =	100% moss, pine litter, and lichen.

Location = E0497795, N3877460: Bulldozed cross-section of gully channel; elevation 586

Oi -- 1 to 0 cm. lichen, moss, and decomposing pine litter.

A -- 0 to 11 cm; very dark brown (10YR2/2) silt loam; moderate fine granular structure; very soft, friable; non-sticky; and non-plastic; many (10/cm^2) very fine roots; many very fine pores (5/cm^2); no redoximorphic features; mycorrhizae present; 2% fine (0.5 to 1.5 cm) angular basalt pebbles. Smooth gradual contact.

C -- 11 to 21 cm: very dark brown (10YR2/2) silt loam; massive; common (4) medium to fine pores; few (2) medium roots; gradual irregular contact.

R -- 21 cm plus: fractured basaltic bedrock; fractures filled with SiL and few medium roots to 150cm depth; black manganese stains and reddish, oxidized-iron stains on rock faces.